



<https://theses.gla.ac.uk/>

Theses Digitisation:

<https://www.gla.ac.uk/myglasgow/research/enlighten/theses/digitisation/>

This is a digitised version of the original print thesis.

Copyright and moral rights for this work are retained by the author

A copy can be downloaded for personal non-commercial research or study, without prior permission or charge

This work cannot be reproduced or quoted extensively from without first obtaining permission in writing from the author

The content must not be changed in any way or sold commercially in any format or medium without the formal permission of the author

When referring to this work, full bibliographic details including the author, title, awarding institution and date of the thesis must be given

Enlighten: Theses

<https://theses.gla.ac.uk/>
research-enlighten@glasgow.ac.uk



UNIVERSITY
of
GLASGOW

**Structure-Function Studies of Prx III, A
Mitochondrial Typical 2-Cys Peroxiredoxin**

Zhenbo Cao M.Res

This thesis is presented for the degree
Doctor of Philosophy
February 2006

Institute of Biomedical and Life Sciences
University of Glasgow

ProQuest Number: 10391434

All rights reserved

INFORMATION TO ALL USERS

The quality of this reproduction is dependent upon the quality of the copy submitted.

In the unlikely event that the author did not send a complete manuscript and there are missing pages, these will be noted. Also, if material had to be removed, a note will indicate the deletion.



ProQuest 10391434

Published by ProQuest LLC (2017). Copyright of the Dissertation is held by the Author.

All rights reserved.

This work is protected against unauthorized copying under Title 17, United States Code
Microform Edition © ProQuest LLC.

ProQuest LLC.
789 East Eisenhower Parkway
P.O. Box 1346
Ann Arbor, MI 48106 – 1346

GLASGOW
UNIVERSITY
LIBRARY

For parents and wife

"Chance favours the prepared mind"

--Louis Pasteur

Acknowledgements

A journey is easier when you travel together. Interdependence is certainly more valuable than independence. This thesis is the result of three and half years of work, whereby I have been accompanied and supported by many people. I am very pleased to have this opportunity to express my gratitude to them all.

Firstly, I would like to thank my supervisor, Prof. Gordon Lindsay, who has continually supported my work all the way through and for his gentle prompting during the write-up. In particular, I am grateful to him for allowing me to work on such an interesting project and for giving me the freedom to choose in which direction the project would develop. I would also like to express my appreciation for the encouragement, expert guidance and assistance provided by Prof. Neil Isaacs. Especially when I'd almost been convinced that it was an impossible mission to solve the structure, Prof. Isaacs still kept faith with me and the result turned out to be jolly good. I would also like to thank my assessor, Prof. Richard Cogdell, for keeping an eye on the progress of my work and for always being available if I needed his advice.

My colleagues in Lab 233; Alison, Donna, Heather, Mischa, Iliba, Audrey and Louise all gave me the feeling of being at home at work. Many thanks for welcoming me as your friend in addition to your work colleague. I would also like to thank everyone from the Protein Crystallography Lab, especially Aleks, Yanshi, Karen and Alan for making "crystallography crystal clear".

My pals Alastair and Michael, as well as the Chinese girls, including Malaysian-Chinese, in the department, are thanked from the bottom of my heart for their friendship and emotional support over these past years.

I am very grateful for my parents, and most of all to my wife Fan, for their love and patience during the course of my studies in Glasgow.

Many thanks to Wellcome Trust for funding my Ph.D studentship.

Abstract

The peroxiredoxins (Prxs) are a ubiquitous family of antioxidant enzymes that regulate intracellular levels of H_2O_2 where they are implicated in both tissue protection against oxidative stress and H_2O_2 -mediated signalling pathways (Wood *et al.*, 2003). This thesis describe our results on the structure-function studies of PrxIII, a mitochondrial typical 2-Cys peroxiredoxin.

Bovine PrxIII was cloned previously in our laboratory; however PrxIII requires its cognate partners, mammalian mitochondrial thioredoxin (Trx2) and mammalian mitochondrial thioredoxin reductase (TRR2), to reconstitute the complete antioxidant defence system. To establish a direct *in vitro* assay for PrxIII, Trx2 and TRR2 were cloned, overexpressed and purified in this study. As TRR2 is a selenocysteine (SeCys) protein, a suitable selenocysteine insert sequence (SECIS) for the translation of its penultimate SeCys codon was introduced by incorporating it into the reverse primer for PCR. A combination of different approaches was used for the successful overexpression of active TRR2. Overexpression in modified rich LB media at 15°C in the presence of low IPTG concentrations gave good overexpression of soluble enzyme. Moreover, the addition of the SECIS at the C-terminal of the insert, in the presence of 1 μ M Na_2SeO_3 and co-expression of the SelABC plasmid ensured an optimal supply of the relevant tRNA, tRNA synthase and elongation factor for translation of the UGA SeCys codon.

Assays showed that NADPH-linked oxidation needed the presence of all three enzymes to reduce H_2O_2 . PrxIII was also shown to reduce other organic peroxides, although with lower activity. Cys47 and Cys168, but not Cys66, proved to be crucial for peroxiredoxin activity. Interestingly, at high H_2O_2 concentrations in the non-physiological range, TRR2 also had the capacity to reduce H_2O_2 directly in an NADPH-dependent manner. PrxIII is also shown to be susceptible to overoxidation and loses peroxidase activity at increased H_2O_2 levels in the range 50 μ M to 1mM. This

was monitored by SDS-PAGE analysis of partially or fully overoxidised forms of H₂O₂-mediated PrxIII and PrxIII pathway assays.

Gel filtration chromatography was used to determine under which conditions the PrxIII dodecamer would dissociate into dimers. The results show that redox state, protein concentration and the N-terminal His-tag all affect the oligomerization of PrxIII.

The crystal structure of the PrxIII C168S mutant from bovine mitochondria has been determined at a resolution of 3.3 angstroms. The structure reveals that the toroid is composed of 12 (not 10) monomers with a 6(2,2) symmetry. Each ring has an external diameter of 150 angstroms and encompasses a central cavity 70 angstroms in width. Surprisingly, two PrxIII rings are mechanically interlocked in the crystal to form a protein catenane. Interestingly, the catenated form represents only a small proportion (3-5%) of the total PrxIII population, as observed by electronic microscopy studies at dilute concentration (10-50µg/ml). Preliminary analytical ultracentrifugation data suggest that 2-ring catenane formation is concentration dependent. A general model illustrating catenane formation arising from polar contacts between two basic dimeric units is described. It is not clear whether the catenated form of PrxIII has any physiological function. However, the observation that Prxs can protect cells from heat shock in a peroxidase-independent process might provide new insights into possible novel functions.

ABBREVIATIONS

Å	angstrom
AhpC	alkyl hydroperoxidase C
ALS	amyotrophic lateral sclerosis
Amp.	ampicillin
Approx.	approximately
ATP	adenosine triphosphate
AUC	analytical ultracentrifugation
CIAP	calf intestinal alkaline phosphatase
Da	Daltons
DTNB	5,5'-dithionitrobenzoic acid
DTT	dithiothreitol
EDTA	ethylenediaminetetraacetic acid
EF	elongation factor
EM	electron microscopy
ESRF	european synchrotron radiation facility
EtBr	ethidium bromide
FAD	flavin-adenine dinucleotide
GFC	gel filtration chromatography
GPx	glutathione peroxidase
GR	glutathione reductase
HBP23	haem-binding protein 23
HEPES	4-(2-hydroxyethyl)-1-piperazineethanesulfonic acid
hORF6	human open reading frame 6
IPTG	isopropyl-beta-D-thiogalactopyranoside
LB	luria broth
Lpd	dihydrolipoamide dehydrogenase
MAD	multiwavelength anomalous diffraction

MOPS	3-(N-Morpholino)propanesulfonic acid
MPD	2-Methyl-2,4-Pentanediol
M _r	molecular weight
MR	molecular replacement
NADH	β-nicotinamide adenine dinucleotide, reduced form
NADPH	β-nicotinamide adenine dinucleotide 2'-phosphate, reduced form
NCS	non-crystallographic symmetry
NMR	nuclear magnetic resonance
NTB	nitrothiobenzoate
PAGE	polyacrylamide gel electrophoresis
PCR	polymerase chain reaction
PDB	protein data bank
PDGF	platelet-derived growth factor
PEG	polyethylene glycol
Prx	peroxiredoxin
RNAi	RNA interference
ROS	reactive oxygen species
SBP	SECIS-binding protein
SDS	sodium dodecyl sulphate
SECIS	selenocysteine insertion sequences
SeCys	selenocysteine
SeMet	selenomethionine
SOD	superoxide dismutase
SRS	synchrotron radiation source
Srx	sulphiredoxin
SucB	dihydrolipoamide succinyltransferase
TAE buffer	tris-acetate-EDTA buffer
TCA	trichloroacetic acid
TNF-α	tumor necrosis factor-alpha

TPxB	thioredoxin peroxidase B
Tris	2-amino-2-(hydroxymethyl)-1,3-propanediol
TRR	thioredoxin reductase
TRR2	mitochondrial thioredoxin reductase
Trx	thioredoxin
Trx2	mitochondrial thioredoxin
TryP	tryparedoxin peroxidase
UTR	untranslated region
UV	ultraviolet
V_e	elution volume
V₀	void volume

Contents

Declaration	
Quotation	
Acknowledgements	
Abstract	
Abbreviations	
Table of contents	

1	CHAPTER 1	5
1.1	OXIDATIVE STRESS	6
1.2	SOD	7
1.3	CATALASE AND GPX	8
1.4	PEROXIREDOXINS (PRXS)	8
1.5	PRX FUNCTION	12
1.6	PRX EVOLUTION AND THE FLOODGATE THEORY	12
1.7	SULPHIREDOXIN (SRX)	15
1.8	MOLECULAR CHAPERONE FUNCTION	15
1.9	PRXIII	18
1.10	THIOREDOXIN (TRX)	19
1.11	THIOREDOXIN REDUCTASE (TRR)	20
1.12	MAMMALIAN SECYS ENZYMES	24
1.13	STRUCTURAL BIOLOGY	25
1.14	X-RAY CRYSTALLOGRAPHY	27
1.15	RESEARCH AIMS	31
2	CHAPTER 2	33
2.1	MOLECULAR BIOLOGY REAGENTS	34
2.1.1	ENZYMES	34
2.1.2	KITS	34
2.1.3	MOLECULAR WEIGHT MARKER	34
2.1.4	SYNTHETIC OLIGONUCLEOTIDES	34
2.1.5	BACTERIAL STRAINS	34

2.1.6	GROWTH OF BACTERIAL CELLS	34
2.1.7	M9 MEDIUM	35
2.1.8	PLASMID VECTORS	35
2.2	MOLECULAR BIOLOGY METHODS	36
2.2.1	POLYMERASE CHAIN REACTION (PCR)	36
2.2.2	RESTRICTION ENDONUCLEASE DIGESTION OF INSERT AND VECTOR DNA	36
2.2.3	DNA GEL ELECTROPHORESIS	37
2.2.4	LIGATION	37
2.2.5	PRODUCTION OF COMPETENT CELLS	37
2.2.6	TRANSFORMATION OF COMPETENT BACTERIA	38
2.2.7	PLASMID PROPAGATION AND PURIFICATION	38
2.2.8	EXPRESSION OF RECOMBINANT PROTEIN IN BACTERIA	38
2.2.9	EXPRESSION OF SEMET PROTEIN IN BACTERIA	39
2.2.10	BACTERIAL CELL LYSIS	39
2.3	MATERIALS FOR PROTEIN PURIFICATION AND ANALYSIS	40
2.3.1	CHEMICALS	40
2.3.2	MOLECULAR WEIGHT MARKERS AND EQUIPMENT	40
2.3.3	SPECTROPHOTOMETRIC EQUIPMENT	41
2.4	PROTEIN METHODS	42
2.4.1	PREPARATION OF THE METAL CHELATE AFFINITY COLUMNS	42
2.4.2	PURIFICATION OF HIS-TAGGED PROTEIN	42
2.4.3	PREPARATION OF BIOCAD PROTEIN FRACTIONS FOR SDS-PAGE	43
2.4.4	SDS-PAGE	43
2.4.5	PROTEIN DIALYSIS AND CONCENTRATION	43
2.4.6	DETERMINATION OF PROTEIN CONCENTRATION	44
2.4.7	ANION EXCHANGE	44
2.4.8	GEL FILTRATION	44
2.4.9	ELLMAN ASSAY FOR THIOLS	45
2.4.10	CLEAVAGE OF HIS-TAG FROM PROTEIN	45
3	CHAPTER 3	46
3.1	INTRODUCTION	47
3.2	RESULTS	50
3.2.1	PRIMERS FOR TRX2	50
3.2.2	PCR AMPLIFICATION OF HUMAN TRX2	50
3.2.3	LIGATION	51

3.2.4	DNA SEQUENCING	51
3.2.5	PROTEIN EXPRESSION OF Trx2	53
3.2.6	PROTEIN SOLUBILITY AND PURIFICATION	53
3.2.7	ESTIMATION OF ACCESSIBLE REACTIVE CYSTEINES IN PURIFIED TRX2	57
3.2.8	CLONING OF TRR2	58
3.2.9	PRIMERS	58
3.2.10	CATALYTIC ACTIVITY OF TRR2	63
3.2.11	OPTIMIZATION OF THE TRR2 ACTIVITY	63
3.3	DISCUSSION	65
3.3.1	CHECKING OF RECOMBINANT CLONES	65
3.3.2	EXPRESSION OF HETEROLOGOUS PROTEINS	65
3.3.3	OVEREXPRESSION OF SOLUBLE ACTIVE RECOMBINANT TRR2 IN <i>E. COLI</i>	66
4	CHAPTER 4	68
4.1	INTRODUCTION	69
4.2	RESULTS	71
4.2.1	RECONSTITUTION OF THE PRXIII PATHWAY	71
4.2.2	BROAD SUBSTRATE SPECIFICITY OF PRXIII	72
4.2.3	EFFECT OF H ₂ O ₂ CONCENTRATION ON OVERALL PRXIII PATHWAY ACTIVITY	73
4.2.4	ANALYSIS OF THE OXIDATION-REDUCTION STATE OF PRXIII	74
4.2.5	ACTIVITY OF THE PRXIII PATHWAY OVER A WIDE RANGE OF H ₂ O ₂ CONCENTRATIONS	77
4.2.6	ROLE OF THE CONSERVED CYSTEINES IN PRXIII PEROXIDASE ACTIVITY	79
4.2.7	GEL FILTRATION ANALYSIS OF THE OLIGOMERIC STATE OF PRXIII	80
4.3	DISCUSSION	82
5	CHAPTER 5	85
5.1	RESULTS	86
5.1.1	PROTEIN PURIFICATION FOR CRYSTALLIZATION	86
5.1.2	SITTING DROP VAPOUR DIFFUSION	86
5.1.3	CRYSTALLIZATION SCREENING	86
5.1.4	CRYSTALLIZATION AND DATA COLLECTION OF NATIVE PRXIII AND ITS MUTANT	88
5.1.5	SEMET PRXIII C168S	95
5.1.6	DATA COLLECTION	96
5.1.7	LOCATING THE SE	101

5.1.8	PHASER	101
5.1.9	MODEL BUILDING AND REFINEMENT	104
5.1.10	SELF-ROTATION FUNCTION	105
5.1.11	THE ANOMALOUS SIGNAL CONTAINED CONTRIBUTION FROM THE SE ATOMS	107
5.2	DISCUSSION	108
6	CHAPTER 6	110
6.1	INTRODUCTION	111
6.2	RESULTS	114
6.2.1	MONOMER STRUCTURE	114
6.2.2	DIMER STRUCTURE	116
6.2.3	DODECAMER STRUCTURE	120
6.2.4	CATENANE STRUCTURE	125
6.3	DISCUSSION	130
7	CHAPTER 7	135
7.1	POSSIBLE MULTIPLE FUNCTIONS OF PRXS	136
7.2	OVEROXIDATION OF PRXIII	137
7.3	PRXIII PATHWAY	137
7.4	SRX AND MOLECULAR CHAPERONE FUNCTION	138
7.5	PRXIII OLIGOMERIZATION	139
7.6	CRYSTAL STRUCTURE OF PRXIII	140
	APPENDIX	143
	REFERENCES	147

Chapter 1

Introduction

1.1 Oxidative stress

Oxidative stress is a term used to describe severe damage to cells, arising from an imbalance in the metabolism of redox-active species. The reduction of O_2 to H_2O requires four electrons. If this happens in 2-electron steps, only H_2O_2 is produced as an intermediate. However, O_2 has a preference for univalent pathways of reduction, resulting in several partially-reduced products of O_2 , the so called reactive oxygen species (ROS). There are three major ROS generated via O_2 reduction: the superoxide anion ($O_2^{\cdot -}$), hydrogen peroxide (H_2O_2) and the hydroxyl radical ($\cdot OH$) (Fig. 1.1). When ROS levels exceed the antioxidant capacity of cells, oxidative stress results. Both $O_2^{\cdot -}$ and $\cdot OH$ are extremely reactive and can cause damage to all the major types of cellular macromolecules, among which the unsaturated lipids, proteins and DNA appear most sensitive. Failure to respond to damage can lead to abnormalities of function and ultimately cell death.

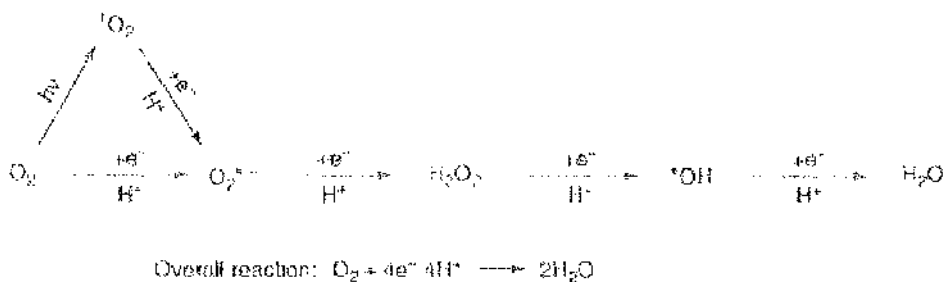


Figure 1.1 Pathways in the univalent reduction of oxygen to water leading to the formation of various intermediate reactive oxygen species (ROS)

Taken from (Scandalios, 2002)

Mitochondria do not only produce ATP, but they also increase the production of ROS as by-products of aerobic metabolism. Most ROS in unstimulated mammalian cells are generated as a result of the univalent reduction of molecular oxygen to $O_2^{\cdot -}$ by electrons that leak from the mitochondrial electron transport chain, mainly from complexes I and III (Boveris and Chance, 1973; Cadenas *et al.*, 1977; Turrens, 1997). As $O_2^{\cdot -}$ is a charged molecule, it cannot cross membranes;

therefore it inhibits mitochondrial function, principally by inactivating the Fe-S centres in the electron transport chain (complexes I, II and III) and the tricarboxylic acid cycle (aconitase) (Wallace, 1999).

Oxidative stress produces reactive oxygen species that damage DNA and most other biological macromolecules. To prevent this kind of damage, living organisms have a series of defence systems involving several antioxidant enzymes, such as superoxide dismutase (SOD) and catalase, as well as the glutathione and thioredoxin systems.

1.2 SOD

SODs are found widely distributed in prokaryotic and eukaryotic cells (Fridovich, 1995). They are an enzyme family that catalyzes the conversion $O_2^{\cdot -}$ to H_2O_2 . Three types of SODs are known in humans. SOD1, or CuZn-SOD, was the first enzyme to be characterized and is a copper and zinc-containing homodimer that is found almost exclusively in intracellular cytoplasmic spaces (McCord and Fridovich, 1969). SOD2, or Mn-SOD, exists as a tetramer and is initially synthesized containing a leader peptide, which targets this manganese-containing enzyme exclusively to the mitochondrial matrix (Chance *et al.*, 1979). SOD3, or EC-SOD is the most recently characterized SOD and exists as a copper and zinc-containing tetramer which is synthesized containing a signal peptide that directs this enzyme exclusively to extracellular spaces (Marklund *et al.*, 1982). The rate of reaction between superoxide anion and nitric oxide was found to be very fast ($2 \times 10^{10} M^{-1}s^{-1}$). Therefore, high levels of SOD are needed to compete for superoxide anions when nitric oxide is present. Evidence has accumulated to show that SOD is involved in a number of diseases and pathologies such as amyotrophic lateral sclerosis (ALS) (Rosen *et al.*, 1993), Down's syndrome (Avraham *et al.*, 1988), and premature aging (Rosenblum *et al.*, 1996).

However, the SOD reaction only partially relieves oxidative stress in mitochondria, since its product, H_2O_2 , is itself a mild oxidant and is readily converted to the more powerful oxidant $\cdot OH$ via the Fenton reaction (Fig 1.2). Intracellular H_2O_2 is removed mostly by catalase, glutathione peroxidase (GPx), and the peroxiredoxins

(Prxs).

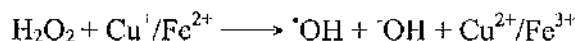


Figure 1.2 The Fenton reaction

1.3 Catalase and GPx

Catalase is a haem-containing enzyme that is located only in peroxisomes and breaks down hydrogen peroxide to water and oxygen. It is believed to remove H_2O_2 that passively diffuses into the organelle or to prevent H_2O_2 leakage (Putnam *et al.*, 2000).

GPx catalyzes the reduction of H_2O_2 and of various organic hydroperoxides with glutathione as the electron donor. There are at least four GPx isoforms in mammalian cells. GPx1 is the major isoform and is expressed in all tissues; it is localized predominantly in the cytosol, but a small proportion (10%) of GPx1 molecules are also present in the matrix of mitochondria (Panfili *et al.*, 1991; Esworthy *et al.*, 1997; Ho *et al.*, 1997; Legault *et al.*, 2000). As catalase is not available in mitochondria in most cell types except in rat myocytes (Radi *et al.*, 1991), GPx1 has been thought to play the major role in the protection of these organelles against oxidative damage by reducing H_2O_2 (Makino *et al.*, 1994; Turrens, 1997; de Haan *et al.*, 1998; Kokoszka *et al.*, 2001). However, homozygous GPx1 knockout mice appear healthy and do not manifest an increased sensitivity to hyperoxia or show an increased content of protein carbonyl groups or lipid peroxides (Ho *et al.*, 1997), suggesting that other antioxidant enzymes are also involved in the protection from ROS.

1.4 Peroxiredoxins (Prxs)

The peroxiredoxins (Prxs) are a ubiquitous family of antioxidant enzymes that regulate intracellular levels of H_2O_2 where they are implicated in both tissue protection against oxidative stress and H_2O_2 -mediated signalling pathways. In recent years, their key role in antioxidant defence has been emphasised by their high abundance in both bacterial and mammalian cells. Prxs can be classified as 1-

Cys or 2-Cys Prxs based on the number of cysteine residues participating in catalysis. There is a further subdivision into two classes called the 'typical' and 'atypical' 2-Cys Prxs based on structural and mechanistic data. This diverse group of antioxidant enzymes is widespread in nature with many organisms producing a number of isoforms, leading to a further division into six subclasses (Wood *et al.*, 2003).

Typical 2-Cys Prxs function as thioredoxin-dependent hydroperoxide reductases and are organised as homodimers in which the adjacent subunits interact in a 'head-to-tail' fashion. During the catalytic cycle, the N-terminal peroxidatic cysteine is oxidised to a cysteine sulphenic acid by its peroxide substrate, which subsequently forms an inter-subunit disulphide bond with the conserved C-terminal resolving cysteine of its partner (Fig 1.3a). The catalytic cycle of typical 2-Cys Prxs was described in a recent review (Wood *et al.*, 2003). Atypical 2-Cys Prxs exist as monomers or dimers and generate an intramolecular disulphide bond during the reaction. Crystal structures have now been reported for 5 atypical 2-Cys, 8 typical 2-Cys and 4 1-Cys Prxs (Table 1). In 5 of the typical 2-Cys structures, the basic dimeric unit is further assembled into decameric rings. In the remaining 2-Cys and 1-Cys Prxs, the structures are monomers or dimers, with two exceptions. Recently an octameric organisation has been reported for a 1-Cys Prx from *Mycobacterium tuberculosis* (Li *et al.*, 2005) and another 2-Cys Prx from the same organism has been shown to exist as a dodecamer (Guimaraes *et al.*, 2005). As the basic functional unit of all Prxs is either a monomer or dimer, the precise relationship between peroxidase activity and the oligomeric state of these enzymes is unclear.

All the typical 2-Cys Prxs show very similar monomer structures with a thioredoxin fold, consisting of a seven stranded β -sheet with parallel and anti-parallel alignments. The sheet is surrounded by four or five α -helices of varying length (Fig 1.3b). Typical 2-Cys Prxs form stable homodimers with the two subunits arranged in a "head-to-tail" fashion. The dimer interface, which has an NCS 2-fold, is created mainly by the formation of an anti-parallel β -sheet (β 7 from each monomer), which produces a 14-stranded, twisted β -sheet running through the centre of the dimer.

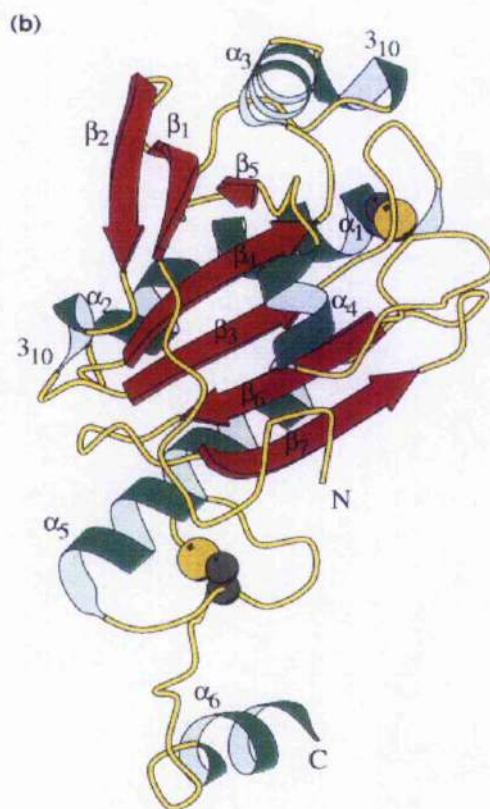
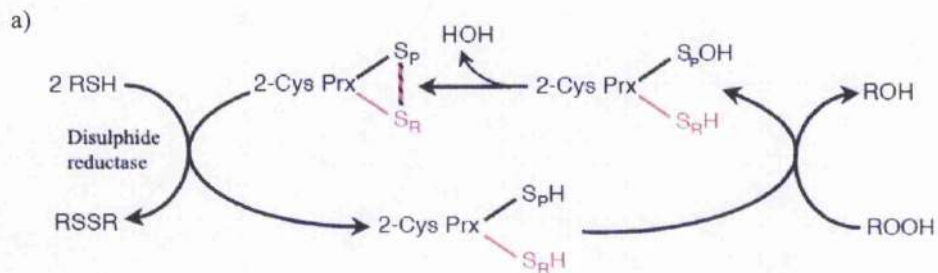


Figure 1.3 Proposed catalytic mechanism and crystal structure of typical 2-Cys peroxidases

a) Peroxidatic cysteines (S_pH) and resolving cysteines (S_RH) in their reduced form. In the case of dimeric 2-Cys Prxs, the black S_p and pink S_R from different subunits condense to form an intersubunit disulphide bond (black and pink striped bar). b) crystal structure of Thioredoxin peroxidase B (TPxB) from red blood cells. Taken from (Schroder *et al.*, 2000).

PDB ID	Res	Prx type	Oligomeric state	Year	Name
1prx	2.0A	1-cys	2	1998	Human open reading frame 6 (hORF6) (Choi <i>et al.</i> , 1998)
1xcc	2.3A	1-cys	2	2004	1-Cys peroxiredoxin from <i>Plasmodium yoelli</i> (To be published)
1xiy	1.8A	1-cys	2	2004	1-Cys peroxiredoxin from <i>Plasmodium falciparum</i> (Sarna <i>et al.</i> , 2005)
1xvw	1.9A	1-cys	8	2004	AhpE from <i>Mycobacterium tuberculosis</i> (Li <i>et al.</i> , 2005)
1hd2	1.5A	atypical	1	2000	Human Prx5 (Declercq <i>et al.</i> , 2001)
1nm3	2.8A	atypical	2	2003	<i>Haemophilus influenzae</i> Hybrid-Prx5 (Kim <i>et al.</i> , 2003)
1psq	2.3A	atypical	2	2003	Probable thiol peroxidase from <i>Streptococcus pneumoniae</i> (To be published)
1qXH	2.2A	atypical	2	2003	Thiol peroxidase from <i>Escherichia coli</i> (Choi <i>et al.</i> , 2003)
1q98	1.9A	atypical	2	2003	Thiol peroxidase from <i>Haemophilus influenzae</i> (To be published)
1e2y	3.2A	typical	10	2000	Tryparedoxin peroxidase from <i>Criethidia fasciculata</i> (Alphey <i>et al.</i> , 2000)
1n8j	2.17A	typical	10	2002	Alkyl hydroperoxide reductase C (AhpC) C46S (Wood <i>et al.</i> , 2003)
1qmv	1.7A	typical	10	1999	Thioredoxin peroxidase B (TPxB) from red blood cells (Schroder <i>et al.</i> , 2000)
1qq2	2.6A	typical	2	1999	Heme-binding protein 23 (HBP23) (Hirotsu <i>et al.</i> , 1999)
1tp9	1.62A	typical	2	2004	Prx D (Type II) from <i>Populus tremula</i> (Echalier <i>et al.</i> , 2005)
1uul	2.8A	typical	10	2003	Tryparedoxin peroxidase from <i>Trypanosoma cruzi</i> (Pineyro <i>et al.</i> , 2005)
1vgs	2.31A	typical	10	2004	Peroxiredoxin from <i>Aeropyrum pernix K1</i> (Mizohata <i>et al.</i> , 2005)
1we0	2.9A	typical	10	2004	AhpC from <i>Amphibacillus xylanus</i> (Kitano <i>et al.</i> , 2005)
2bmx	2.4A	typical	12	2005	AhpC from <i>Mycobacterium tuberculosis</i> (Guimaraes <i>et al.</i> , 2005)

Table 1.1 Peroxiredoxin crystal structures

1.5 Prx function

Apart from their antioxidant functions, resulting from their ability to regulate levels of hydrogen peroxide, Prxs have also been implicated in peroxide-mediated signalling cascades (Fujii and Ikeda, 2002). Prxs are associated with diverse cellular functions, such as regulation of NF- κ B activation (Kang *et al.*, 1998); they can reduce intracellular hydrogen peroxide induced by p53 (Wong *et al.*, 2000), epidermal growth factor (Wong *et al.*, 2000) and tumor necrosis factor- α (Kang *et al.*, 1998). Although compared to catalase or GPx, Prxs are thought to have moderate catalytic efficiencies, it is Prxs, but not GPx or catalase, which are reported to be negative regulators of PDGF signaling (Choi *et al.*, 2005). Bacterial Prxs are also found to have peroxynitrite reductase activity (Bryk *et al.*, 2000).

In *Mycobacterium tuberculosis* (Mtb), dihydrolipoamide dehydrogenase (Lpd) and dihydrolipoamide succinyltransferase (SucB) are components of the 2-oxoacid dehydrogenase complexes which play a very important role in metabolism. In these organisms the peroxiredoxin AhpC removes H₂O₂ in a system which lacks thioredoxin. Instead, AhpC is reduced by NADH via Lpd and SucB by a thioredoxin-like adaptor protein, AhpD (Bryk *et al.*, 2002). This interaction between antioxidant and metabolic pathways is unique and may provide important insights into the physiological roles of mitochondrial Prxs.

1.6 Prx evolution and the floodgate theory

The 2-Cys Prxs were originally identified as antioxidant enzymes but there is increasing evidence that they play important roles in H₂O₂-mediated cell signaling as well.

The yeast *Saccharomyces cerevisiae* has at least five Prxs that have partially overlapping functions in detoxifying peroxides. In mammalian cells, Prxs typically constitute 0.1 to 0.8% of the total soluble protein of the cell (Chae *et al.*, 1999). Many organisms produce more than one Prx isoform. The abundance of Prxs may partly relate to their moderate catalytic proficiency; however, Prxs have received a great deal of attention recently owing to their role in regulating levels of hydrogen peroxide, an intracellular signaling molecule common to many cytokine-induced

signal-transduction pathways (Hofmann *et al.*, 2002).

Wood *et al.* (Wood *et al.*, 2003) found that bacterial 2-Cys Prxs are much less sensitive to oxidative inactivation than are eukaryotic 2-Cys Prxs. In bacteria, peroxiredoxins appear to be required only to protect against ROS. For example, in *Escherichia coli*, the abundant peroxiredoxin AhpC is the primary scavenger of H₂O₂, generated during aerobic metabolism, and also detoxifies alkyl hydroperoxides. Recent *in vivo* studies show that human PrxI and PrxII are inactivated under conditions of peroxide signaling (Rabilloud *et al.*, 2002; Koshkin *et al.*, 2003) by irreversible over-oxidation of the peroxidatic cysteine to sulphinic acid (Cys-SO₂H) at a low steady-state level (<1 μM) of H₂O₂. Wood *et al.* (2003) concluded that the sensitivity of 2-Cys Prxs to inactivation by over-oxidation is not a limitation of the 2-Cys Prx catalytic mechanism; rather it is a feature that has been selected for during the evolution of eukaryotes. This additional property of mammalian 2-Cys Prxs has led to the development of the floodgate model (Fig 1.4). The activity of some Prxs also been shown to be regulated by phosphorylation (Chang *et al.*, 2002).

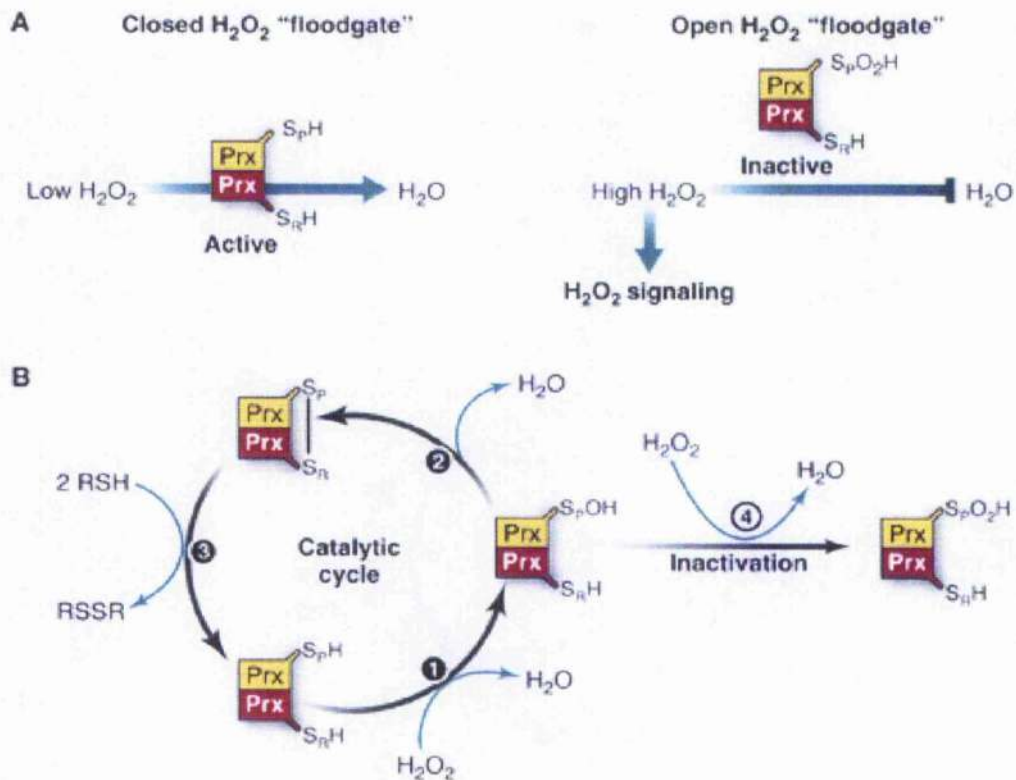


Figure 1.4 A floodgate model for Prx-mediated regulating intracellular H_2O_2 levels

(A) The floodgate model of peroxiredoxin (Prx) regulate H_2O_2 signaling. At low H_2O_2 concentrations, active peroxiredoxin catalyzes the reduction of H_2O_2 to H_2O , preventing signaling. High H_2O_2 concentrations result in overoxidation of peroxiredoxin, thus preventing the reduction of H_2O_2 and allowing it to participate in signaling. (B) The peroxiredoxin catalytic cycle. (1) Oxidation of the peroxidatic cysteine (S_p) to sulphenic acid by H_2O_2 . (2) Attack of the sulphenic acid by the thiol group of the resolving cysteine (S_r) results in the formation of a disulphide bond. (3) Reduction of the disulphide bond by an external thiol-reducing agent such as thioredoxin. Other processes that involve the peroxiredoxin catalytic site are (4) inactivation of peroxiredoxin by overoxidation of the peroxidatic cysteine from sulphenic acid to sulphinic acid. Adapted from (Georgiou and Masip, 2003)

1.7 Sulphiredoxin (Srx)

Srx is a new member of the antioxidant family in eukaryotes, first identified in yeast. Srx contains a C-terminal cysteine residue that is conserved in all family members. Studies with the yeast and human homologue show this residue is critical for its antioxidant function (Biteau *et al.*, 2003). Inactivated Prxs, caused by cysteine over-oxidation to cysteine sulphinic acid, can be reduced by Srx and ATP, although this over-oxidation was previously thought to be irreversible. A recent study on the molecular mechanism of the reduction of cysteine sulphinic acid of peroxiredoxin to cysteine by mammalian sulphiredoxin reveals that the presence of the sulphinic form (but not the reduced form) of PrxI induces phosphorylation of the conserved cysteine of Srx and then the phosphate is immediately transferred to the sulphinic moiety of PrxI to generate a sulphinic acid phosphoryl ester [Prx-Cys-SOOP₃]²⁻. This ester is reductively cleaved by a thiol molecule (RSH) such as GSH, thioredoxin and DTT to produce a disulphide-S-monoxide [Prx-Cys-S(=O)-S-R]. The disulphide-S-monoxide is further reduced through the oxidation of three thiol equivalents to complete the catalytic cycle and regenerate Prx-Cys-SH (Jeong *et al.*, 2006). Interestingly, Srx is not found in prokaryotes. This could be because Srx is involved in the restoration of over-oxidized Prxs, whose counterparts in prokaryotes are not sensitive to oxidative inactivation as reported by Wood *et al.* (2003). This may suggest that Prx inactivation and recovery by Srx has been selected for during evolution (Biteau *et al.*, 2003).

1.8 Molecular Chaperone Function

Cytosolic PrxI and PrxII are found to be responsible for yeast survival during heat shock although the ability of cytosolic PrxI to protect the cells lacking PrxI/II from heat shock is not exclusively due to its peroxidase activity (Jang *et al.*, 2004). Jang *et al.* also find that heat shock and oxidative stress induce a structural change in PrxI which results in a functional switch from a peroxidase to a molecular chaperone *in vitro*. They have developed a new model taking into account these additional observations (Fig 1.5). At low ROS concentrations, Prxs form mainly low molecular weight species (dimers or oligomers) with peroxidase activity that remove low levels of ROS and regulate H₂O₂ signaling. However, when yeast are placed under extreme conditions like heat shock or oxidative stress, the

peroxidized cysteine is overoxidized to cysteine sulfinic acid (-SO₂H) and acts as a highly efficient "H₂O₂-sensor" with the help of the Trx system. The overoxidized 2-Cys Prxs then multimerize into a high molecular weight super-chaperone complex. That is postulated to aid cell survival under stress conditions. After oxidative stress, the Cys-sulphinic acid is reduced to Cys-SH by Srx in the presence of ATP and the high molecular weight complex gradually dissociates into low molecular weight species, thus restoring peroxidase activity. The molecular mechanisms by which Prxs function as chaperones are unclear at present as these recent data demonstrate solely that Prxs can enhance yeast survival under stress conditions.

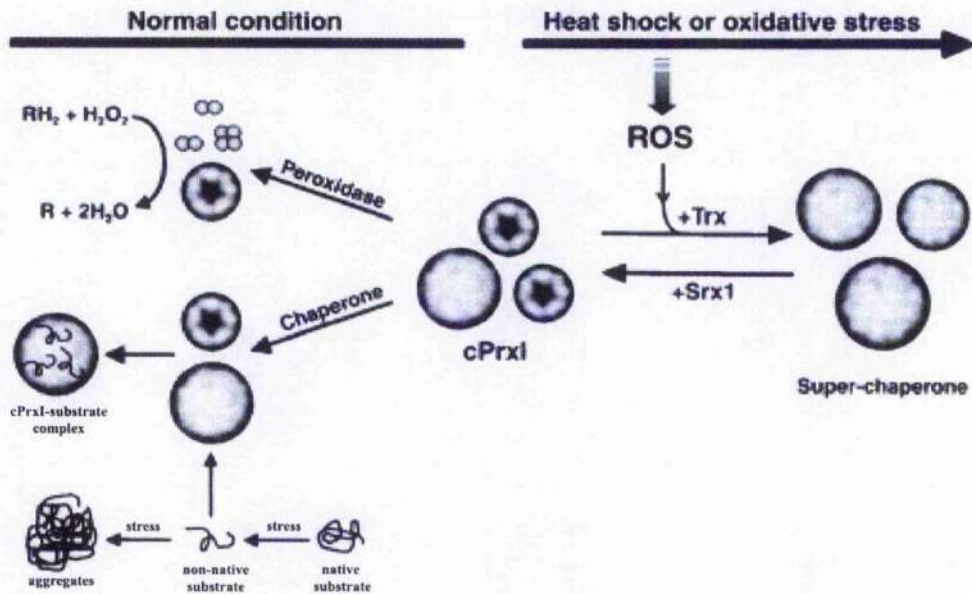


Figure 1.5 A Model of the Heat Shock or Oxidative Stress-Dependent Structural and Functional Switching of cPrxI from a Peroxidase to a Molecular Chaperone

In normally growing cells, cPrxI exhibits both peroxidase and chaperone activity with a mixture of different oligomeric states. However, during heat shock or oxidative stress, Prxs are overoxidised and shift to a high molecular weight state with the help of the Trx system to act as super-chaperones. Srx1 is essential for the dissociation of complexes into low molecular weight protein species. Taken from (Jang *et al.*, 2004).

1.9 PrxIII

PrxIII (also called SP-22) is a small (22kDa) mitochondrial protein that was originally isolated from bovine adrenal cortex as a substrate protein for a mitochondrial ATP-dependent protease (Watabe *et al.*, 1994; Watabe *et al.*, 1995). Analysis of its amino acid sequence revealed that PrxIII is a member of the Prx family and belongs to the typical 2-Cys PrxIII subclass. Among the members of this family, PrxIII is the only protein specifically located in mitochondria. PrxV, an atypical 2-Cys Prx, is localized intracellularly to mitochondria but also to cytosol and peroxisomes (Seo *et al.*, 2000). Owing to the limited study of PrxIII at present, its exact physiological function *in vivo* and the biochemical mechanisms involved remain to be fully concluded. However PrxIII has been demonstrated to protect several free-radical sensitive enzymes from oxidative damage *in vitro* (Watabe *et al.*, 1997). *In vivo*, current results indicate that PrxIII plays a crucial role in the antioxidant defence mechanism of mitochondria in the cardiovascular system (Araki *et al.*, 1999) and is also found to protect hippocampal neurons from excitotoxic injury (Hattori *et al.*, 2003).

A recent RNAi study in HeLa cells suggests PrxIII depletion promotes increased intracellular levels of H₂O₂ and sensitizes cells to induction of apoptosis by staurosporine or TNF- α (Chang *et al.*, 2004). The authors conclude that PrxIII is a critical regulator of the abundance of mitochondrial H₂O₂, which itself induces apoptosis with other mediators of apoptotic signaling.

The amino acid sequence of PrxIII has been determined, in both its precursor and mature forms (Iliroi *et al.*, 1996). PrxIII has a 62 amino acid long mitochondrial targeting presequence. By comparison with other 2-Cys Prxs, PrxIII also contains the conserved peroxidatic cysteine (C47), the resolving cysteine (C168) and a third cysteine residue C66.

The specific localization of Prx III in mitochondria (Araki *et al.*, 1999) together with the identification of its mitochondrial-specific electron suppliers, thioredoxin 2 (Trx2) and thioredoxin reductase 2 (TRR2) (Spyrou *et al.*, 1997; Lee *et al.*, 1999), suggest that these three proteins might cooperate to provide a primary line of defence against H₂O₂ produced by the mitochondrial respiratory chain (Miranda-

Vizuete *et al.*, 2000; Pedrajas *et al.*, 2000). Moreover, it has been shown that PrxIII is 30-fold more abundant in the mitochondria of HeLa cells than is GPx1 and is a critical regulator of the mitochondrial H₂O₂ concentration, in contrast to the widely held view that GPx1 is the only important H₂O₂-metabolizing enzyme in mitochondria (Turrens, 1997; de Haan *et al.*, 1998; Kokoszka *et al.*, 2001).

Transmission electron microscopy has shown that bovine PrxIII exists as an oligomeric ring, with external and internal diameters of 150 and 70 Å, respectively (Gourlay *et al.*, 2003). The size of the ring is larger than other typical 2-Cys Prxs that exist as decamers.

1.10 Thioredoxin (Trx)

Thioredoxins are a family of proteins containing a conserved catalytic site (-Trp-Cys-Gly-Pro-Cys-Lys-) that undergoes reversible oxidation to the cysteine disulphide through the transfer of reducing equivalents from cysteine residues to a disulphide substrate (X-S₂). The oxidized thioredoxin is then reconverted back to its reduced form by an NADPH-dependent thioredoxin reductase.

Human Trx1 is a small, compact protein (104 amino acids) with a M_r value of 12 kDa (Deiss and Kimchi, 1991). A slightly larger form was first identified in pig heart mitochondria (Bodenstein and Follmann, 1991). This second Trx, Trx2, was cloned from a rat heart library and contained a putative 60 amino acid long N-terminal mitochondrial targeting signal. Including the leader sequence, Trx2 is synthesised initially as a 166 amino acid, 18 kDa precursor protein containing the conserved Trx catalytic site but lacking the other Cys residues found in mammalian Trx1 (Spyrou *et al.*, 1997).

The molecular basis for the reducing action of Trx is that substrate X-S₂ binds to a conserved hydrophobic surface and in the hydrophobic environment of the complex, the thiolate of Cys31 acting as a nucleophile, combines with the protein substrate to form a covalently linked mixed disulphide (-Cys31-S-S-protein). Finally, the now deprotonated Cys34 attacks the -Cys31-S-S-protein disulphide bond, releasing the reduced protein substrate and forming a Cys31-Cys34 disulphide bond in Trx, which is then reduced by thioredoxin reductase (Holmgren,

1995).

Although Trx1 forms homodimers in solution and in the crystal structure (Weichsel *et al.*, 1996), it is not yet clear if dimer formation occurs under physiological conditions. The crystal structure of Trx2 shows that the folding of Trx2 is similar to that of human Trx1 and dimerization still occurs in the crystal structure mainly mediated by hydrophobic contacts (Fig 1.6a) (Smeets *et al.*, 2005).

The physiological roles of Trxs in different organisms range from a common fundamental reaction to a series of different specialized functions. Their primary highly conserved role is as a high-capacity hydrogen donor system for reductive enzymes to highly specialized functions such as forming a complex with apoptosis signal-regulating kinase 1 preventing downstream signalling for apoptosis (Saitoh *et al.*, 1998). Trxs are also implicated in the onset and progression for a number of human diseases including cancer, viral infection, ischaemia-reperfusion injury, aging and cardiac conditions (Burke-Gaffney *et al.*, 2005). Studies on Trx2 are limited but Trx2 has been shown to interact with specific components of the mitochondrial respiratory chain, play a key role in the regulation of the mitochondrial membrane potential (Damdimopoulos *et al.*, 2002) and also in protection against peroxide-induced apoptosis (Chen *et al.*, 2002).

1.11 Thioredoxin reductase (TRR)

Thioredoxin reductase is the only enzyme that is known to be able to reduce the active site of thioredoxin with the use of electrons from NADPH (Tamura and Stadtman, 1996). It belongs to a superfamily of flavoprotein disulphide oxidoreductases that includes glutathione reductase (GR), dihydrolipoamide dehydrogenase, mercuric reductase and alkylhydroperoxide reductase (Russel and Model, 1988). Mammalian TRR is distinct from those of prokaryotes and yeast. The mammalian enzyme exhibits a broader substrate specificity, having the ability to reduce chemically unrelated compounds and is larger in subunit size (58 kDa, compared with 35 kDa for the prokaryote and yeast enzymes), as it contains a much longer C-terminal region (Gasdaska *et al.*, 1995; Zhong *et al.*, 1998). In addition, mammalian TRR is a selenoprotein that contains a penultimate

selenocysteine (SeCys) residue in the sequence –Gly-Cys-SeCys-Gly (Stadtman, 1996; Tamura and Stadtman, 1996), which serves as a redox centre (Arscott *et al.*, 1997).

Two full-length human thioredoxin reductases have been cloned, a 54.4 kDa thioredoxin reductase-1, which is predominantly in the cytosol (Gasdaska *et al.*, 1995), and a 56.2 kDa thioredoxin reductase-2, which has a 33-amino-acid N-terminal extension identified as a mitochondrial import sequence (Lee *et al.*, 1999). A third, incomplete thioredoxin reductase sequence has been reported (Pedrajas *et al.*, 1999). The overall structure of the SeCys498Cys mutant of rat TRR1 is similar to that of glutathione reductase (GR), including conserved amino acid residues binding the cofactors FAD and NADPH with the two subunits in a head-to-tail arrangement (Fig 1.6b) (Sandalova *et al.*, 2001). The electrons are first transferred from NADPH to FAD and then the C-terminal selenocynylsulphide bond from the adjacent subunit is reduced by FAD. At this stage the Cys-SeCys acts as a second redox centre in which the electrons are transferred from this redox-active selenosulphide to the substrate Trx (Fig 1.7) (Zhong *et al.*, 1998; Zhong *et al.*, 2000). Mutagenesis of TRR1 in which SeCys is replaced by Cys shows that the TRR1 mutant lacks hydroperoxidase activity. Therefore selenium is required for catalytic activity. TRR1 is also involved in many aspects of cellular redox regulation (Sun and Gladyshev, 2002). It is capable of inducing apoptosis if the enzyme does not contain selenocysteine or if this residue is blocked by chemotherapeutic agents (Anestal and Arner, 2003). A TRR2 mouse knockout study shows an essential role for TRR2 in hematopoiesis, heart development, and heart function (Conrad *et al.*, 2004). In this study also, cardiac tissue-restricted ablation of TRR2 results in fatal dilated cardiomyopathy, a condition reminiscent of that observed in Keshan disease and Friedreich's ataxia.

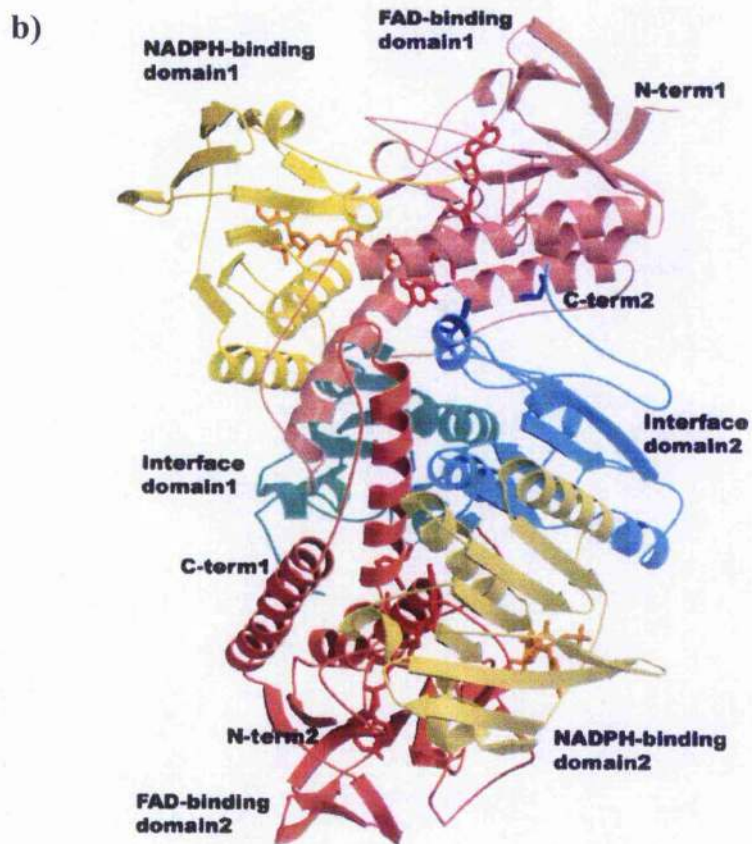
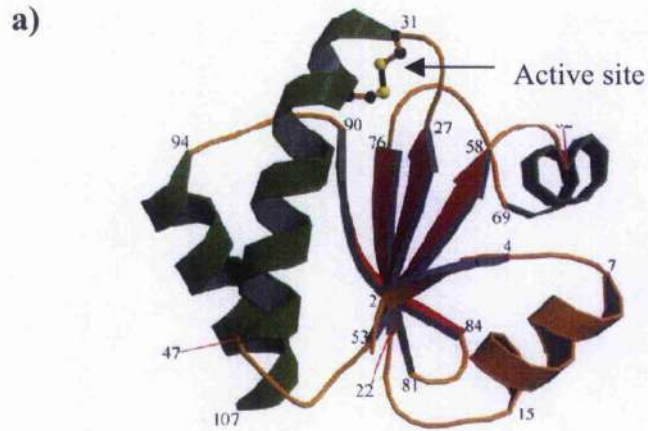


Figure 1.6 Crystal Structure of (a) human Trx2 and (b) rat TRR1 SeCys498Cys

Taken from (Biterova *et al.*, 2005) and (Zhong *et al.*, 2000).

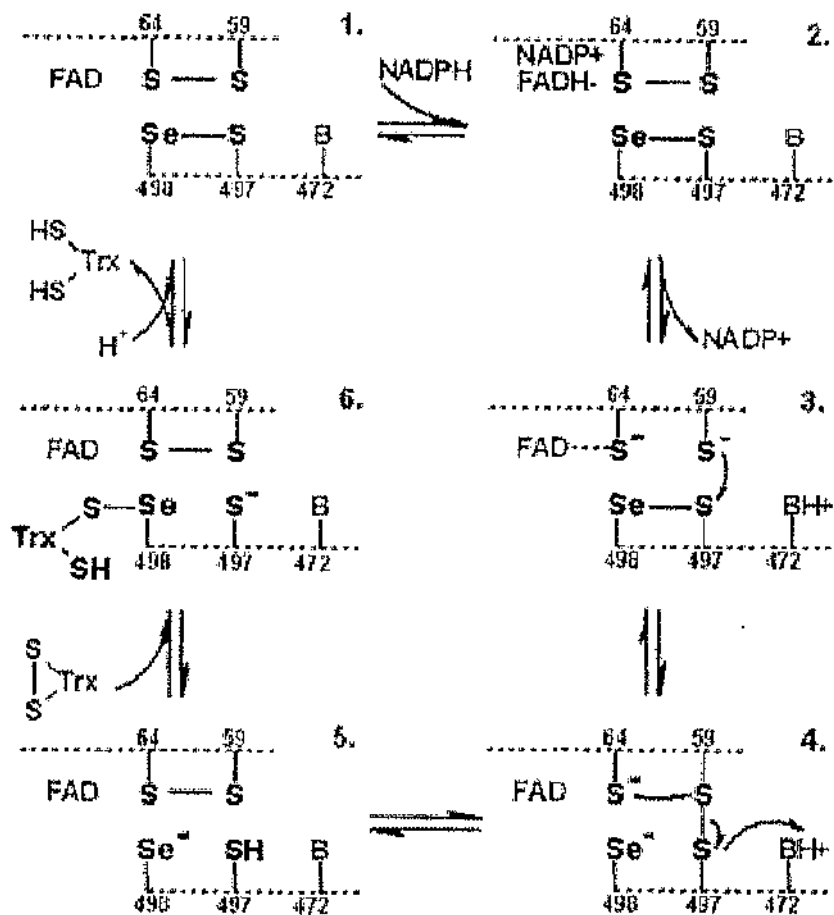


Figure 1.7 Postulated reaction mechanism for mammalian TRR
 The upper part of each figure shows a FAD centre and the lower part shows the Cys-SeCys redox centre from adjacent subunit. Taken from (Zhong *et al.*, 2000).

1.12 Mammalian SeCys enzymes

Although most derivatives are toxic, selenium is recognized as an essential trace element for health. It is incorporated into proteins to make selenoproteins, most of which are important antioxidant enzymes. After glutathione peroxidase (Rotruck *et al.*, 1973), the first specific mammalian selenoprotein discovered, it has been estimated that there are 25 human selenoproteins through genomic analysis (Kryukov *et al.*, 2003). Until now, only two types of seleno amino acids have been found in proteins, selenomethionine (SeMet) and selenocysteine (SeCys). However, in normal cellular metabolism methionine and selenomethionine are essentially treated equally (Birringer *et al.*, 2002). Due to the unselective nature of selenomethionine incorporation, the physiological relevance of SeMet is still unknown. On the other hand, UGA, normally interpreted as a stop codon, is also the codon for the 21st amino acid, selenocysteine, with additional signals. Unlike SeMet, SeCys is incorporated specifically into proteins. In mammalian cells, it is incorporated into SeCys proteins by a translational recoding event at specific UGA codons. These are found upstream of stable stem-loop structures known as SeCys insertion sequences (SECIS) that reside in the 3'-untranslated region (UTR). A minimum distance of 58-111 nucleotides up to a maximum of 5.4 kb in an extreme case (Buettner *et al.*, 1998), has been identified between the SECIS and its cognate upstream SeCys-encoding UGA (Low and Berry, 1996; Grundner-Culemann *et al.*, 1999). While the UGA codon and the SECIS element are the only known *cis*-acting elements required for SeCys incorporation, at least three *trans*-acting factors are also required: 1) the SeCys-specific elongation factor (EFSeCys), 2) a SECIS-binding protein (SBP2), and 3) the tRNA^{SeCys}. Our understanding of the mechanism of SeCys incorporation into polypeptides is still not totally clear.

Both selenium and sulphur are members of the Group VI elements and hence have similar properties. However, the redox potential of selenium compounds is lower compared to their respective sulphur-containing equivalents. Furthermore, selenium compounds are generally more reactive (Huber and Criddle, 1967). Studies have shown that selenoenzymes use SeCys because it expands the metabolic capacity of enzymes in terms of activity toward a wider variety of substrates and over a broader range of pH (Gromer *et al.*, 2003).

Selenoenzymes have long been known to play important roles in protection from oxidative stress and the damaging effects of reactive oxygen species. The glutathione peroxidases, the best characterized family of selenoenzymes, were originally thought to be solely responsible for anti-oxidative defence. Many studies show that overexpression of GPx-1 can protect cells against reactive oxidative species, for example, damage caused by hydrogen peroxide and lipid hydroperoxides and redox cycling compounds such as paraquat (Taylor *et al.*, 1993). However, overexpression of GPx-1 can also inhibit hydrogen peroxide-induced apoptosis in cell lines (Laskowski *et al.*, 1993). By using alternative splice sites, GPx4 can generate mitochondrial and cytoplasmic isoforms. GPx4 also exhibits the broadest substrate specificity of all glutathione peroxidases and can even reduce phospholipid hydroperoxides. It is also capable of reducing hydrogen peroxide still present in membranes and may thus play a role as a universal antioxidant in the protection of biomembranes (Ursini *et al.*, 1985). GPx4 is also involved in redox signaling and regulatory processes, such as inhibiting lipoxygenases and apoptosis (Brigelius-Flohe, 1999).

Defects in selenoproteins are also implicated in a few diseases. The most prominent examples in humans are Keshan disease, a dilatative cardiomyopathy primarily affecting children (Ge *et al.*, 1983), and Kashin-Beck disease, a disabling chondronecrosis (Peng *et al.*, 2000).

1.13 Structural Biology

Currently, electron microscopy and small angle scattering are used to obtain low-resolution structural information. Although the resolution is relatively low (10-25Å), these techniques give valuable information about large protein complexes and, in combination with high-resolution data, provide us with a comprehensive picture of how proteins interact with each other in multi-component complexes.

To obtain detailed structural information on a protein of interest, high-resolution data are needed. X-ray crystallography and NMR spectroscopy are the two techniques of choice for solving high-resolution structures of macromolecules. X-

ray crystallography is the traditional approach that gives the best resolution. However, a major rate limiting step is often the production of good quality crystals. NMR spectroscopy does not give as high resolution as X-ray crystallography; moreover, the protein must be relatively small (normally less than 50 kDa). NMR has its own advantages as structures are determined in solution, which may be closer to normal physiological conditions. In addition, mobile loops of the protein can be “seen” by NMR whereas they are normally not sufficiently ordered to be visualised in crystallography.

The Protein Data Bank (PDB) is the single worldwide repository for the processing and distribution of 3-D structural data relating to large molecules, namely proteins and nucleic acids. Every year the number of deposited structures in the PDB is increasing dramatically, especially in the past ten years (Appendix I). The vast majority of structures of biological macromolecules have been determined by protein crystallography. There are several factors contributing to the success of this approach. Firstly, recombinant DNA methods have made it possible to clone, express and purify large quantities of the majority of biological macromolecules. Secondly, rapid and improved automated methods are introduced each year. In addition, synchrotrons provide intense sources of X-rays, while new detectors allow rapid data collection. Thirdly, new and powerful software for crystal structure determination as well as cheaper and more powerful computers have also reduced the time for data processing and analysis. With these advantages, not only the number of structures, but also the complexity of structures in the PDB is increasing rapidly (Appendix II). Therefore, the focus of structural biology is gradually moving towards the analysis of macromolecular interactions in the cell, including attempts to capture the dynamic nature and high precision of localized interactions, as well as the involvement of multiple ligands.

1.14 X-ray Crystallography

A well-ordered crystal that will diffract X-rays strongly is the first requirement for solving the three-dimensional structure of a protein by X-ray crystallography. After that an X-ray beam will interact with the crystal, which is a regular, repeating array of many identical molecules, so that the X-rays are diffracted from it in a diffraction pattern, from which the structure of an individual molecule can be retrieved. The repeating unit forming the crystal is called the unit cell. Each unit cell may contain one or more molecules.

There are several techniques for setting up crystallization experiments including sitting drop vapour diffusion, hanging drop vapour diffusion, sandwich drop, batch, microbatch, under oil, microdialysis, and free interface diffusion. Sitting and hanging drop methodologies are most popular because they are easy to perform, require a small amount of sample, and allow a large amount of flexibility during screening and optimization.

Using the sitting drop technique (Fig 1.10), a small (0.5 to 20 μ l) droplet of the sample is mixed with crystallization reagent on a platform in vapour equilibrium with the reagent such that the initial reagent concentration in the droplet is less than that in the reservoir. Over time the reservoir will remove water from the droplet in the vapour phase until equilibrium is reached between the drop and the reservoir. During this equilibration process the protein is concentrated, increasing the relative supersaturation of the protein in the drop. The advantages of the sitting drop technique are that it is convenient and simple to use. The disadvantages are that crystals can sometimes stick to the sitting drop surface which makes "looping out" of crystals difficult. The sitting drop technique is a good routine choice for screening and optimization.

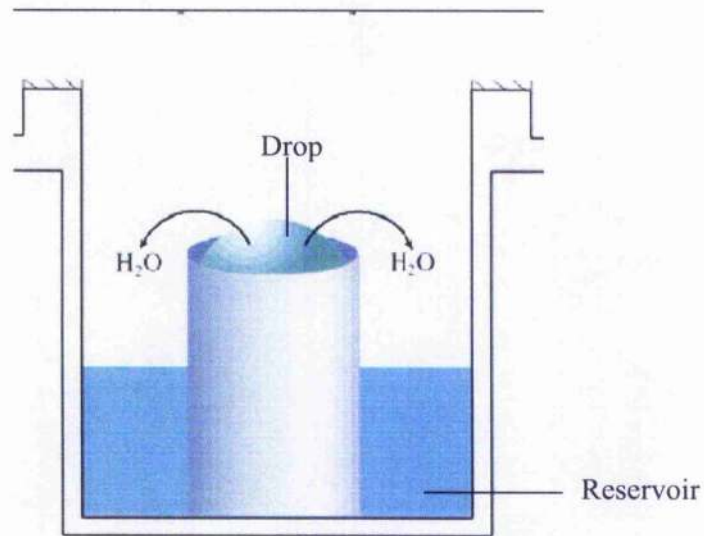
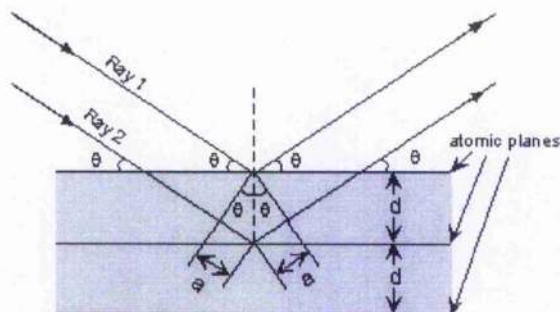


Figure 1.10 Sitting drop crystallization technique

When an X-ray beam hits the crystal, most of the X-rays travel straight through it. Some, however, interact with the electrons on each atom and cause them to oscillate. The oscillating electrons serve as a new source of X-rays which are emitted in almost all directions as scattering. X-ray scattering from a single molecule would be unimaginably weak and could never be detected above the noise level, which would include scattering from air and water. A crystal arranges huge numbers of molecules in the same orientation, so that scattered waves can add up in phase and raise the signal to a measurable level. In a sense, a crystal acts as an amplifier. Diffraction by a crystal can be regarded as the reflection of the primary beam by sets of parallel planes. The relationship between the reflection angle, θ , the distance between the planes, d , and the wavelength, λ , is given by Bragg's law (Fig 1.11).



$$2d \sin\theta = n\lambda$$

Figure 1.11 Bragg's Law

A set of parallel planes with interplanar spacing, d , produces a diffracted beam when X-rays of wavelength λ impinge on the planes at an angle θ and are reflected at the same angle. If the difference in path length (that is $2a$, also $2d \sin\theta$) for Ray1 and Ray2 from successive planes is equal to an integral number of wavelengths of the X-rays ($n\lambda$), then they will produce a strong diffracted beam.

Each atom in a crystal scatters X-rays in all directions, and only those that positively interfere with one another, according to Bragg's law, give rise to diffracted beams that can be recorded as a distinct diffraction spot above background. Each diffraction spot is the result of interference of all X-rays with the same diffraction angle emerging from all atoms. To extract information about individual atoms from such a system Fourier transform analysis is employed. Each diffracted beam, which is recorded as a spot on the detector, is defined by two properties: the amplitude, which can be measured from intensity of the spot; and the phase, which is "lost" in X-ray experiments. Both properties for all of the diffracted beams have to be known to determine the position of the atoms. This is the so-called phase problem in X-ray crystallography. There are quite a few methods available now for solving the phase problem.

When identical or similar structures exist in different crystallographic environments, similarities between their diffraction patterns, which are directly related to their Fourier transforms, would be expected. The technique of Molecular Replacement (MR) uses this similarity to determine phases. Molecular replacement

is usually a two-step process. Firstly, the orientation of the search model is found from the rotation function and then, the position of the search model is found using the translation function. In recent years with access to more and more powerful computers, some programs like PHASER employing maximum likelihood methods have made it possible to obtain large scale improvement in relatively poor datasets.

Phase information can also be obtained by multiwavelength anomalous diffraction (MAD) experiments. For certain X-ray wavelengths, the interaction between the X-rays and electrons of an atom causes the electrons to absorb the energy of the X-ray. This causes a change in the X-ray scattering of the atom, called anomalous scattering. The intensity differences obtained in the diffraction pattern by illuminating such a crystal with X-rays of different wavelengths can be used to obtain the phases of the diffracted beams. The MAD method requires access to synchrotron radiation since different wavelengths are used.

The amplitudes and the phases of the diffraction data from the protein crystals are used to calculate an electron-density map of the repeating unit of the crystal. This map then has to be interpreted as a polypeptide chain with a particular amino acid sequence. The quality of the map depends on the resolution of the diffraction data, which in turn depends on the degree of order in the original crystals. The initial model will contain errors, which can be subsequently removed by crystallographic refinement of the model. In this process the model is changed to minimize the difference between the experimentally observed diffraction amplitudes and those calculated for a hypothetical crystal containing the model instead of the real molecule. This difference is expressed as an R factor, residual disagreement, which is 0 for exact agreement and around 0.6 for total disagreement. In general R factors should be between 0.15 and 0.20 for a well-determined protein structure but also depends on resolution, number of reflections, the refinement and other parameters. In refined structures at high resolution there should be no major errors in the positions of all atoms.

1.15 Research Aims

The major goals of this research programme were (a) to obtain a detailed picture of the mitochondrial antioxidant defence pathway involving PrxIII; (b) to study the properties of the reconstituted pathway in detail and analyse the effect of various point mutations in its key enzyme and (c) to conduct detailed structure (X-ray crystallographic) studies on PrxIII.

Initial research was directed towards the cloning and expression of the human mitochondrial isoforms of thioredoxin, Trx2 and thioredoxin reductase, TRR2 in high yields to facilitate their purification in sufficient quantities to permit the reconstruction of the complete, 3-component antioxidant pathway *in vitro*. This was successfully achieved as described in chapter 3 although overexpression of active, SeCys-containing TRR2 required the insertion of a selenocysteine insert sequence (SECIS) at the 3'-end of the open reading frame. The presence of the SECIS is required for promote incorporation of a SeCys residue at the appropriate UGA codon which normally functions in termination of translation. A number of other genetic tricks were also employed to optimise the expression of active, soluble TRR2.

In chapter 4, the successful reconstitution of the PrxIII pathway is described and the pathway is characterised with respect to its substrate specificity, H₂O₂ concentration dependence and susceptibility to inactivation by overoxidation. The oxidation of PrxIII and the appearance of abnormal oxidation states was also detected by SDS-PAGE. Finally, the protein concentration, redox state dependence and the influence of the N-terminal His-tag on the stability of the toroidal form of PrxIII was also investigated.

Comprehensive crystallographic trials were conducted on wild-type PrxIII and various active-site mutants. However, only the C168S mutant produced well-ordered crystals that were employed subsequently to solve a 3-D structure of this enzyme to 3.3 Å as described in chapter 5. A number of difficulties were encountered during the data processing so several different approaches and a variety of programs were employed before a final solution could be obtained.

In Chapter 6, the remarkable subunit organisation of PrxIII was analysed in detail and compared to other Prxs structures. A model is proposed which accounts for the tendency of PrxIII to assemble into a 2-ring catenane.

Chapter 2

Materials and Methods

2.1 Molecular biology reagents

2.1.1 Enzymes

Restriction endonucleases and calf intestinal alkaline phosphatase (CIAP) were purchased from Roche. T4 DNA ligase and *Pfu* DNA polymerase were purchased from Promega.

2.1.2 Kits

Wizard® Plus Mini Preps purification system was purchased from Promega. The QIAchange Gel extraction kit was purchased from QIAGEN.

2.1.3 Molecular weight marker

The 1kb DNA Step Ladder, supplied with Blue/Orange Loading Dye (6X) was purchased from Promega.

2.1.4 Synthetic oligonucleotides

Primers for gene amplification by Polymerase Chain Reaction (PCR) were designed in house and synthesized by Sigma (25 mmole scale).

2.1.5 Bacterial strains

Escherichia coli DH5 α (Stratagene, Amsterdam, The Netherlands) and *Escherichia coli* BL21 (DE3) pLysS and BL21 (DE3) CodonPlus (Novagen, Nottingham, UK) bacterial strains were used for propagation of plasmid vectors and the expression of recombinant proteins employing the pET vector system, respectively. *E. coli* M15 cells were used for expression of recombinant protein employing the pQE vector system.

2.1.6 Growth of bacterial cells

Luria Broth (LB) (1% (w/v) bacto-tryptone, 1% (w/v) NaCl, 0.5% (w/v) yeast extract, pH 7.2) or LB/agar plates (LB containing 1.5% (w/v) agar) were the

growth media of choice for most bacterial strains. When appropriate, media were supplemented with ampicillin (50 μ g/ml), kanamycin (30 μ g/ml) or chloramphenicol (34 μ g/ml).

Modified-rich LB (Rich LB) (0.5% (w/v) NaCl), 1.2%(w/v) Bactotryptone, 2.4%(w/v) yeast extract, 4.0% (v/v) glycerol, 0.5%(w/v) K₂HPO₄ and 0.0142%(w/v) Na₂SO₄) with appropriate antibiotics, as indicated above, were the growth media of choice for production of recombinant mitochondrial thioredoxin reductase.

2.1.7 M9 medium

5x M9 stock: 3%(w/v) Na₂HPO₄, 1.5%(w/v) KH₂PO₄, 0.5%(w/v) NH₄Cl, 0.25% (w/v) NaCl was first autoclaved to prepare the M9 medium. M9 medium (1l) was made from: 200ml 5x M9 stock, 700ml water (autoclaved), 1ml 1M MgSO₄ stock, 100ml 4% (w/v) glucose stock (sterile filtered), 100 μ l 0.5% (w/v) thiamine (sterile filtered), 1ml FeSO₄, 4.2g/l (sterile filtered) and the required antibiotic.

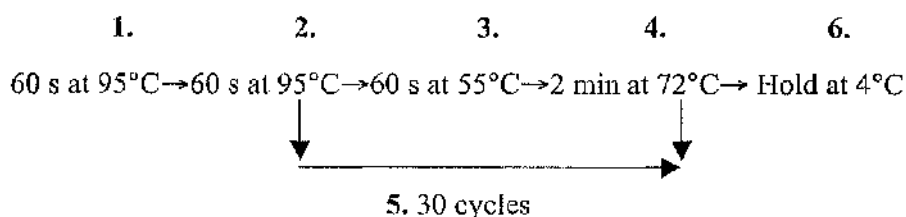
2.1.8 Plasmid vectors

pET-14b vector was purchased from Novagen and pQE-31 vector was purchased from QIAGEN.

2.2 Molecular Biology Methods

2.2.1 Polymerase Chain Reaction (PCR)

Clones of human mitochondrial thioredoxin (Trx2) (IMAGE ID 5554051) and human mitochondrial thioredoxin reductase (TRR2) (IMAGE ID 5588243) obtained from Geneservice Ltd (100ng) were used as the PCR template. The PCR reaction contained 5 μ l reaction buffer (10x), 1 μ l dNTP mix (0.25mM each of dATP, dCTP, dGTP, and dTTP), 1 μ l (250ng) forward and reverse specific primers, and 1 μ l *Pfu* DNA polymerase (3U/ μ l) prepared in a total volume of 50 μ l with sterile dH₂O. Amplification was carried out in a PTC-100™ programmable thermocycler (MJ Research Inc.). The typical reaction cycle comprising six steps is shown below:



The quality and quantity of PCR product obtained was analyzed by agarose gel electrophoresis.

2.2.2 Restriction Endonuclease Digestion of Insert and Vector DNA

Following PCR amplification, *Bam*HI restriction endonuclease was used to generate sticky ends for ligation. Both insert and vector DNA (approx. 5 μ g) were digested in a reaction containing 3 μ l of the appropriate buffer as provided by the manufacture (10x), and 3 μ l *Bam*HI (10U/ μ l) made up to a total volume of 30 μ l with sterile dH₂O. Digestion was carried out at 37°C for 3h.

To prevent re-joining of the vector DNA during ligation, the 5' protruding termini were dephosphorylated immediately following restriction digestion. This was carried out by incubating the linear vector with 1 unit of calf intestinal alkaline phosphatase for 30 min at 37°C. The treated vector was then purified using the

QIAquick® Gel Extraction Kit, purifying directly from the reaction mix. After each purification step, 5µl of the insert DNA was analyzed on a 1.0% (w/v) agarose gel.

2.2.3 DNA Gel Electrophoresis

DNA fragments were separated by agarose gel electrophoresis, prepared by dissolving the required amount of agarose, typically 0.7-2.5% (w/v) in (1x) TAE buffer, pH 7.6. TAE buffer was prepared as a (10x) stock in 1litre (11.4ml glacial acetic acid, 20ml 0.5M EDTA and 48.8g Tris-HCl, pH 8.0). The gel was placed in an electrophoresis tank and submersed in TAE buffer (1x). In general, 3µl loading buffer (50% (v/v) glycerol, 0.01% (w/v) SDS, 0.01% (w/v) bromophenol blue) was added to 5µl of DNA prior to electrophoresis which was carried out at 100 volts (V) and 250 mA. DNA fragments were visualized by ethidium bromide (EtBr) staining in distilled water (0.5-1µg/ml in dH₂O) for 30 min with shaking at room temperature. The gel was rinsed in dH₂O to remove background stain, and then visualized under 320nm UV light. Photographs were taken with a Polaroid DS34 direct screen-imaging camera, and recorded onto K65HM-CE glossy thermal film. Where necessary, linear DNA fragments were excised from the gel using a scalpel, and subsequently purified using a Qiagen DNA gel extraction kit.

2.2.4 Ligation

Following *Bam*HI treatment, the DNA encoding PrxIII, and pET-14b were joined via the actions of T4 DNA ligase. Three ratios of plasmid to insert were prepared (1:1, 1:3 and 1:7), in a reaction mix containing 2µl reaction buffer (10x), 1.5µl T4 DNA ligase (3U/µl) diluted to 20µl with sterile dH₂O. These were incubated at room temperature overnight before being transformed into competent *E. coli* DH5α cells following the standard protocol above. The resulting colonies were then screened to check for the presence of the insert of interest.

2.2.5 Production of Competent Cells

Competent cells were made using the rubidium chloride method. The appropriate bacterial *E. coli* strain was streaked overnight on a LB plate without antibiotics. A single colony was used to inoculate a 5ml overnight culture. This was subcultured into 100ml LB and grown at 37°C with shaking until the culture reached an optical

density of 0.5 at 600nm. The culture was then chilled for 5 min before centrifugation at 8,000g for 10 min at 4°C. The pellet was resuspended in 40ml buffer 1 (100mM rubidium chloride, 10mM calcium chloride, 50mM manganese chloride, 15% (v/v) glycerol in 30mM potassium acetate, pH 5.8). Cells were centrifuged as before and the pellet resuspended in 4ml buffer 2 (75mM calcium chloride, 10mM rubidium chloride, 15% (v/v) glycerol in 10mM MOPS buffer, pH 6.5). The cells, now competent, were divided into aliquots and stored at -80°C.

2.2.6 Transformation of competent bacteria

To 50µl of competent bacteria, 1-10ng of DNA was added. The mixture was chilled for 15 min before heat shocking at 42°C for 90s and returning to ice. After 2 min LB medium (450µl) was added and this was incubated at 37°C with shaking for 45 min. This mix was plated on an LB plate containing the appropriate antibiotic and incubated overnight at 37°C.

2.2.7 Plasmid Propagation and Purification

Vector and recombinant plasmid DNA amplified in *E. coli* DH5α cells was purified from 5ml overnight cultures using a Wizard® Plus Mini Preps DNA purification kit. Purified DNA (5µl) was analyzed by agarose gel electrophoresis.

2.2.8 Expression of Recombinant Protein in Bacteria

A single colony was picked from a LB-agar antibiotic plate and grown at 37°C with shaking in 5ml growth media plus antibiotic for 16h. An aliquot was subcultured into 50ml of growth media plus antibiotic. Cultures were incubated at 37°C with shaking until an A₆₀₀ of 0.5 was reached. Induction of heterologous protein expression was initiated by addition of 1mM IPTG. Induction temperatures varied according to the protein of interest. Bacterial growth was monitored; samples (1ml) were removed at the point of induction and at regular intervals thereafter, and their absorbance recorded at 600nm. Cells were harvested by centrifugation in a bench top microfuge for 2 min; the pellet was resuspended in Laemmli sample buffer (10% (w/v) sucrose, 2% (w/v) SDS, 62.5mM Tris-HCl, pH 6.8 and a small amount of Pyronin Y dye), adding 10µl per 0.1-absorbance unit of original culture.

Successful overexpression was determined following reducing SDS-polyacrylamide gel electrophoresis (SDS-PAGE) analysis.

2.2.9 Expression of SeMet Protein in Bacteria

A single colony was picked from an LB-agar antibiotic plate and grown at 37°C with shaking in 5ml growth media plus antibiotic for 16h. The M9 medium was pre-warmed to 37°C. LB overnight cultures (1ml) were centrifuged at 13,000 rpm for 1 min at room temperature and the cell pellet was gently resuspended in 1ml of M9 medium. The resuspended cell suspension was returned to a 250 ml culture. Growth was continued until A_{600} reached 0.3 which normally took 4-8h. Solid amino-acid supplements were added to the cultures to the final concentrations given: L-lysine 100mg/l, L-phenylalanine 100mg/l, L-threonine 100mg/l, L-isoleucine 50mg/l, L-leucine 50mg/l, L-valine 50mg/l and L-selenomethionine 50mg/l. After culturing for 15 min to permit inhibition of methionine synthesis, heterologous protein expression was induced as normal (1 mM IPTG) at 22°C. Growth was continued for a further 16h before cells were harvested as described above.

2.2.10 Bacterial Cell Lysis

Bacterial cells from small (50ml) cultures were harvested by centrifugation and resuspended in 5ml of the appropriate buffer. For large (500ml) cultures, bacterial cells were harvested and the pellet resuspended in 20ml of buffer. The bacterial extract was passed four times through a French Pressure Cell (AMINCO) at a pressure of 750Psi/950Psi for small/large cultures, to lyse the cells. Insoluble and soluble fractions were separated from the cell extract by centrifugation at 10,000rpm for 15 min in a JA-17 rotor in a Beckman J2-MC centrifuge.

2.3 Materials for Protein Purification and Analysis

2.3.1 Chemicals

The following chemicals were purchased from Sigma Chemical Co, Poole, Dorset, UK: benzamidine, DL-6,8-thioctic acid amide (DL-lipoamide, oxidized form), 5,5'-dithionitrobenzoic acid (DTNB), hydrogen peroxide (H₂O₂), N-(2-hydroxyethyl)piperazine-N'-(4-butanesulphonic acid) (HEPES), imidazole, leupeptin, β -nicotinamide adenine dinucleotide, reduced form (β -NADH), β -nicotinamide adenine dinucleotide 2'-phosphate, reduced form (β -NADPH), potassium phosphate (KH₂PO₄), trichloroacetic acid (TCA). DTT was bought from Melford Laboratories Ltd., Suffolk, UK. All chemicals were at least of analytical grade. Distilled water was of Millipore-Q quality.

2.3.2 Molecular Weight Markers and Equipment

The Low Molecular Weight Marker Kit was purchased from Amersham Pharmacia Biotech UK Ltd, for subunit molecular weight determination of proteins run on denaturing SDS-PAGE. The calibration mix was supplied as a lyophilized sample containing six highly purified proteins with a M_r range of 14,400-94,000. The calibration mix (250 μ g) was resuspended in 250 μ l Laemmli sample buffer (section 2.2.8) to give a 1X concentration, and 10 μ l was routinely loaded on a gel. The subunit M_r value of the protein of interest was determined by comparing its electrophoretic mobility with that of the molecular weight standards.

A pre-packed HiPrep (16mm x 600mm), Sephacryl S-300 High Resolution column was purchased from Pharmacia with a bed volume of 120ml and fractionation range of 1 X 10⁴- 2 X 10⁶ M_r. The column was run using a BioCAD[®] 700E Perfusion Chromatography[®] Workstation.

The BioCAD[®] SPRINT[™] and BioCAD 700 Series Perfusion Chromatography[®] Workstations and SelfPack POROS 20 Metal Chelate Affinity Packing equipment were purchased from PerSeptive Biosystems, Framingham, MA, U.S.A. Chelating Sepharose[®] Fast Flow gel matrix was purchased from Amersham Pharmacia Biotech.

2.3.3 Spectrophotometric Equipment

All spectrophotometric measurements for enzyme assays, protein concentration determination, and Ellman's assay, were recorded using an Ultrospec 4300 Pro UV/Visible spectrophotometer (Biochrom). UV quartz cuvettes (1ml, Jencons) with a 10mm pathlength were used routinely.

2.4 Protein Methods

2.4.1 Preparation of the Metal chelate Affinity Columns

Metal chelate chromatography used to purify His-tagged proteins was carried out using a BioCAD® SPRINT™ or BioCAD 700 Workstation. A column (10mm x 100mm) with a bed volume of 8.5ml was packed with Self Pack POROS 20 Metal Chelate Affinity Packing according to the manufacturer's instructions. Zinc ions (Zn^{2+}) were loaded onto the matrix by passage of 24 column volumes (CV) of 0.1M $ZnCl_2$ at a low pH of 4.5-5.0 to minimize precipitation of metal hydroxide complexes. The column was then washed with 5 CV of dH_2O to remove excess zinc ions followed by 5 CV of 0.5M NaCl to remove non-specifically bound metal ions. To improve selectivity and recovery of the His-tagged protein, the column was saturated with elution buffer (0.5M imidazole, 1.0M NaCl, 20mM HEPES buffer, pH 6.0). The metal chelate column was primed with 5 CV of starting buffer (0.5mM imidazole, 1.0M NaCl, 20mM HEPES buffer, pH 8.0) prior to protein loading.

2.4.2 Purification of His-tagged protein

Bacterial cultures (500ml) were routinely employed in purification of high yields of protein per single purification. Bacterial cell lysis was performed as described in section 2.2.10. The clarified supernatant of the extract was maintained on ice for further purification. Four 5ml injection steps were incorporated into the BioCAD elution protocol to load the 20ml sample onto the metal chelate affinity column. An increasing imidazole gradient, from 0.5mM - 0.5M over 6 CV was carried out, eluting the His-tagged protein in 2ml fractions. Column regeneration was achieved by stripping with 1.0M NaCl containing 50mM EDTA followed by a water wash. The column was stored in dH_2O or 20% (v/v) ethanol for longer time periods. Fractions were stored at 4°C.

2.4.3 Preparation of BioCAD Protein Fractions for SDS-PAGE

Following elution of the His-tagged recombinant protein, aliquots (20 μ l) of peak fractions were mixed with 20 μ l Laemmli sample buffer supplemented with DTT (150mM) for subsequent SDS-PAGE analysis.

2.4.4 SDS-PAGE

Electrophoresis of protein samples was carried out in SDS, according to the method of Laemmli (1970). Each gel comprised a 3% stacking gel and a 10-15% resolving gel depending on the molecular weight of the protein of interest. Polymerization of the gel was achieved on addition of 0.03% (v/v) TEMED, and 0.05% (w/v) ammonium persulphate (APS) to a 30:0.8 ratio of acrylamide:bisacrylamide. Typically a 10 μ l sample was loaded per well. Electrophoresis was carried out at a constant voltage (400V) and 50mA/gel in 1X SDS running buffer prepared from a 10X stock (144g glycine, 10g SDS and 29.8g Tris-HCl, pH 8.8 prepared to 1l with distilled water). Protein bands were stained with Coomassie Brilliant Blue G250 in 50% (v/v) methanol and 10% (v/v) glacial acetic acid with shaking for 30 min at room temperature. The gel was immersed in an appropriate volume of destain (10% (v/v) methanol and 10% (v/v) glacial acetic acid) to remove excess stain and enable clear band visualization.

For superior resolution when necessary, samples were run on pre-cast 4-12% NUPAGE[®]Novex Bis-Tris gels (Invitrogen) held within a XCell *SureLock*[™] Mini-Cell. The preparation of protein samples for electrophoresis was the same as for standard SDS-PAGE. Electrophoresis was carried out in 1X NUPAGE[®] MES SDS Running buffer at constant voltage (200V) and 110mA/gel. The staining procedure was as for conventional SDS polyacrylamide gels.

2.4.5 Protein Dialysis and Concentration

Peak fractions following metal chelate chromatography were pooled and dialyzed routinely against 10l of dialysate (5 x 2l changes) at room temperature or 4°C. Dialysis tubing had a molecular weight cut-off of 10,000 M_r. The dialysate was typically 150mM NaCl, 50mM HEPES, pH 7.2 for the majority of experiments.

2.4.6 Determination of Protein Concentration

Protein concentration was determined according to the absorbance of the protein at 280nm. To determine the A_{280} , it was necessary to derive an extinction coefficient for the protein under investigation. The protein was analyzed in the far UV spectrum over 240–400nm, using buffer only as the reference. The extinction coefficient was calculated using the following equation:

$$\frac{\text{No. of Tryptophan Residues} \times 5690 + \text{No. of Tyrosine Residues} \times 1280}{\text{Monomeric molecular weight of Protein}}$$

The A_{280} divided by the extinction coefficient enabled protein concentration determination. The extinction coefficient for PrxIII (1mg/ml) was 0.735, for TRR2 was 1.053 and for Trx2 was 0.485. In all cases the $A_{280}:A_{260}$ ratio of the protein was checked to ensure minimal DNA or RNA contamination.

2.4.7 Anion exchange

Anion exchange chromatography was performed on a BioCAD® SPRINT™ or BioCAD 700 Workstation at room temperature with a POROS® HQ column. The sample buffer was exchanged with 50mM Tris-HCl, pH 8.5. A gradient of 1M NaCl in 50mM Tris-HCl, pH 8.5 was used to elute the protein from the HQ column over 30CV.

2.4.8 Gel Filtration

Gel exclusion chromatography was performed at room temperature using a pre-packed HiPrep 16/60 Sephacryl S-300 High Resolution column connected to a BIOCAD® 700E Perfusion Chromatography® Workstation. The flow rate was 1ml/min and the volume of protein loaded was 1ml (recommended < 2% of bed volume). Fractions (2ml/tube) were collected. All buffers were filtered through a 0.2µm vacuum filter (Millipore). The column was equilibrated with 2 CV of the appropriate buffer, washed with 2 CV of dH₂O between runs and stored in 20% (v/v) ethanol for longer periods.

2.4.9 Ellman Assay for Thiols

Protein samples of known concentration were prepared in 150mM NaCl, 50mM HEPES, pH 7.0. The amount of nitrothiobenzoate (NTB) released upon reaction of a thiol with DTNB was measured by monitoring the absorbance at 412nm. The absorbance was set to zero with a 1ml protein sample. To the protein sample, 25 μ l 10mM DTNB prepared in 0.1M HEPES, pH 7.0 was added and inverted to mix. The absorbance was recorded over 40 min at room temperature. The absorbance difference between the protein sample and the buffer only control was measured. The absorbance of the TNB anion ($\epsilon_{412} = 14,150\text{M}^{-1}\text{cm}^{-1}$) produced was used to calculate the molar concentration of the thiols present:

$$\mu\text{M protein} \times \epsilon_{412} = \text{Expected } A_{412} \text{ per thiol.}$$

2.4.10 Cleavage of His-tag from protein

The serine protease thrombin, supplied as a lyophilized powder, was used to cleave recombinant fusion proteins containing a His-tag. Cleavage was achieved by overnight incubation at room temperature with the protein (1U cleaves $\geq 90\%$ of 100 μ g protein). Protein with intact His-tag was removed by metal affinity chromatography using a PD-10 column prepared with 2ml of Chelating Sepharose® Fast Flow (Amersham Pharmacia Biotech Ltd.) employing immobilized zinc ions according to the manufacturer's instructions. Successfully cleaved protein was collected in 1ml fractions by washing through with buffer containing 150mM NaCl, 50mM HEPES, pH 7.0.

Chapter 3

Cloning

3.1 Introduction

Bovine PrxIII was cloned previously in our laboratory (Gourlay *et al.*, 2003); however PrxIII requires its cognate partners, mammalian mitochondrial thioredoxin (Trx2) and mammalian mitochondrial thioredoxin reductase (TRR2), to reconstitute the complete antioxidant defence pathway. To establish a direct *in vitro* assay for PrxIII, Trx2 and TRR2 were cloned, overexpressed and purified. The successful cloning of recombinant human Trx2 and the crystal structure of Trx2 was published very recently (Smeets *et al.*, 2005) but no successful cloning, expression and purification of active recombinant of TRR2 has been reported to date.

The pET (plasmid for expression by T7 RNA polymerase) system vectors were chosen to produce Trx2 and TRR2 as N-terminally His-tagged proteins. This system enables high-level expression of cloned genes in *E. coli* and is presently the preferred choice of prokaryotic system for heterologous expression. The bacteriophage T7 RNA polymerase is integrated into the bacterial genome in the *E. coli* BL21 expression strain and its cognate promoter on the pET vector tightly controls heterologous protein production from the pET plasmid. Expression of T7 RNA polymerase is induced in *E. coli* BL21 (DE3) pLysS cells on addition of IPTG.

As described in the first chapter, TRR2 contains the C-terminal active site motif Gly-Cys-SeCys-Gly in which the SeCys is encoded by UGA, normally a 'stop' codon and so requires the presence of a SECIS for correct translation. However, the SECIS of mammalian selenoproteins has different secondary structural characteristics and conserved features than in *E. coli* (Fig 3.1 a). Moreover, the mammalian SECIS is often situated in the 3'-untranslated region several hundred nucleotides downstream of the UGA codon (Low and Berry, 1996). Thus mammalian selenoprotein genes are unsuitable for direct recombinant expression in *E. coli*. A technique, however, to by-pass the barriers to heterologous expression of mammalian selenoproteins in bacteria was employed by mimicking the mechanism used in *E. coli* formate dehydrogenase H (Fig 3.1 b).

Adding the entire SECIS of *E. coli* presents difficulties for standard PCR insertion procedures. Therefore, a minimal SECIS capable of forming the secondary structure loop was designed and incorporated into the PCR primers. The loop region of the SECIS is the SelB binding site and is base specific whereas the stem region is length specific but not base specific requiring at least 11 nucleotides downstream of the Sec UGA codon (Arner *et al.*, 1999). Overall, there are 13 matched bases and 30 unmatched bases in the 3' primer.

3.2 Results

3.2.1 Primers for Trx2

Human Trx2

Forward: GAGGATGGATCCGACAACCTTTAATATCCAGG

Reverse: CATCCCGGATCCCTCAGCCAATCAGCTTCTTC

Figure 3.2 Oligonucleotide primers for Trx2 clone

BamHI site is underlined.

3.2.2 PCR Amplification of Human Trx2

The PCR template for the human Trx2 gene was IMAGE clone 5588243, obtained from Geneservice Ltd. A standard PCR method was performed to amplify the gene from the initial template. In order to use the pET-14b vector, it was necessary to incorporate an extra base immediately before the start codon of the inserted gene to give the correct reading frame. *Bam*HI restriction sites were incorporated into the primers so that the amplified gene product could be incorporated into the pET-14b vector (Fig 3.2). All primers terminated with either a guanine or cytosine nucleotide to reduce the occurrence of base mismatches. To minimise errors in base incorporation, the *Pfu* DNA polymerase was used in the PCR reaction. *Pfu* is a magnesium-dependent, thermostable enzyme with 3'→5' exonuclease proofreading activity.

PCR products were gel-purified and analysed on a 1% (w/v) agarose gel, alongside a 1kb DNA Step Ladder (Materials and Methods, section 2.2.3). A band of ~320bp was observed, corresponding to the expected size of the human Trx2.

The purified Trx2 insert gene and pET-14b vector were treated with *Bam*HI to generate cohesive ends. To prevent pET-14b self-ligation, 5'-phosphates were removed by adding 1 unit of calf intestine alkaline phosphatase (CIAP) for 30 min before the end of digestion.

3.2.3 Ligation

Different ratios (1:1, 1:3 and 1:7) of vector to insert were added together and a control ligation with vector only was used to determine the efficiency of the dephosphorylation step. Ligated plasmid was then transformed into *E. coli* DH5 α cells. Colonies were not seen on the control plate. Six clones were selected to grow a series of 5ml overnight cultures. Plasmid minipreps were performed next day from the 5ml overnight cultures. Purified DNA was either sent for sequencing or subjected to PCR analysis.

A set of 2 parallel PCR reactions was performed. One set used the T7 promoter primer and Trx2 reverse primer while the other uses the T7 terminator primer and Trx2 forward primer. An example of a positive result, in which the correct size of PCR product is observed on the gel with the T7 promoter primer and Trx2 reverse primer of the target insert, shows successful ligation in the correct orientation (Fig 3.3 lane 1R).

Purified positive plasmids were transformed into *E. coli* BL21(DE3) pLysS cell for protein expression.

3.2.4 DNA sequencing

Overnight cultures (5ml) were harvested and sent for DNA sequencing. The sequencing was performed on a MegaBACE1000 instrument in the Sir Henry Wellcome Functional Genomics Facility (SHWFGF), University of Glasgow. Typically there were 400-600 bases with good signal from each sequence run. Sequencing from both ends of the insert was performed routinely.

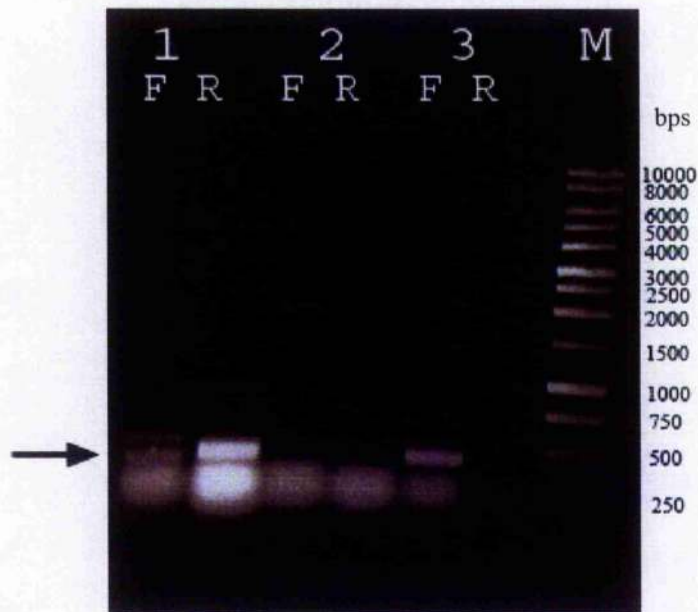


Figure 3.3 PCR check of putative Trx2 clones

Following PCR amplification of Trx2 from the Trx2/pET-14b template, 5 μ l was analysed on a 1% (w/v) agarose gel. Bands were stained with ethidium bromide, and sizes were determined by comparison with a 1kb DNA Step Ladder (M), shown to the right of the gel, with units in base pairs (bps). Two parallel PCR reactions were performed for each clone. The T7 terminator primer and Trx2 forward primer were used as a pair of primers for one PCR (marked as F in the figure) while the T7 promoter primer and Trx2 reverse primer were used as the other pair of primers for the other PCR (marked as R in the figure). A typical agarose gel of the PCR results from 3 clones (1,2,3) is shown in this figure. Arrow indicates the PCR products. In this gel, clone 1 shows a PCR product with T7 promoter primer and Trx2 reverse primer which indicates the presence of insert in the correct orientation in contrast to clone 3 where the insert is in the opposite orientation.

3.2.5 Protein Expression of Trx2

E. coli BL21 (DE3) pLysS cells with the Trx2 gene were grown to log phase before IPTG was added. To confirm the correct orientation of the Trx2 insert gene, both clones 1 and 3 shown in the previous gel were induced. Following reducing SDS-PAGE, a band at 17 kDa was observed, corresponding to the predicted M_r value of Trx2 together with its N-terminal His-tag. Clone 1, which is the positive clone, produced this band after induction (Fig 3.4); however, as expected, clone 3 did not give a similar product.

3.2.6 Protein solubility and purification

Bacterial cell lysis was performed as described in Material and Methods section 2.2.10. Trx2 was found in the supernatant fraction but not in the pellet as visualized on SDS-PAGE analysis (data not shown), indicating that Trx2 was soluble under these conditions. Soluble protein from large-scale (500ml) bacterial cultures was then purified by Zn^{2+} chelate affinity chromatography using a BioCAD[®] 700E[™] Workstation. Samples from peak fractions were analysed by SDS-PAGE to assess sample purity (Fig 3.5).

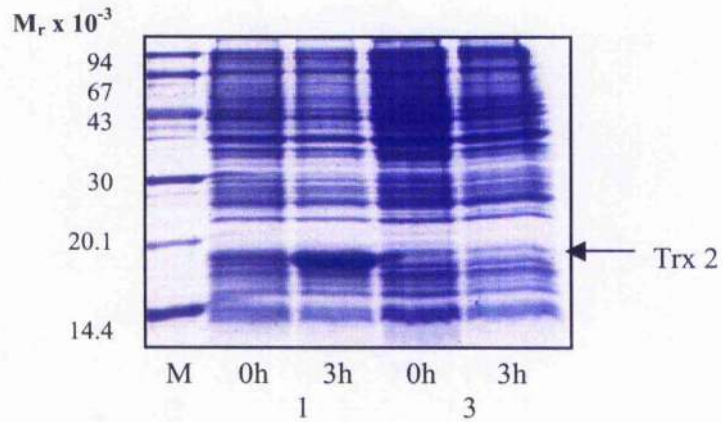


Figure 3.4 Overexpression of Trx2

Trx2 were overexpressed at 37°C in BL21(DE3)pLysS cells, by induction with 1mM IPTG. Samples (1ml) were removed at the point of induction (0h) and after 3 hours (3h). Bacterial pellets were resuspended in Laemmli sample buffer (10 μ l/0.1 OD₆₀₀ of original culture), and denatured for 5 min at 100°C in the presence of DTT (150mM). Samples were analysed on a 10% SDS/polyacrylamide gel, and stained with Coomassie Brilliant Blue. The expression of Trx2 from the clones analysed in the previous section (clones 1 and 3) is shown in the lanes indicated. Molecular weight markers (M) are shown to the left of the gel.

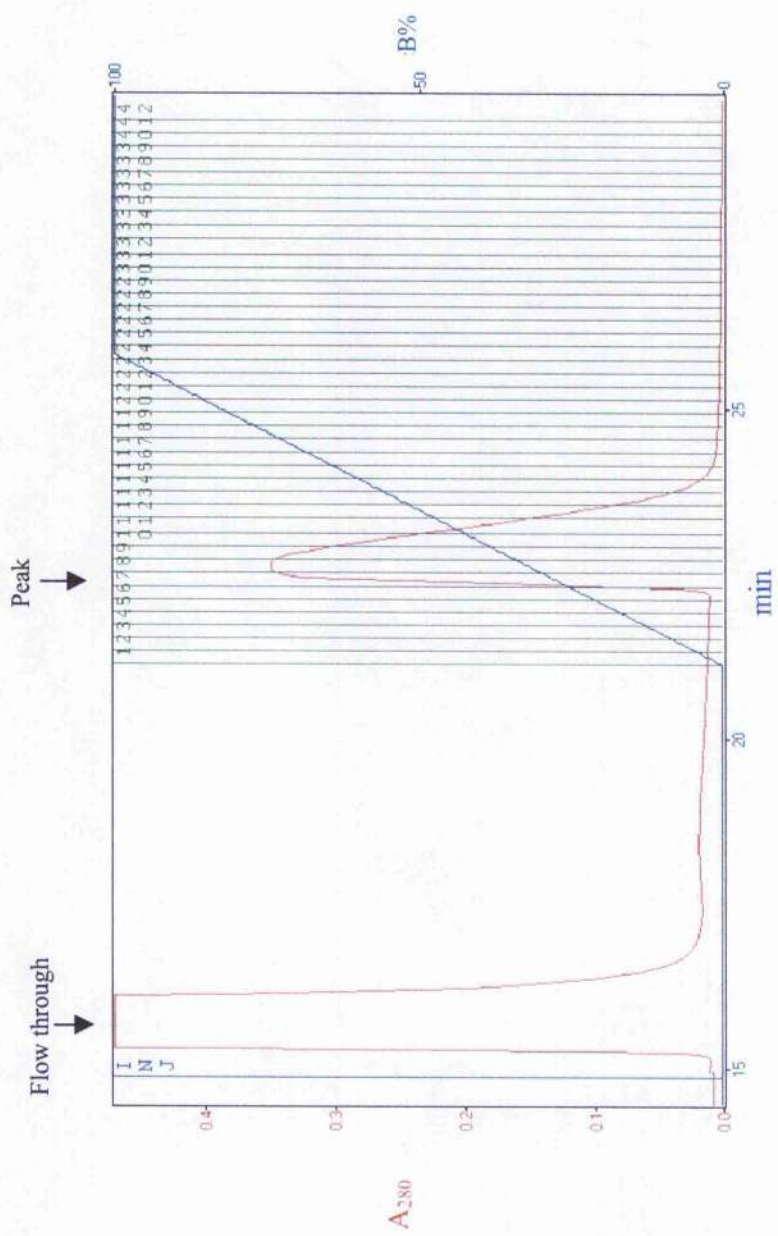


Figure 3.5 BioCAD elution profile of Trx2

The soluble fraction (20ml) of a 500ml bacterial culture containing overexpressed Trx2 was loaded onto a zinc metal chelate column (Materials and Methods section 2.4.1). The protein was eluted over an increasing imidazole gradient (0.5mM-0.5M) show as the blue line in the figure and expressed as a percentage of buffer B containing the high level of imidazole. The A_{280} (red) of Trx2 was recorded over time in minutes. Fraction numbers are highlighted in green.

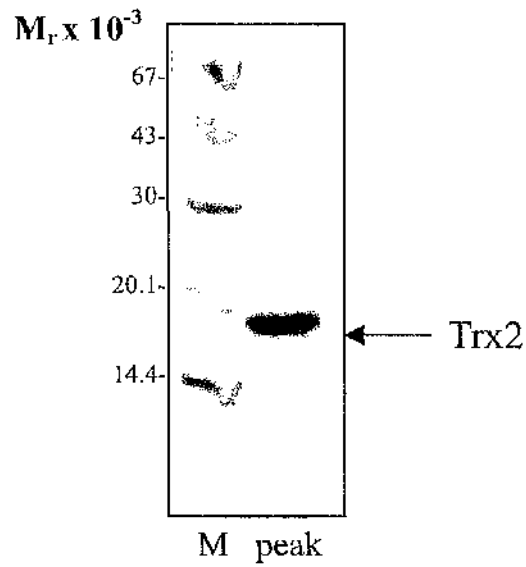


Figure 3.6 BioCAD fractions of purified Trx2

A sample (10 μ l) from the peak fraction was diluted with an equal volume of Laemmli sample buffer, supplemented with DTT (150mM) and denatured for 5 min at 100°C, prior to loading on a 10% SDS/polyacrylamide gel. Bands were stained with Coomassie Brilliant Blue. Molecular weight markers (M) are shown to the left of the gel.

3.2.7 Estimation of accessible reactive cysteines in purified Trx2

Ellman's assay was used to confirm the number of reduced cysteines in purified Trx2 that were accessible to thiol modification by the reactant 5,5'-dithionitrobenzoic acid (DTNB). The number of thiols accessible to DTNB was assessed by measuring the A_{412} of the nitrothiobenzoate (NTB) product released during the reaction. Purified Trx was reduced by 10mM DTT and passed through a PD-10 desalting column to remove excess DTT. The A_{412} of reduced Trx was measured over two weeks using the DTNB assay as described in Materials and Methods, section 2.4.9 (Fig 3.6). Two cysteines were accessible initially but they gradually lost their ability to reduce DTNB after 2 weeks. This implies there are 2 free cysteines as expected but they are reoxidised over a 2-week period in the absence of reducing agent during storage at 4°C.

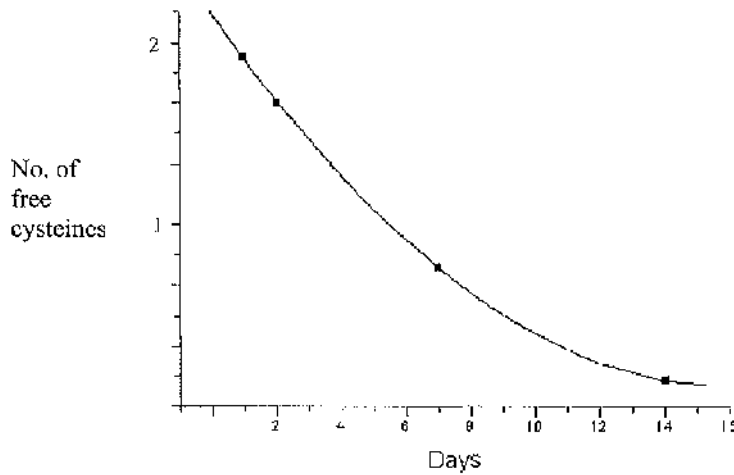


Figure 3.7 Reoxidization of Trx2 in solution as monitored by loss of reactivity with DTNB

3.2.8 Cloning of TRR2

TRR2 was cloned using a similar strategy to Trx2 from IMAGE clone 5554051, purchased from Geneservice Ltd. A band of ~1,500 bp was observed after PCR amplification, corresponding to the expected size of the human TRR2 (Fig 3.8). PCR products were then ligated into the pET-14b vector via its unique *Bam*HI site. However, for this unusual SeCys protein, the presence of a SECIS is important for SeCys incorporation for TRR2 to have activity. SECIS was introduced by designing C-terminal primers so that the adjacent 3' untranslated sequence contained the required sequence elements (Fig 3.7).

3.2.9 Primers

Human TRR2 without SECIS

Forward: CGCAGCGGATCCTCAGCGGGACTATGATCTCC

Reverse: CAGGGAGGATCCTTACCCTCAGCAGCC

Human TRR2 with SECIS

Forward: CATATGGATCCTCAGCGGGACTATGATCTC C

Reverse: GAGGATCCGGTGCAGACCTGCAACCGAATTATTACCCTCAGCAG

Figure 3.7 Oligonucleotide primers for TRR2 clone

The BamHI site is underlined. The loop region of SECIS is highlighted in blue. The double stop codon is highlighted in red. The SeCys UGA codon is highlighted in plum.

Unlike Trx2, the solubility of TRR2 under standard expression conditions was very poor. As shown in Fig 3.9, although the expression at 22°C was much better than at 15°C, the majority of the TRR2 was still insoluble. By optimizing various parameters, the best conditions for maximal TRR2 yield and solubility involved growth in a modified rich LB media (Material and Methods, section 2.1.6) and appropriate antibiotics. Cells were induced by 0.3mM IPTG at 15°C for 18h at a starting OD₆₀₀ of 0.5. Na₂SeO₃ (1 μM) was added as a supplement when cultures were induced. Cells were then lysed by French Press treatment in high-salt buffer (0.5mM imidazole, 1.0M NaCl, 20mM HEPES pH 8.0).

Two peaks emerged from the Zn^{2+} metal chelate column during the elution step. SDS-PAGE gel analysis shows that peak 2 corresponds to the target protein (Fig 3.10). The purified enzyme was yellow in colour and showed significant absorbance at 450nm indicating the incorporation of the FAD cofactor. Approximately 4-5 mg soluble protein could be purified per litre of original culture. Peak 1 contained a single unidentified protein which exhibited no TRR2 activity.

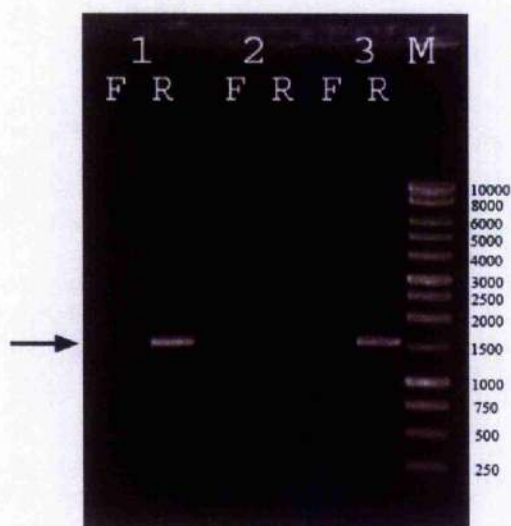


Figure 3.8 PCR check of recombinant TRR2 pET14b plasmid

Following PCR amplification of TRR2 from the TRR2/pET-14b template, the product (5 μ l) was analysed on a 1% (w/v) agarose gel. Bands were stained with ethidium bromide, and sizes were determined by comparison with a 1kb DNA Step Ladder (M), shown to the right of the gel, with units in base pairs (bp). Three templates were used (1,2,3). T7 terminator primer and TRR2 forward primer were used as a pair of primers for one PCR (R) while T7 promoter primer and TRR2 reverse primer were used as a pair of primers for the other PCR (F). Arrows indicate the PCR products. Both clones 1 and 3 show a PCR product with T7 promoter primer and TRR2 reverse primer which indicates the presence of insert in the correct orientation.

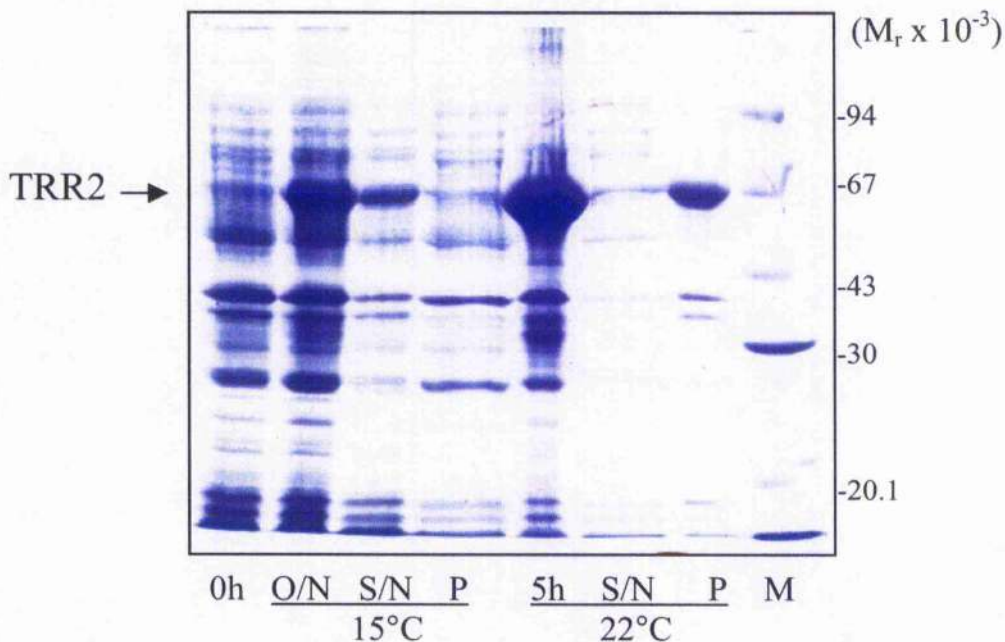


Figure 3.9 Assessment of TRR2 expression and solubility

TRR2 overexpression was attempted at different temperatures in *E. coli* BL21(DE3)pLysS cells, by induction with 0.3mM IPTG. Samples (1ml) were removed at the point of induction (0h). Samples from overnight (O/N) induction at 15°C and 5 hours (5h) at 22°C induction were also removed. After induction, the bacterial culture (500ml) was centrifuged and the pellet resuspended in 20ml 20mM HEPES buffer, pH 8.0 containing 1M NaCl. Cells were lysed by two passages through a French Pressure Cell at a pressure of 950Psi. The cell extract was separated into its soluble (S/N), and insoluble (P) fractions by centrifugation. All samples were diluted with an equal volume of Laemmli sample buffer, supplemented with DTT (150mM) and denatured for 5 min at 100°C, prior to loading on a 10% SDS/polyacrylamide gel. Bands were stained with Coomassie Brilliant Blue. Molecular weight markers (M) are shown to the right of the gel.

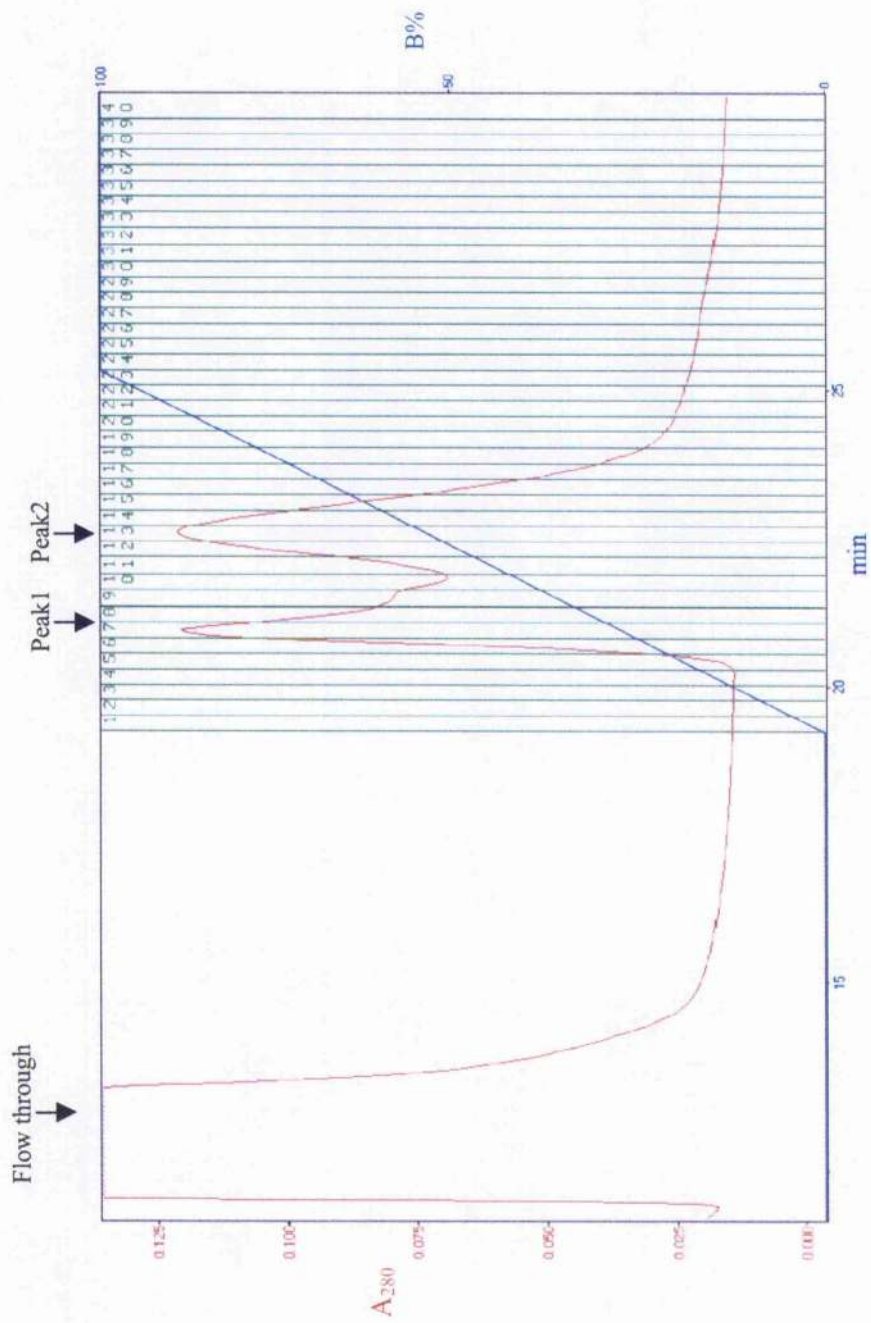


Figure 3.10 BioCAD elution profile of TRR2

The soluble fraction (20ml) of a 500ml bacterial culture containing overexpressed TRR2 was loaded onto a zinc metal chelate column (Materials and Methods section 2.4.1). The protein was eluted over an increasing imidazole gradient (0.5mM-0.5M) shown as the blue line in the figure and expressed as a percentage of buffer B containing the high level of imidazole. The A_{280} (red) of TRR2 was recorded over time in minutes.

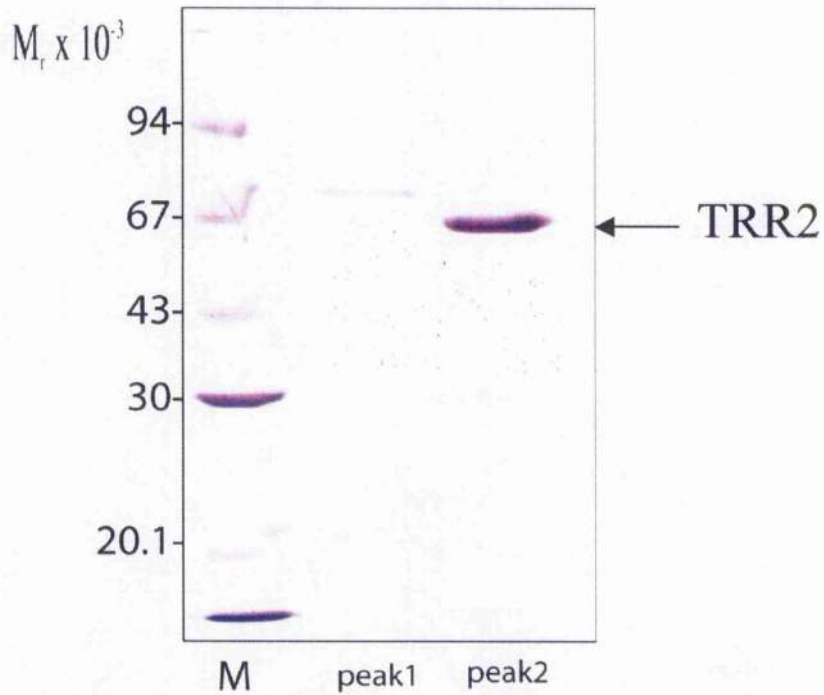


Figure 3.11 BioCAD fractions of purified TRR2

Sample (10 μ l) from the 2 peak fractions were withdrawn and diluted with an equal volume of Laemmli sample buffer, supplemented with DTT (150mM) and denatured for 5 min at 100°C, prior to loading on a 10% SDS/polyacrylamide gel. Bands were stained with Coomassie Brilliant Blue. Molecular weight markers (M) are shown to the left of the gel.

3.2.10 Catalytic activity of TRR2

Measurement of DTNB reductase activity was performed at 25°C in freshly prepared 100 mM Tris-HCl, pH 7.5, 2 mM EDTA. TRR2 (1 µg) and 1.5 mM DTNB was also added. The reaction was initiated by adding 0.2 mM NADPH. Absorbance is read at 412 nm and the activity is expressed as µmol/min/mg protein and can be calculated by $\Delta A_{412} \times 1000 / (13.6 \times 2) / \text{min}$.

3.2.11 Optimization of the TRR2 activity

To screen for the highest activity of TRR2, different constructs were made and analyzed, including the pET and pQE expression systems. The TRR2 sequence and the SECIS were amplified by PCR and ligated into the pQE31 vector via the *Bam*HI site as described previously for pET-14b. The TRR2/pQE31 plasmid was then transformed into *E. coli* M15 cells for maximum overexpression. To increase the efficiency of selenoprotein production, a plasmid carrying the selABC genes (generously gifted by E.S. Arner) was also co-expressed. A construct without SECIS was employed as the negative control. Data from native TRR1 isolated from rat liver was included as positive control data (Bar-Noy, 2001).

Constructs	Specific activity of TRR2 (µmol/min/mg protein)
pET vector without SECIS	0.14
pET vector with selABC plasmid	2.2
pQE vector without selABC plasmid	3.2
pQE vector with selABC plasmid	4.2
Native isolated rat liver TRR1	40-50

Table 3.1 Specific activities of purified recombinant human TRR2 expressed from different constructs

By comparing the catalytic activities of purified human TRR2 produced from different constructs, it is clear that the SECIS is very important in improving

recombinant TRR2 activity. Constructs with SECIS showed 15-30 fold more activity than the control enzyme with the pQE vector system performing better than the pET system. Surprisingly, the inclusion of the selABC plasmid did not promote significant improvement in TRR2 specific activity. In addition, the most active recombinant TRR2 only attained approx. 10% of the specific activity of native rat liver TRR1 which is in line with reported literature values obtained for recombinant forms of TRR1 (Arner *et al.*, 1999).

3.3 Discussion

3.3.1 Checking of recombinant clones

To ensure successful ligation of the required insert a digestion of the recombinant plasmid was performed with the restriction enzymes employed for the original ligation. In addition, if the insert has been ligated non-directionally at a single restriction site, as in this case, then an orientation check is also necessary. Traditionally, to achieve this, restriction endonucleases are chosen which will cut both within the insert and also the vector, thereby producing predicted fragment sizes that differ with orientation. By judging the fragment sizes from the agarose gel, a conclusion can be made on the orientation. However, this traditional method has some limitations as suitable restriction endonucleases need to be found to cut both the insert and vector and give different results for different orientations. To achieve this is not always possible or the most convenient restriction enzyme is expensive or not readily available.

Here, a method was employed using PCR analysis, which is quick and convenient involving only 2h for a standard PCR and gel running time. No specific enzymes are employed, as only the original primers employed in the cloning procedure plus T7 promoter primer and terminator primer are necessary and therefore independent of insert sequence. Positive clones from the PCR check were all sent for DNA sequencing to verify the accuracy of the amplified sequence and its correct insertion in frame.

3.3.2 Expression of heterologous proteins

For producing recombinant soluble proteins, *E. coli* is still the organism of choice in most cases. It produces large biomass, is very cheap to grow, and the equipment needed to culture and harvest *E. coli* is easy to obtain. Unfortunately, *E. coli* are not particularly amenable hosts for many human proteins. Expression of large proteins (>60 kDa) is often difficult, and toxicity and solubility remain huge obstacles. Some alterations in the conditions of expression can help reduce the solubility problem. Lowering the temperature at induction to 16°C-25°C has been extremely helpful in increasing solubility. Other possible solutions include *E. coli* strain

choice, co-expression of chaperones, and the inclusion of additives in the media. However, so far there is no routine and reliable route to achieve high-level expression of all soluble heterologous proteins so optimal conditions must be determined on a case by case basis.

3.3.3 Overexpression of soluble active recombinant TRR2 in *E. coli*

Previously, in the absence of soluble recombinant TRR2, PrxIII activity had to be measured by an indirect method, in which PrxIII activity was determined *in vitro* by assessing its protective effect towards enolase in the presence of a metal-catalysed free-radical generating system (Gourlay *et al.*, 2003). Quantitative comparison of the activity of various PrxIII mutants is extremely difficult to assess by this indirect approach. Thus successful cloning, overexpression and purification of TRR2 and Trx2 is crucial for further structure-function studies of PrxIII and its reconstituted antioxidant pathway.

The C-terminal primer for amplification of TRR2 was designed to incorporate the correct SECIS for the translation of its penultimate SeCys codon. An additional 11 nucleotides were included between the UGA codon and the sequence-specific loop region. A double stop codon was also added which was shown to give a higher specific activity for TRR1 (Arner *et al.*, 1999).

Standard protocols, such as 3h at 37°C, for overexpression of TRR2 yielded only insoluble protein. Overexpression at 22°C and 15°C was tried as was protein refolding after solubilisation of inclusion bodies in 8M urea. Only insoluble aggregate protein was obtained by these approaches. Different growth media and lysis buffers were tried and a low concentration (0.3mM instead of 1mM) of IPTG was added to give a slower rate of overexpression. A 42°C heat shock step before induction was also performed to produce endogenous chaperones as an aid to protein folding. However, none of the above methods were successful in improving TRR2 solubility. The reasons for the failure of these approaches could be:

- a) TRR2 is a relatively large (55kDa) protein which exceeds the protein mass limitation of the *E. coli* system, thereby requiring a very slow overexpression to give maximum time for correct protein folding.

- b) TRR2 is a SeCys protein. Translating SeCys proteins in *E. coli* is a complex event. It needs the SECIS, tRNA for the SeCys, a supply of selenium and elongation factors.

The optimal solution for the successful overexpression of active TRR2 proved to be a combination of different approaches. Overexpression at 15°C in the presence of low IPTG concentration in a modified rich LB media gave good overexpression of soluble enzyme. Moreover the addition of the SECIS at the C-terminal of the insert, in the presence of 1 µM Na₂SeO₃ and co-expression of the SelABC plasmid ensured an optimal supply of the relevant tRNA, tRNA synthase and recognition factor for translation of the UGA SeCys codon.

After achieving successful expression and purification of soluble, active His-tagged TRR2, an additional affinity purification step was attempted employing a 3'-5'-ADP Sepharose column using the NADPH binding capacity of the enzyme. However, this step was abandoned for two reasons. Firstly, there was no increase in specific activity by comparing the results from activity assays. Secondly, this additional affinity purification step resulted in a significant decrease in the yield of TRR2.

Chapter 4

Assays

4.1 Introduction

To date, the activity of PrxIII has only been determined indirectly *in vitro* by assessing its protective effect towards enolase in the presence of a metal-catalysed free-radical generating system (Gourlay *et al.*, 2003). After successful cloning, overexpression and purification of PrxIII, Trx2 and TRR2, the PrxIII pathway was reconstituted and studied *in vitro* in this chapter. NADPH oxidation was monitored coupled to H₂O₂ reduction by TRR2, Trx2 and PrxIII (Fig 4.1). NADPH has an absorbance peak at 340nm that is absent in NADP⁺; therefore the oxidation of NADPH can be monitored to assess the activity of the PrxIII pathway and various mutants.

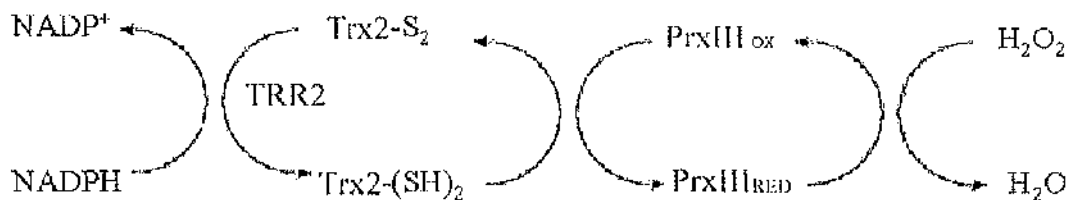


Figure 4.1 The PrxIII mitochondrial antioxidant defence pathway

A unique property of mammalian peroxiredoxins is their sensitivity to overoxidation in the presence of elevated levels of H₂O₂. PrxIII sensitivity in this case is examined both by the H₂O₂ concentration dependence of the pathway and the appearance of abnormal oxidised forms of PrxIII on SDS-PAGE analysis.

Recently, TEM (transmission electron microscopy) and studies of the crystal structure of several typical 2-Cys Prxs have revealed two distinct oligomeric forms: dimer and decamer. While the rat haem binding protein HBP23 has just one dimeric form (Hirotzu *et al.*, 1999), some other members like tryparedoxin peroxidase (TryP) from *Crithidia fasciculata* (Alphey *et al.*, 2000), thioredoxin peroxidase B (TPx-B) from human erythrocytes (Schroder *et al.*, 2000) and alkyl hydroperoxidase C (AhpC) from *Salmonella typhimurium* (Wood *et al.*, 2002) can exist as dimers or decamers. The factors that govern oligomeric assembly are not well understood. High or low ionic strength and low pH have been reported as key

factors (Kitano *et al.*, 1999; Kristensen *et al.*, 1999; Chauhan and Mande, 2001) and more importantly, oligomerization has been shown to be redox sensitive, with the reduced enzyme strongly favouring the decameric form and oxidation favouring dissociation into dimers (Wood *et al.*, 2002).

In this chapter, gel filtration chromatography (GFC) was employed for assessment of the overall molecular weight and oligomeric state of PrxIII. This technique is especially useful for monitoring alterations in the quaternary structure of a protein over a wide variety of conditions including pH, temperature and ionic strength. In gel filtration, the stationary phase consists of porous beads with a well-defined range of pore sizes. Proteins that are small enough can fit inside all the pores in the beads and are said to be included. These small proteins have access to the mobile phase inside the beads as well as the mobile phase between beads and elute last in a gel filtration separation. Proteins that are too large to fit inside any of the pores are excluded and are eluted at the void volume (V_o) of the column which is approx. 30% of the total column volume. They have access only to the mobile phase between the beads and, therefore, elute first. Proteins of intermediate size are partially included and gain access to some but not all of the pores in the beads. These proteins will then elute between the large ("excluded") and small ("totally included") proteins. Therefore, GFC is a simple and reliable chromatographic method for separating native proteins according to size.

The approx. size of a globular protein of interest is determined by comparing the ratio of the elution volume (V_e) to the void volume (V_o) for the unknown protein. The void volume is based on the elution volume of a large macromolecule usually for the pre-packed HiPrep 16/60 Sephacryl S-300 column with a M_r of 2×10^6 or greater. A calibration curve is generated using the logarithms of the known molecular weights of the protein standards, against their respective V_e/V_o values. From this calibration curve the apparent M_r value of the protein under investigation can be determined.

4.2 Results

4.2.1 Reconstitution of the PrxIII pathway

Assay of PrxIII pathway activity was performed by measuring the disappearance of NADPH when H₂O₂ was added to the reaction. A 1 ml assay mix containing 50 mM Tris-HCl, pH 7.5, 100 μ M NADPH, 2 μ M Trx2, 1 μ M TRR2 and 5 μ M PrxIII was incubated at 25 °C. The reaction was initiated by adding 0.2 mM H₂O₂. Controls omitting each component of the pathway, in turn, were also carried out. The A₃₄₀ were recorded by using an Ultrospec 4300 pro UV/Visible spectrophotometer over 180 s to monitor the oxidation of NADPH as the reducing substrate donor (Fig 4.2).

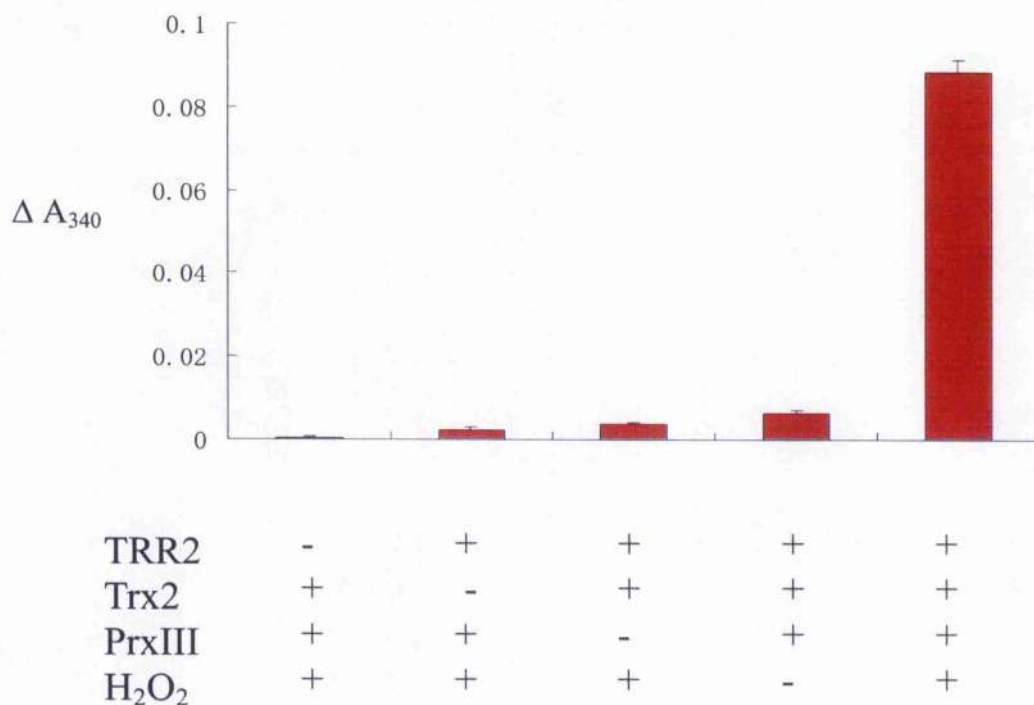


Figure 4.2 NADPH oxidation coupled to H₂O₂ reduction by various combinations of TRR2, Trx2 and PrxIII

NADPH oxidation was monitored at 340nm in a 1ml reaction mixture containing 50 mM Tris-HCl, pH 7.5, 100 μ M NADPH and the indicated combinations of 2 μ M Trx, 1 μ M TRR, 5 μ M PrxIII and 0.1mM H₂O₂. All reactions were performed in triplicate.

4.2.2 Broad substrate specificity of PrxIII

Employing the reconstituted PrxIII pathway, the substrate specificity of PrxIII was assessed using two readily available organic hydroperoxides, cumene peroxide and t-butyl peroxide. A_{340} was monitored as an indication of the PrxIII activity and compared to its activity with its natural H_2O_2 substrate (Fig 4.3). The figure shows PrxIII has less ability to reduce organic hydroperoxides under these conditions. t-Butyl peroxide promotes about 80% and cumene peroxide promotes about 40% of control activity with H_2O_2 as substrate.

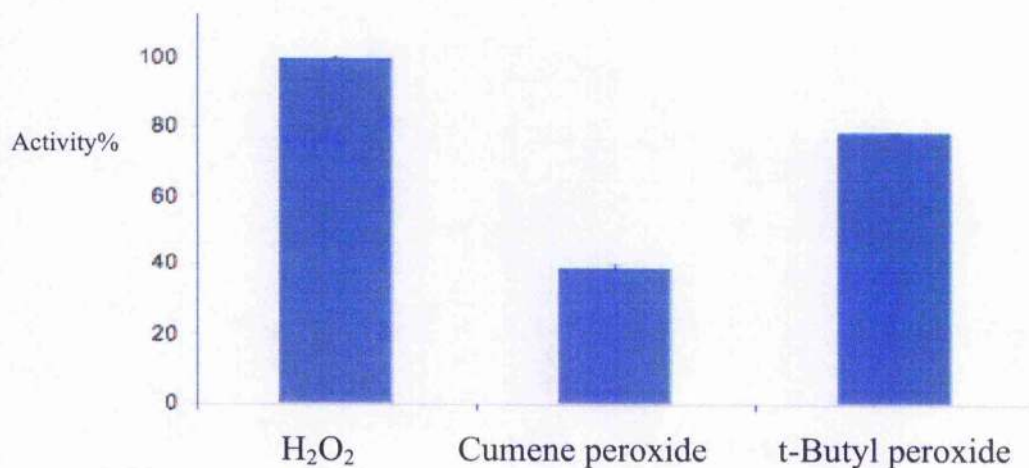


Figure 4.3 Relative activity of PrxIII with organic hydroperoxides as substrate

NADPH oxidation was monitored at 340nm in a 1ml reaction mixture containing 50 mM Tris-HCl, pH 7.5, 100 μ M NADPH and the indicated combinations of 2 μ M Trx, 1 μ M TRR, 5 μ M PrxIII and 0.1mM peroxide substrate. The activity of PrxIII coupled with H_2O_2 was used as the reference which has 100% activity. All reactions were performed in triplicate.

4.2.3 Effect of H₂O₂ concentration on overall PrxIII pathway activity

To examine the substrate concentration dependence of the PrxIII pathway, different concentrations of H₂O₂ were added into the PrxIII assay (Fig 4.4). At the lowest H₂O₂ concentration shown (20 μ M), maximal rates of reaction were already achieved which showed that PrxIII displayed a very high affinity for its peroxide substrate. In the range 20 μ M to 250 μ M H₂O₂, the PrxIII pathway exhibited constant activity. However, at high levels of H₂O₂ (500 μ M-10 mM), there was a progressive decline in overall activity, probably caused by the overoxidation of the active site cysteines of PrxIII (see Fig 4.5).

Maximal rates of reaction with 5 and 10 μ M of H₂O₂ were also observed but not presented owing to the rapid termination of the reaction resulting from exhaustion of the substrate.

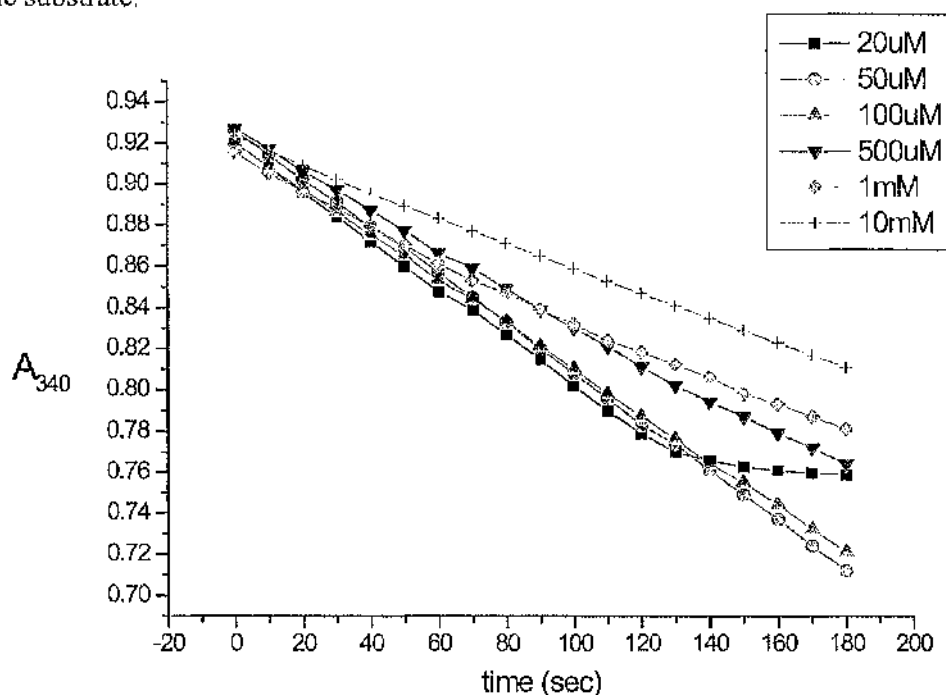


Figure 4.4 Time course of PrxIII dependent NADPH oxidation coupled to H₂O₂ reduction

NADPH oxidation was monitored at 340nm in a 1ml reaction mixture containing 50 mM Tris-HCl, pH 7.5, 100 μ M NADPH, 2 μ M Trx, 1 μ M TRR, 5 μ M PrxIII and different H₂O₂ concentrations as indicated.

4.2.4 Analysis of the oxidation-reduction state of PrxIII

Recombinant PrxIII has a subunit M_r of 25,000; however, in its oxidised state, it appears as a homodimer on SDS-PAGE (-DTT) owing to intersubunit disulphide bond formation between its N and C terminal cysteines. This property of PrxIII was exploited to monitor its change in oxidation state after treatment with increasing levels of H_2O_2 .

Initially, purified PrxIII was reduced by DTT, and excess DTT removed on a Sephadex PD-10 desalting column. Different concentrations (from $0.05\mu M$ to $1M$ H_2O_2) were mixed with $1\mu M$ PrxIII at room temperature for 10 min. Then samples were diluted with an equal volume of Laemmli sample buffer and denatured for 5 min at room temperature, prior to resolving on a 12% SDS/polyacrylamide gel. Bands were stained with Coomassie Brilliant Blue. As PrxIII was fully reduced by DTT, at very low H_2O_2 concentration only monomer (25kDa) (band a in Fig 4.6) was observed on SDS-PAGE analysis (lane 1 in Fig 4.5). With increasing H_2O_2 concentration, more PrxIII is oxidized to form dimers (band b) or partial dimers with a higher M_r (50 kDa) (lanes 2-4). Complete conversion of monomer (reduced) to dimer (oxidised) PrxIII is achieved with $10\mu M$ H_2O_2 (lane 4) confirming the high affinity of PrxIII for its natural substrate. At higher H_2O_2 levels, a more extended band of lower mobility than the normal dimer became increasingly apparent (lanes 5-9). This band may represent a partially overoxidized form of PrxIII (band c). At very high H_2O_2 concentrations, a monomer band (band d) is also evident (lanes 7-9) suggesting the presence of highly oxidised PrxIII that is incapable of dimer formation.

A scheme for the possible oxidation states of PrxIII detected by their differing gel mobility is depicted in Fig 4.6.

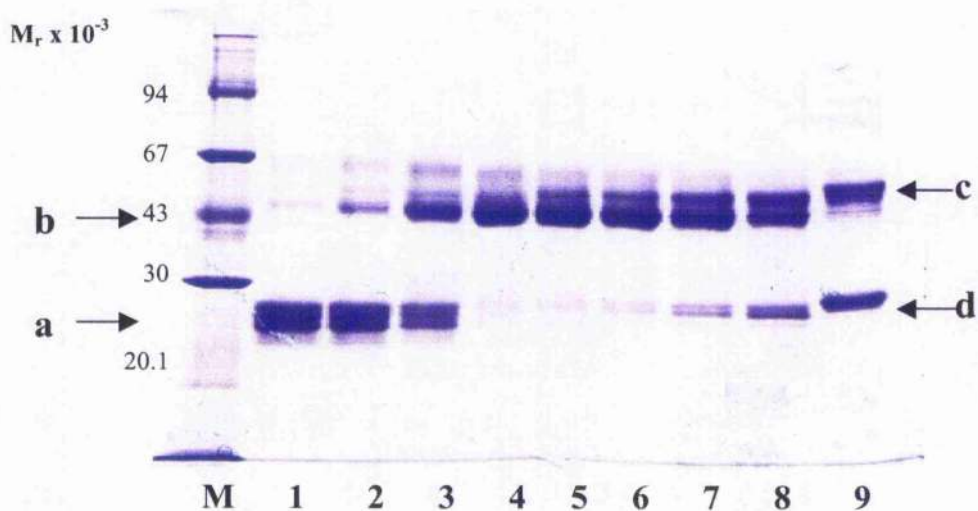


Figure 4.5 PrxIII oxidation by hydrogen peroxide

Non-reducing SDS-PAGE analysis of PrxIII (17.5 μM) oxidation by H₂O₂ at the following concentrations: lane 1, 0.5 μM; lane 2, 1 μM; lane 3, 5 μM; lane 4, 10 μM; lane 5, 50 μM; lane 6, 100 μM; lane 7, 0.5 mM; lane 8, 1 mM; lane 9, 10 mM. The possible identities of bands a, b, c and d are described in Fig 4.6. The apparent heterogeneity of the monomer bands is probably caused by aberrant formation of intra-subunit disulphide bonds in the highly oxidising conditions of the gel.

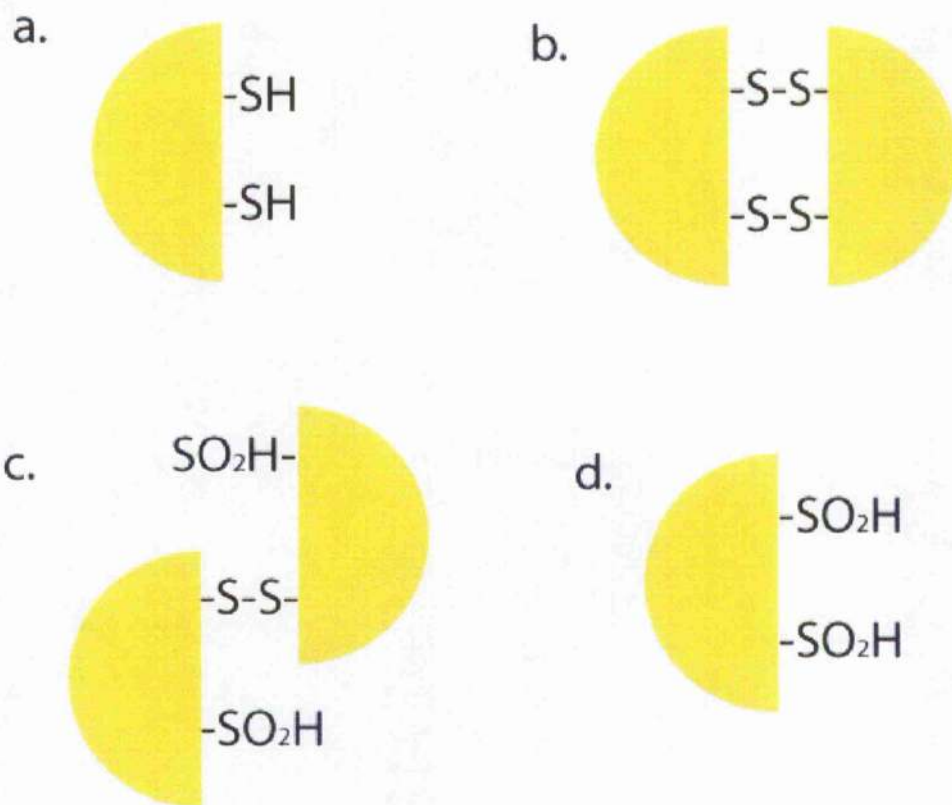


Figure 4.6 Proposed oxidation-reduction states of PrxIII produced by increasing concentrations of H_2O_2

Possible formation of different oxidation-reduction states of PrxIII. a) reduced form of PrxIII. b) oxidized form of PrxIII with two disulphide bonds forming between two adjacent subunit at relatively low H_2O_2 concentration. c) partially overoxidized (more extended) form of PrxIII at high H_2O_2 concentration which shows a dimer band of lower mobility than the normal oxidised form. d) totally overoxidized form of PrxIII at very high concentrations of H_2O_2 . In the absence of reduced sulphhydryl groups, dimer formation is prevented and monomer PrxIII is again observed on the gel. Other forms in which the sulphur is present as a sulphenic acid RSOH are of course possible.

4.2.5 Activity of the PrxIII pathway over a wide range of H₂O₂ concentrations

To examine if PrxIII can be completely overoxidised and therefore inactivated by H₂O₂, a wider range of H₂O₂ concentrations was tested in the PrxIII assay (Fig 4.7).

At very low H₂O₂ concentration (20μM), the PrxIII pathway reaches maximal activity. However, overall activity gradually decreased in the range of 50μM-10mM H₂O₂ predicted by the susceptibility of PrxIII to overoxidation.

Surprisingly, instead of declining to zero at higher H₂O₂ levels, a second burst of NADPH oxidation occurred, peaking at 100mM substrate, which is much higher than the physiological range. Complete inactivation required 1M H₂O₂.

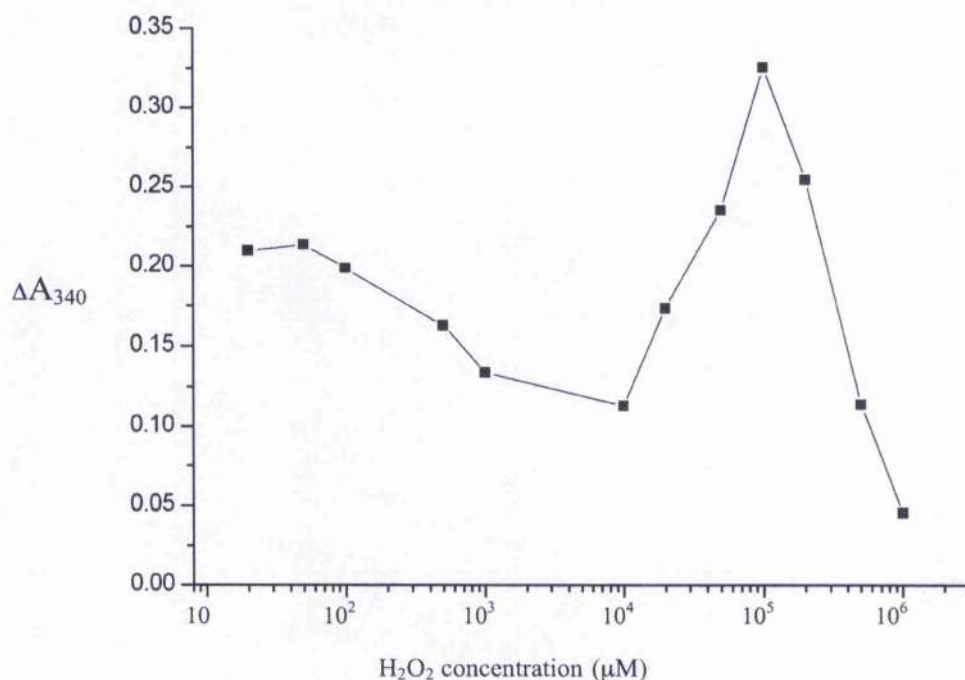


Figure 4.7 Profile of PrxIII pathway activity at different H₂O₂ concentrations
NADPH oxidation was monitored at 340nm in a 1ml reaction mixture containing 50 mM Tris-HCl, pH 7.5, 100 μM NADPH, 2 μM Trx, 1 μM TRR, 5 μM PrxIII and different H₂O₂ concentrations. The linear decrease of A₃₄₀ over 180s against the log₁₀ of H₂O₂ concentration is shown.

To investigate the reason for this unusual activity profile, different combinations of pathway components were checked. It was discovered that TRR2 alone can reduce H_2O_2 directly at high substrate concentrations but makes no contribution at low H_2O_2 levels (Fig 4.8).

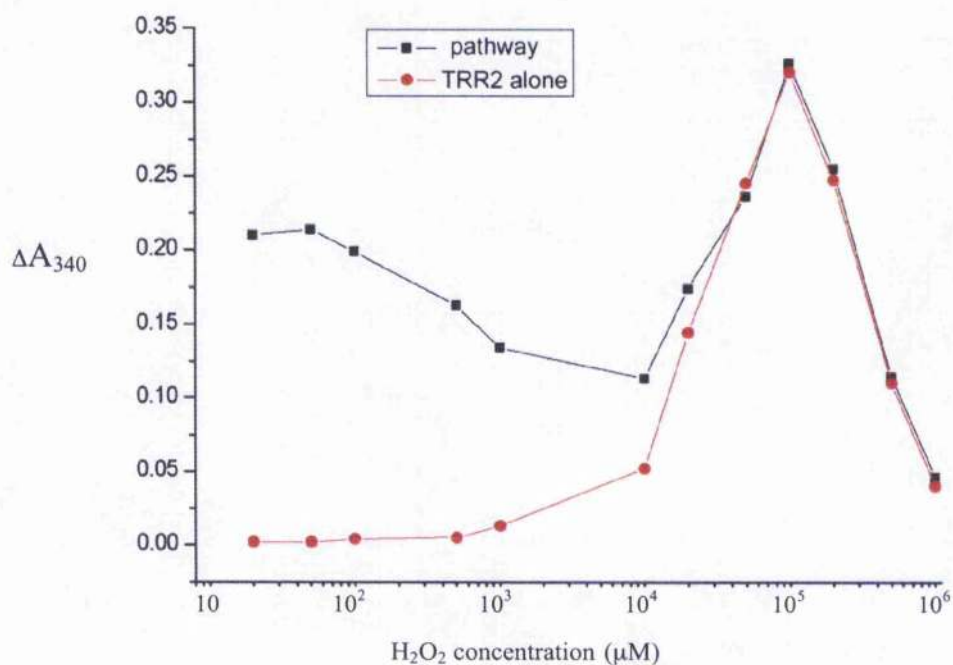


Figure 4.8 Overoxidation study of PrxIII at different H_2O_2 concentrations

NADPH oxidation was monitored at 340nm in a 1ml reaction mixture containing (red line) of 50 mM Tris-HCl, pH 7.5, 100 μM NADPH, and 1 μM TRR, and (black line) of 50 mM Tris-HCl, pH 7.5, 100 μM NADPH, 2 μM Trx, 1 μM TRR, 5 μM PrxIII and different H_2O_2 concentrations. The decrease in A_{340} over 180s against the log of H_2O_2 concentration is shown.

4.2.6 Role of the Conserved Cysteines in PrxIII Peroxidase Activity

To assess the role of the conserved cysteine residues in the catalytic activity of PrxIII, the PrxIII pathway assay was repeated for the cysteine mutants (Fig 4.9).

C47S and C168S show no activity as did the control which had no H₂O₂ added. C66S shows very similar activity to the wild-type enzyme. These results confirm the role of cysteine 47 and 168 in catalysis, and also indicate that the non-conserved Cys 66 is not essential for enzyme activity.

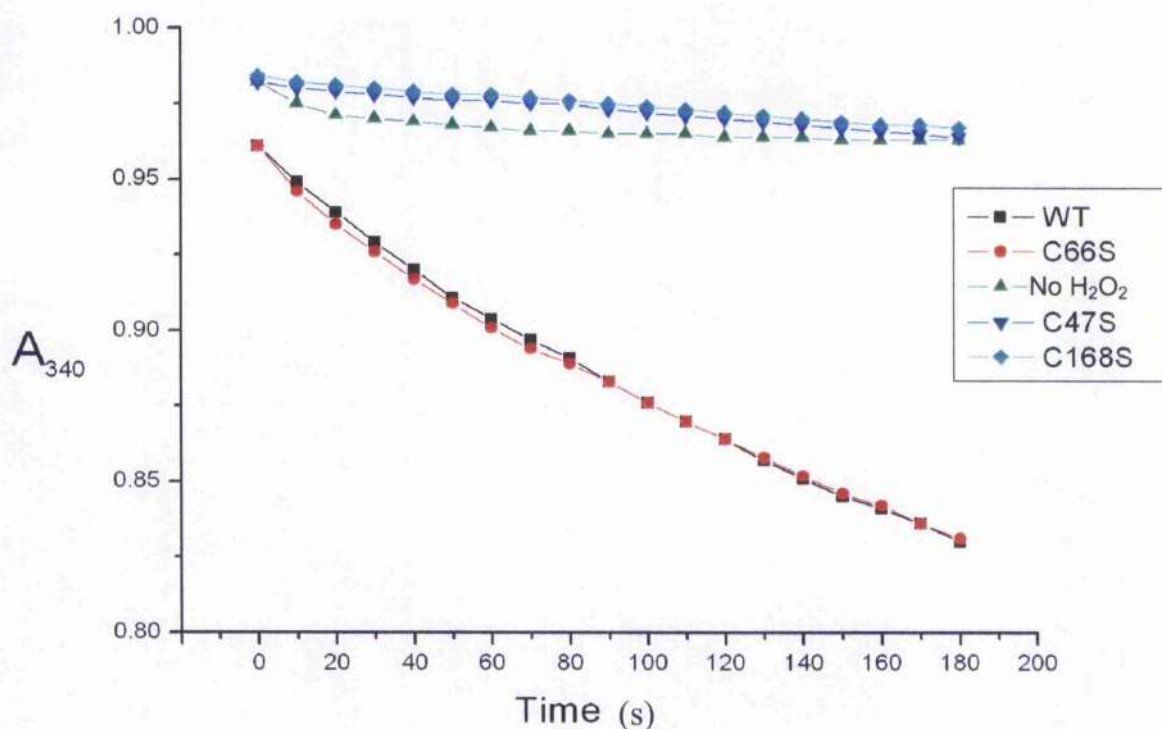


Figure 4.9 Time course of PrxIII dependent NADPH oxidation coupled to H₂O₂ reduction for various cys mutants of PrxIII

NADPH oxidation was monitored at 340nm in a 1ml reaction mixture containing 50 mM Tris-HCl, pH 7.5, 100 μ M NADPH, 2 μ M Trx, 1 μ M TRR, 0.1mM H₂O₂ and 5 μ M of various PrxIII mutants. Reaction without H₂O₂ (green line) was used as the negative control. Reaction with wild type PrxIII (black line) was used as positive control.

4.2.7 Gel filtration analysis of the oligomeric state of PrxIII

Gel filtration chromatography (GFC) was used to study the oligomeric state of PrxIII under various conditions (Fig 4.10).

His-tagged PrxIII, purified by MC chromatography, was buffer exchanged into 25mM HEPES pH 7.2, 50 mM NaCl, 5mM EDTA buffer and run through a Sephacryl S-300 gel filtration column (Material and Methods section 2.4.7). Fractions (1ml) were collected and analysed by SDS-PAGE to confirm that the peaks represented the target protein. V_c was determined from monodisperse, symmetrical peaks.

Previous studies in our laboratory have shown that PrxIII exists as a stable oligomeric toroid with an apparent M_r value of 450-500 kDa. The oligomeric state of PrxIII was found to be independent of changes in influence of pH in the range 5-9 or ionic strength (0-2M NaCl). Therefore, in this study, the redox state, protein concentration and the presence of the His-tag on the stability of the PrxIII oligomer was tested as shown in Fig 4.10. Removal of the His-tag from oxidised PrxIII caused its complete dissociation into a low M_r value, 50 kDa dimeric form at low protein concentration (1mg/ml) whereas at higher levels (10mg/ml), a mixture of high M_r (dodecamer) and dimeric forms was present. In contrast, His tagged PrxIII existed exclusively in its high M_r oligomeric state even at low protein concentration. Reduced PrxIII was present as oligomeric toroids regardless of protein concentration and the presence or absence of the His-tag.

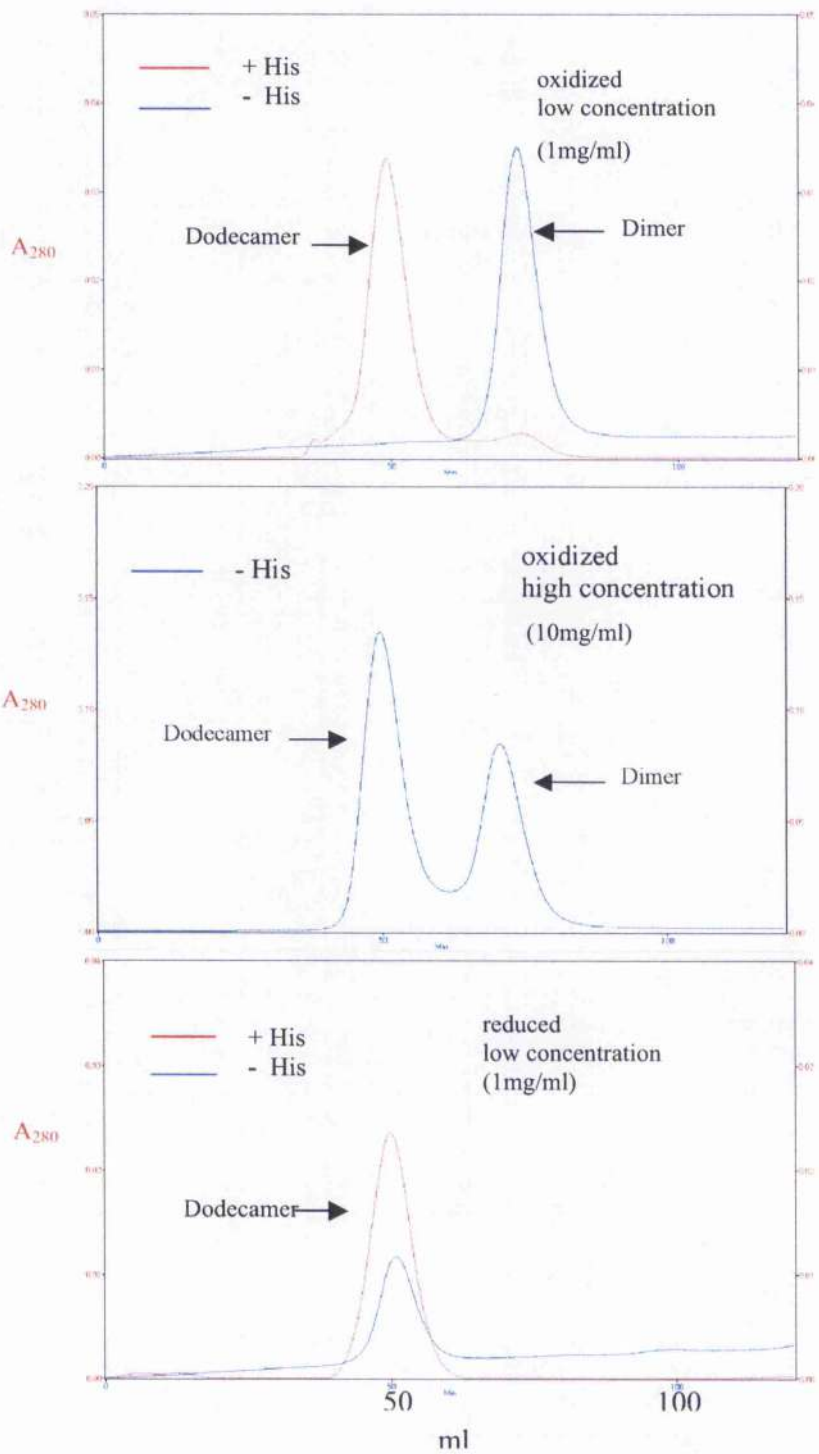


Figure 4.10 Gel Filtration Chromatography (GFC) elution profile for PrxIII
 GFC analyses were used to determine the oligomeric state of PrxIII. Blue lines represent protein without His-tag. Red lines represent protein with His-tag.

4.3 Discussion

By completing the cloning, overexpression and purification of PrxIII, Trx2 and TRR2, it has been possible to reconstitute the entire mitochondrial PrxIII antioxidant defence pathway *in vitro*. To develop the optimal conditions for determination of pathway activity, different concentrations of pathway components were varied independently in the reconstituted pathway assay to achieve a situation where PrxIII levels were rate limiting to the overall reaction. A relatively high concentration of TRR2 was required, presumably reflecting the low specific activity of the recombinant enzyme compared to its wild-type counterpart. However, as TRR2 also has the capacity to reduce H₂O₂ directly in an NADPH-dependent manner, care was also taken to ensure that this secondary reaction did not interfere with direct measurement of the activity of the complete antioxidant defence pathway.

The results show, particularly at low H₂O₂ concentrations in the physiological range, that the presence of all three pathway components is essential for reconstitution of activity. At high H₂O₂ concentrations in the non-physiological range, the NADPH-dependent TRR2 can reduced H₂O₂ directly, presumably by leakage of electrons from its flavin rings. Another mitochondrial member of the pyridine nucleotide family of oxidoreductase family, dihydrolipoamide dehydrogenase, is also reported to have an NADH oxidase activity in which electrons are transferred from the edge of the flavin ring onto dissolved oxygen to form H₂O₂ in solution (Gazaryan *et al.*, 2002).

The susceptibility of other Prxs to overoxidation has been reported previously (Yang *et al.*, 2002). The floodgate theory (Wood *et al.*, 2003) was used to explain the possible physiological reason for this. This theory proposes that at low H₂O₂ concentrations, Prxs will play an anti-oxidant defence role in reducing H₂O₂ levels. However, when H₂O₂ concentrations are elevated sufficiently, the Prxs will tend to lose activity allowing H₂O₂ to act in a signalling capacity. The results from PrxIII also agree with this observation and are clearly shown by SDS-PAGE gel assay. Wood *et al.* (2003) also find that and the AhpC, a bacterial peroxiredoxin, is more than 100 times less susceptible to overoxidation than human Prx I. Thus they have

concluded that bacterial peroxiredoxins only behave as antioxidants whereas their eukaryotic counterparts also regulate H₂O₂-mediated signalling.

Until recently the overoxidation of Prxs was thought to be irreversible. However, Woo *et al.* (2003) showed that the sulphinic acid form of PrxI, produced during the exposure of cells to H₂O₂, is rapidly reduced to the catalytically active thiol form. A protein called sulphiredoxin (Srx), which was first identified in yeast and conserved in higher eukaryotes, was found to be able to reduce cysteine-sulphinic acid in the yeast peroxiredoxin Tsa1 (Biteau *et al.*, 2003). The ability of eukaryote cells to repair the overoxidized protein suggests its function is subject to redox-mediated regulation.

The PrxIII pathway attains maximal activity at very low H₂O₂ concentrations (10µM or lower) owing to its high affinity for this substrate. In these circumstances, it is impossible to measure the K_m of PrxIII for H₂O₂ owing to the rapid exhaustion of substrate. Unexpectedly, when testing for the susceptibility of the pathway inhibition at high H₂O₂ levels, a second peak of NADPH-dependent peroxiredoxin activity was detected, that was contributed by TRR2 only. It is not clear whether this TRR2 activity at 10mM-1M H₂O₂ has any physiological relevance. TRR1 was also reported to have peroxidase activity with a K_m value at 2.5mM for H₂O₂ (Zhong and Holmgren, 2000).

On GFC analysis, dissociation of the dodecamer in its oxidised form was found to occur at low protein concentration. Interestingly, the presence of the His-tag sequence affects the stability of PrxIII oligomerization. No previous studies have reported on the possible contribution of the N-terminal His-tag to the oligomerization of Prxs. Unfortunately, the N-terminal sequence was not ordered enough to see in the crystal structure, so how the N-terminal His-tag affects dimer-dimer interactions is unclear. However, as the His-tag can be cleaved off by thrombin, experiments can be performed in the presence or absence of the His-tag for comparison. Preliminary results (not shown) indicate no difference in peroxidase activity using the PrxIII pathway assay between the enzyme with or without its His-tag protein.

The redox-state of PrxIII also acts like a switch of oligomerization. The oligomeric properties of this 2-Cys Prx have been studied using different methods. Factors such as ionic strength, pH, magnesium or calcium concentration have been shown to affect the oligomeric states of Prxs. Here, our results also showed that concentration affects oligomeric state of non-His-tagged protein in oxidised form. However, reduction of the active-site disulphide bond of typical 2-Cys Prxs is shown to be the primary factor governing the stability of the ring structures (Wood *et al.*, 2002). The exact relationship between peroxidase activity and oligomeric state is still unclear, but they appear to be closely linked.

Chapter 5

Solving the Structure of PrxIII

5.1 Results

5.1.1 Protein purification for crystallization

PrxIII was first purified by zinc metal chelate chromatography as described previously (Gourlay *et al.*, 2003). For the crystallization study a further purification step was needed, therefore the zinc metal chelate chromatography was followed by an anion exchange POROS® HQ column with buffer exchanged into 50mM Tris-HCl pH 8.5 with an NaCl gradient (0-1M) used to elute the protein (Material and Methods section 2.4.7). Another buffer exchange was performed into 50mM NaCl, 20mM HEPES pH 7.2, 10mM dithiothreitol (DTT) and 5mM EDTA followed by gel filtration chromatography with the purified protein used directly for crystallization.

5.1.2 Sitting drop vapour diffusion

All crystallization trials were conducted using the sitting drop technique. Typically, crystallization reagent (1 ml) was added to the reservoir and 2µl of purified protein solution was mixed with 2µl of reservoir solution on the platform of the trays. The crystal trays were then sealed by Crystal Clean™ tape and kept in the incubator at an appropriate temperature for equilibration.

5.1.3 Crystallization screening

Crystallization trials were performed at different temperatures but mainly at 16°C. The initial crystal screening was carried out with Crystal Screen™, Crystal Screen 2™ (Hampton Research), Cryo™ I and II (Jena Bioscience) and Wizard™ Screens I and II (Emerald BioSystems). A protein concentration of 10mg/ml was used for the screen.

Needle crystals of wild type PrxIII appeared in 3 days from condition 5 (5% isopropanol, 2.0M (NH₄)₂SO₄) of the Hampton crystal screen 2 (Fig 5.1). No other conditions gave diffracting protein crystals.

Different cryoprotectant compounds such as MPD (m-phenylene diamine), PEG

(polyethylene glycols) 400 and isopropanol were then tested. The mother liquor, with 25% glycerol added, gave no ice rings and the crystal diffracted to a similar resolution as crystals in a capillary. These crystals diffracted to 10Å resolution at beam line ID11, ESRF, Grenoble, France.



Figure 5.1 Needle crystals obtained from the initial screen
The condition is 5% isopropanol, 2.0M $(\text{NH}_4)_2\text{SO}_4$.

5.1.4 Crystallization and data collection of native PrxIII and its mutant

Many different conditions for crystal growth were screened such as protein concentration, $(\text{NH}_4)_2\text{SO}_4$ concentration, isopropanol concentration and temperature. Wild-type PrxIII crystals could only be optimised to diffract to 5\AA resolution with a relatively small size while the PrxIII C168S mutant with His-tag gave larger crystals with better diffraction (Fig 5.2). The best crystals of PrxIII C168S, grown in the condition 5% isopropanol and 1.7M $(\text{NH}_4)_2\text{SO}_4$, diffracted to 3.3\AA resolution at station 14.1, SRS, Daresbury, UK.



Figure 5.2 Optimized crystals of PrxIII C168S
The condition is 5% isopropanol 1.7M $(\text{NH}_4)_2\text{SO}_4$

After autoindexing the first image by MOSFLM (CCP4, 1994), spacegroup C2 was chosen as the best possible spacegroup with highest symmetry. A simple formula was used to estimate the maximum permitted rotation range to avoid overlap;

$$\Delta\varphi = 180d/\pi a - \eta$$

where the factor $180/\pi$ converts radians to degrees, η is the angular width of the reflection (mosaicity and beam divergence), d is the high-resolution limit and a is the length of the primitive unit-cell dimension along the direction of the X-ray beam (Wonacott, 1977). Due to the low-resolution data (3.3\AA), relatively large mosaicity (0.8°) and relatively long axes ($a=303.5\text{\AA}$; $c=122.3\text{\AA}$), the oscillation angle is required to be between 0.1 to 0.8 degrees to prevent serious overlap of spots. However, as the crystals belong to the C2 spacegroup, 180 degree collection was required to give 100% completeness. The best crystals did not diffract strongly and 180 seconds exposure time at SRS, Daresbury for each frame was needed to give best diffraction. To account for all these factors, a long exposure time was needed to complete the dataset. Although crystals were frozen to 100°K during the data collection, radiation damage still occurred, and also the time was limited at the synchrotron to complete the data collection. Adding up these factors, 0.5 degree of oscillation was used to minimise overlap of neighbouring lunes with most output.

Data were indexed by MOSFLM using three blocks of data 45 degrees apart (0 , 45 and 90). Each block contains 2 images. All together 863 reflections with $I/\sigma(I) > 20$ were used for indexing. C2 was chosen for the highest symmetry with lowest penalty (Table 5.1). Data were processed to 3.47\AA (using a 50% cut-off from R_{merge}). Details of the data collection and processing are summarized in Table 5.2.

No.	Penalty	Latt	a	b	c	alpha	beta	gamma	Possible spacegroups
10	176	mC	264.81	81.08	160.15	105.1	119.6	71.3	C2
9	174	mP	81.08	125.42	154.26	111.1	105.1	90.9	P2,P21
8	128	oC	125.42	288.37	81.08	73.6	90.9	92.9	C222, C2221
7	83	mP	125.42	81.08	154.26	105.1	111.1	90.9	P2, P21
6	82	mI	148.31	276.61	81.08	89.9	122.3	87.7	C2(transformed from I2)
5	52	oI	81.08	125.42	276.61	92.8	89.9	90.9	I222, I212121
4	49	mC	288.37	125.42	81.08	90.9	106.4	87.1	C2
3	7	mC	298.07	81.08	125.42	90.9	112.1	89.7	C2
2	4	aP	81.08	125.42	154.26	69.1	75.1	90.9	P1

Table 5.1 List of possible Laue groups

Indexing using 863 reflections with $I/\sigma(I) > 20$, the possible Laue groups sorted on penalty index. The lower the PENALTY, the better. The chosen one is highlighted in blue.

Space group	C2
Unit cell dimensions (Å)	a=303.5; b=79.1; c=122.3
β (°)	115.5
Resolution (Å)*	35-3.47(3.54-3.47)
Total/unique observations	36651(10923)
Completeness(%)*	96.3(98.2)
Multiplicity*	3.1(3.1)
$R_{\text{merge}}(\%)*$	8.0(50.9)
Mean $I/\sigma(I)*$	9.8(3.2)

*Parentheses refer to final resolution shell.

Table 5.2 Diffraction data statistics of native PrxIII C168S

The Matthews' coefficient (Matthews, 1968) suggested between 10 ($V_m=2.8 \text{ \AA}^3/\text{Da}$) and 12 ($V_m=2.3 \text{ \AA}^3/\text{Da}$) monomeric subunits in the crystal asymmetric unit. Since most (6 out of 8) known typical 2-Cys Prxs structures are decamers, a self-rotation function from program MOLREP was calculated. The result showed no peaks at a 72-degree chi angle indicating there is no 5-fold symmetry in the crystal structure (Fig 5.3). However, there are 3 peaks at 60-degree chi angle indicating three 6-fold symmetry axes and also there are 3 lines of 6 peaks indicating 2-fold symmetry (Fig 5.4). In each line the peaks occur at an angle of 30 degree to each other and are all perpendicular to a 6-fold peak, which also coincident with a 2-fold peak. Taken together these facts suggest a dodecameric rather than a decameric structure.

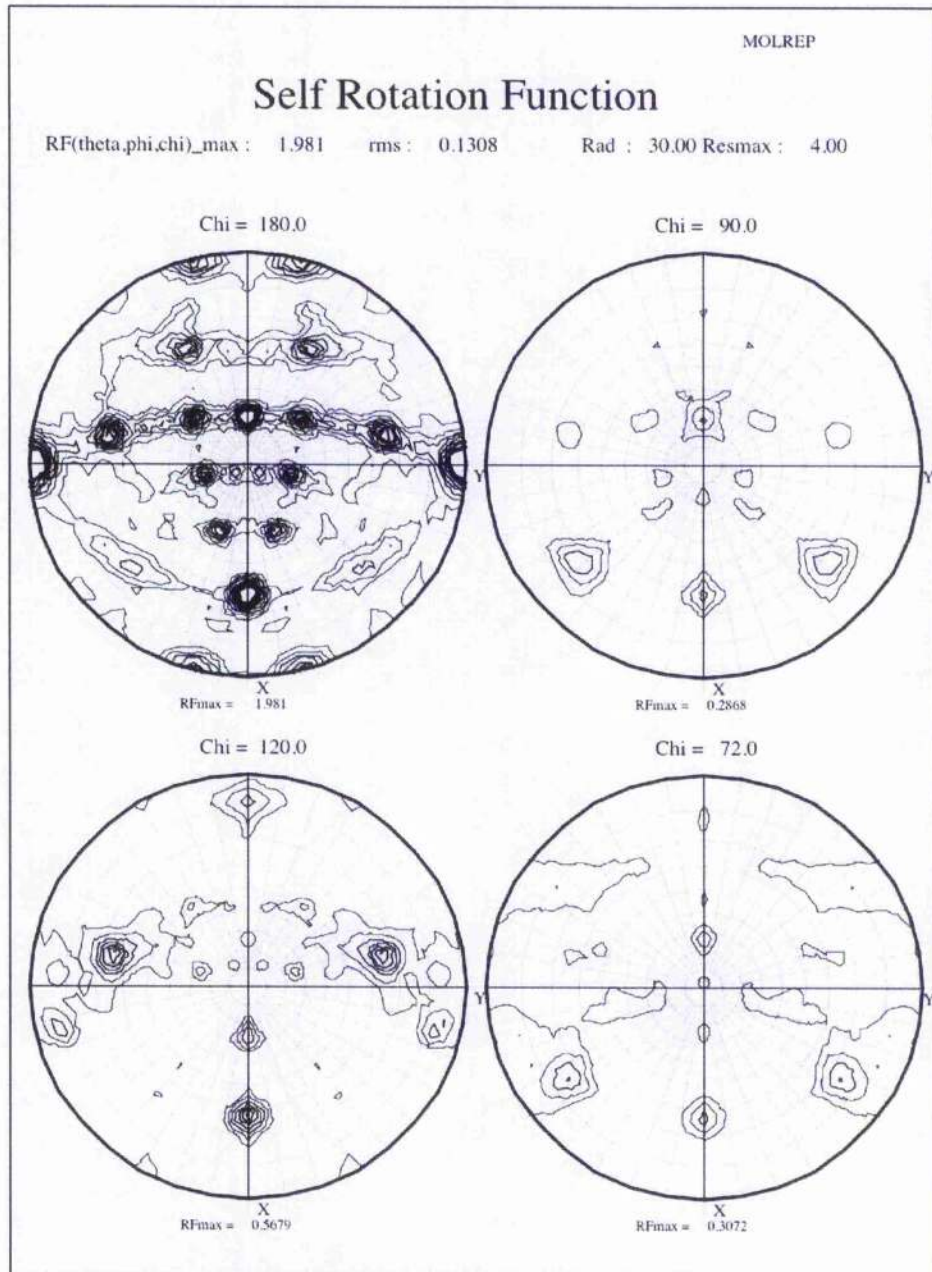


Figure 5.3 The self-rotation function of PrxIII C168S

The self-rotation function was calculated by the program MOLREP with data in the 10-4 Å resolution range and an integration radius of 30 Å with chi angle at 180, 120, 90 and 72 degrees.

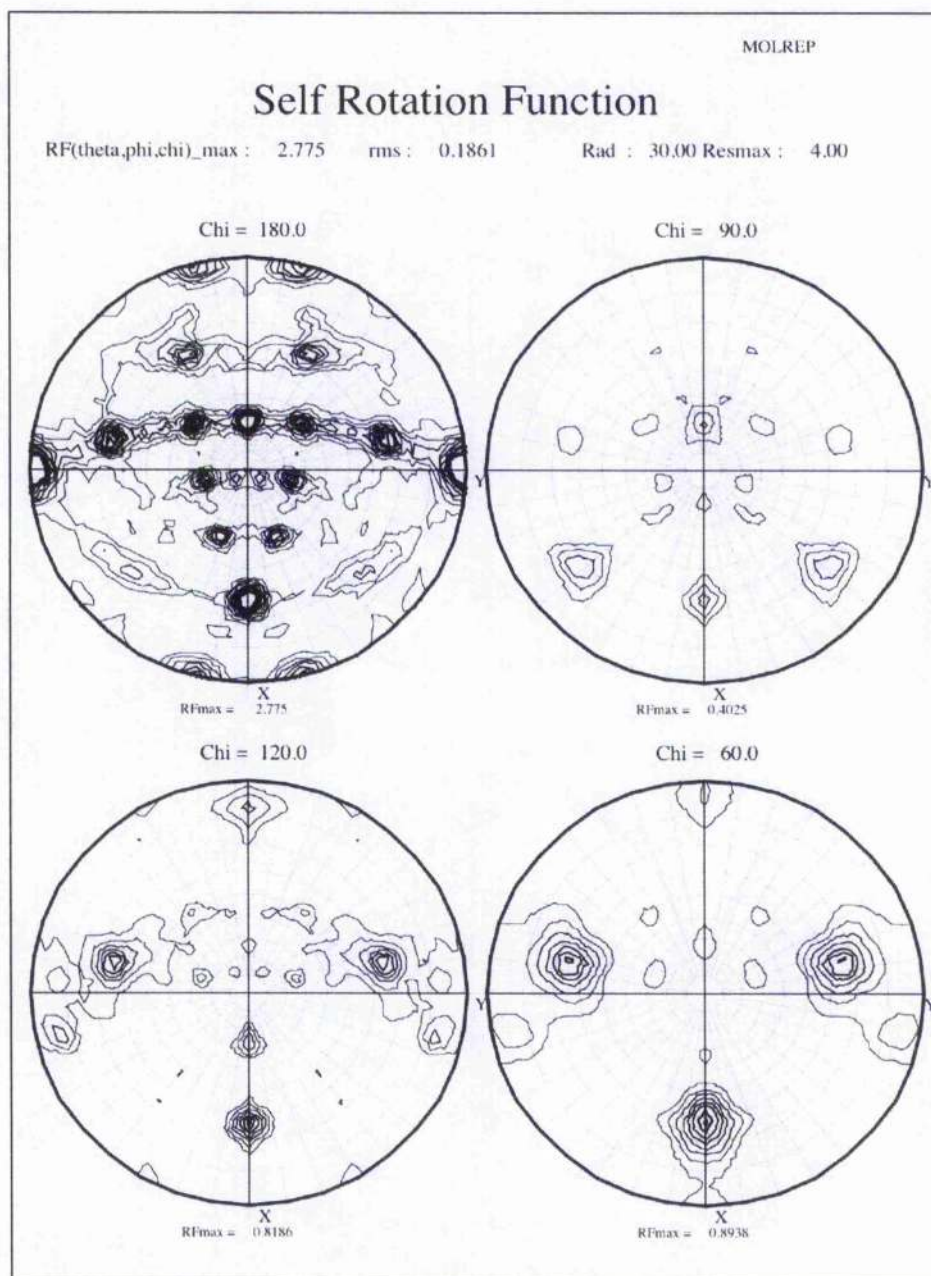


Figure 5.4 The self-rotation function of PrxIII C168S

The self-rotation function was calculated by the program MOLREP with data in the 10-4 Å resolution range and an integration radius of 30 Å with chi angle at 180, 120, 90 and 60 degrees.

Thioredoxin peroxidase B (TPxB, PDB code 1qmv, (Schroder *et al.*, 2000)) was chosen as the search model for the molecular replacement strategy for its high sequence similarity with PrxIII (64% identity and 22% similarity, see Fig 5.5) and high resolution crystal structure (1.7Å). The molecular replacement programs MOLREP (CCP4, 1994), AMoRe (Navaza, 1994) and PHASER (Storoni *et al.*, 2004) with the default parameters using TPxB monomer, dimer and decamer as the starting model were all tried without any successful solutions. For example, AMoRe was run by autoAMoRe mode using data in the 10-4.0Å resolution range with a rotation function search sphere set to 30Å. No solution stood out. Similar parameters were used to run a rotation function using a monomer as the search model and then all peaks were used to run a translation function independently. After the first monomer was located, the program was asked to add the second one and so on. However, after 3 or 4 monomers were added together, clashes were found between monomers. PHASER was run using data in the 20-4.0Å resolution range in an auto search which includes rotation, translation and packing. The sequence identity was set to 65%. The solution had a very low Z-score indicating a failure to find the right solution. With the unsuccessful trial of molecular replacement, ScMet protein was prepared to determine the structure by MAD phasing.

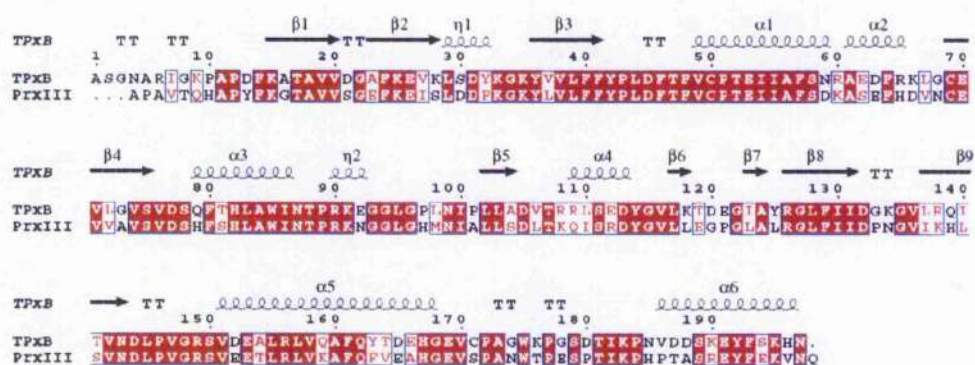


Figure 5.5 Sequence alignment between thioredoxin peroxidase B (PDB code 1qmv) and PrxIII

Identical residues are outlined in red. The secondary structural elements of TPxB are shown. Sequence alignment performed with ClustalW (Chenna *et al.*, 2003) and the figure generated with ESPript (Gouet *et al.*, 1999)

5.1.5 SeMet PrxIII C168S

Within each subunit there are 2 methionines out of a total of 220 amino acids. One methionine is at amino acid 95 and the other is in the vector N-terminal His-tag linker sequence (Fig 2.2).

SeMet PrxIII production is described in Material and Methods section 2.2.9. The SeMet protein purification employed the same protocol as native protein except all buffers were degassed to prevent selenium oxidation.

The best crystals of SeMet PrxIII C168S were obtained from 2 μ l drops of protein solution (38 mg/ml) mixed with a 2 μ l volume of a reservoir solution containing 1.65 M ammonium sulphate and 5% isopropanol. These crystals grew to a size of 0.5 x 0.2 x 0.2 mm in a week.

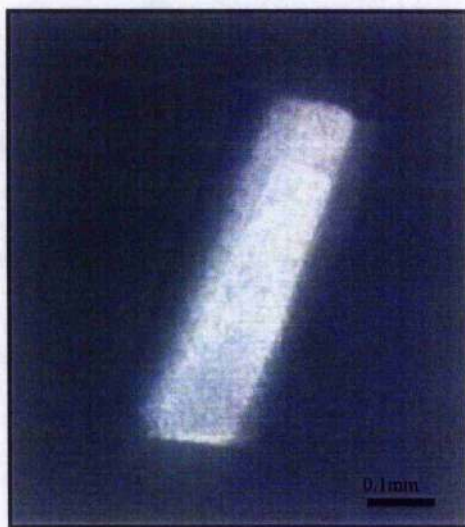


Fig 5.6 SeMet PrxIII C168S crystals

Growth condition was 1.65 M ammonium sulphate and 5% isopropanol

5.1.6 Data collection

Mother liquor with 25% (v/v) glycerol was used as a cryoprotectant. X-ray diffraction data sets were collected at 100°K using synchrotron radiation (European Synchrotron Radiation Facility, Grenoble, France) at the BM14 beamline equipped with a MARMOSAIC225 CCD detector.

An energy scan (Fig 5.7) was performed to determine the wavelengths of peak and inflection point to give the maximum anomalous signal. The wavelength was set at 0.9790Å for the peak, 0.9792 Å for the inflection and 0.9537 Å for the remote. A 30s exposure time was used for each frame. In total 720 frames were recorded for the peak data with a crystal-detector distance of 325 mm and 0.5 degree of oscillation for each frame. Subsequently 360 frames were recorded for the inflection data with a crystal-detector distance of 325 mm and 0.5 degree of oscillation. Finally 360 frames were recorded for the remote data with a crystal-detector distance of 335 mm and 0.5 degree of oscillation with 30s exposure time.

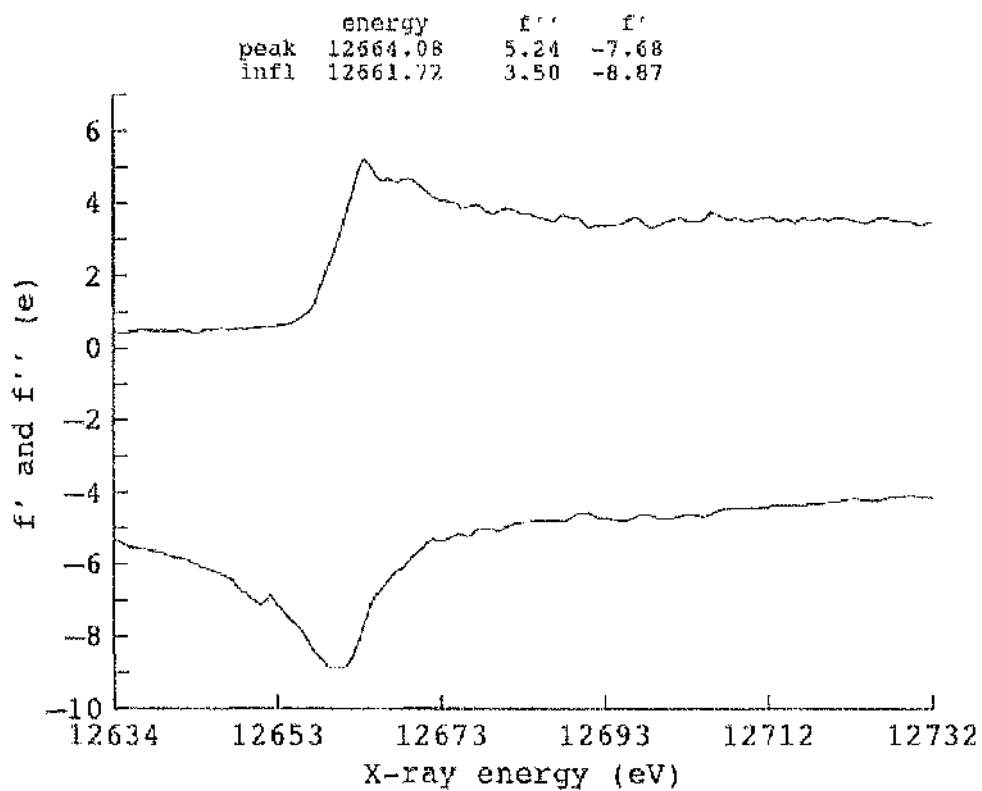


Figure 5.7 Energy scan of SeMet PrxIII C168S crystal

Data were indexed by MOSFLM using a similar strategy to that described in section 5.1.4. C2 was chosen for the highest symmetry with lowest penalty.

All data were processed to a resolution of 3.3Å (using 50% cut-off from R_{merge}) using the programs MOSFLM, SCALA and TRUNCATE from the CCP4 package (CCP4, 1994). Data collection statistics are summarized in Table 5.3. A subset of 5% of reflections was used independently for the calculation of an R_{free} to assist decisions regarding refinement protocols.

The Matthews' coefficient (Matthews, 1968) also suggested between 10 ($V_m=2.8 \text{ \AA}^3/\text{Da}$) and 12 ($V_m=2.3 \text{ \AA}^3/\text{Da}$) monomeric subunits in the crystal asymmetric unit. The acentric moments statistics produced by SCALA (see Fig 5.8) showed no indication of crystal twinning, a result similar to that obtained for the native data.

A self-rotation function, calculated by the program MOLREP with data in the 10-4 Å resolution range and an integration radius of 30 Å showed very similar results to the native data (see Fig 5.9).

	Peak	Inflection	Remote
Wavelength(Å)	0.9790	0.9792	0.9537
Resolution (Å)*	35.8-3.3	35.8-3.3	30-3.3
Total/unique observations	314446/41825	157009/41830	156691/41665
Completeness(%)*	99.9(100)	99.9(100)	99.9(100)
Multiplicity*	7.5(7.6)	3.8(3.8)	3.8(3.8)
R_{merge} (%)*	12.2(50.7)	14.5(52.5)	13.9(62.7)
Mean $I/\sigma(I)$ *	15.9(2.2)	11.0(2.1)	12.0(2.8)

*Parentheses refer to final resolution shell.

Table 5.3 Diffraction data statistics relevant to the MAD experiment on SeMet PrxIII C168S.

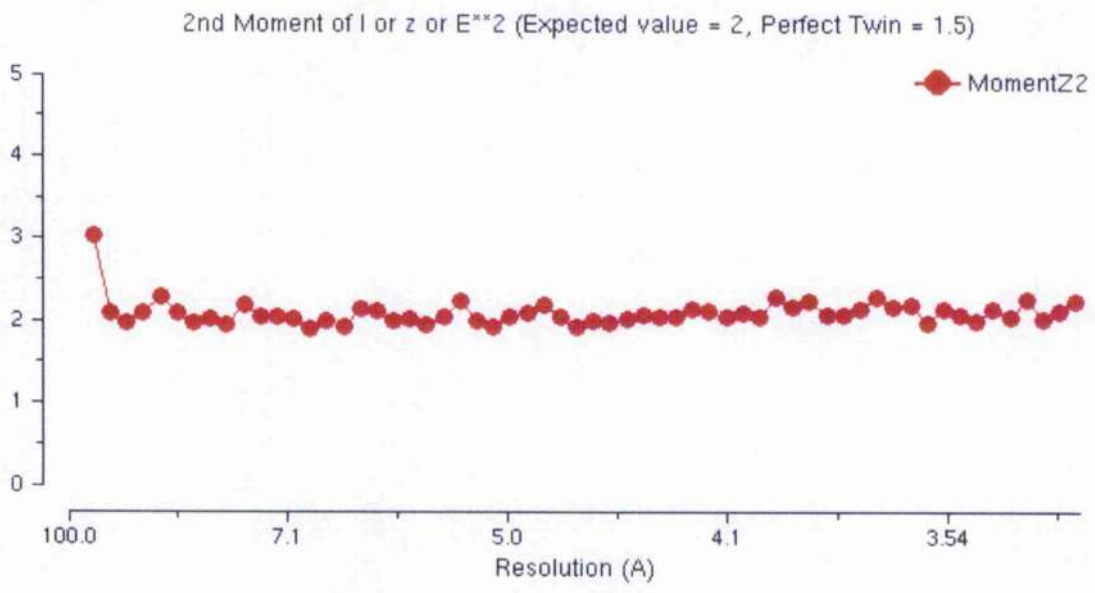
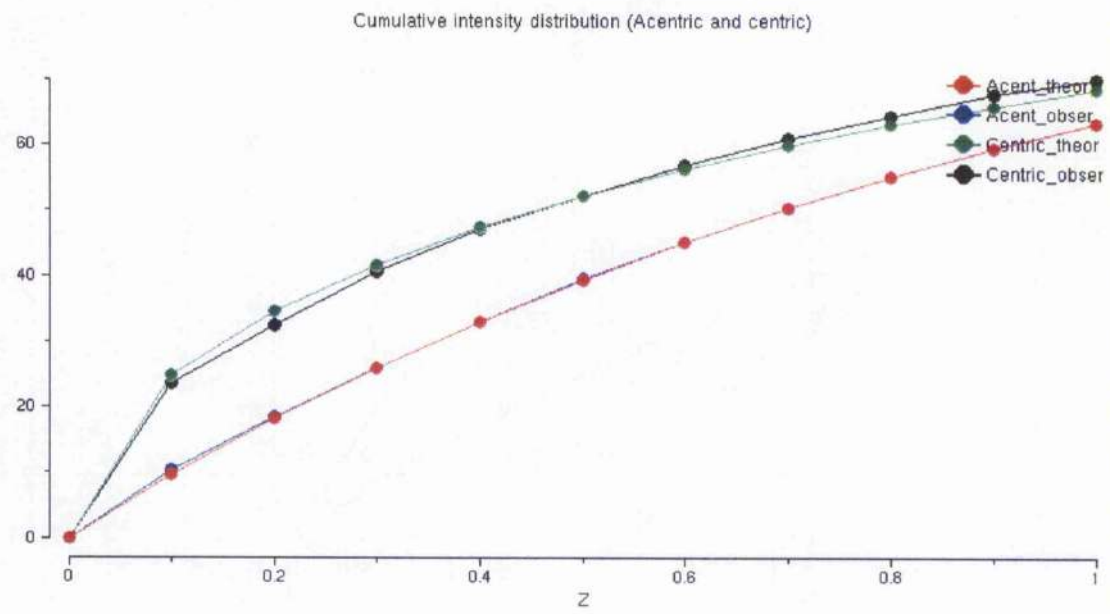


Figure 5.8 The acentric moments statistics produced by SCALA from the CCP4 package show no indication of crystal twinning.

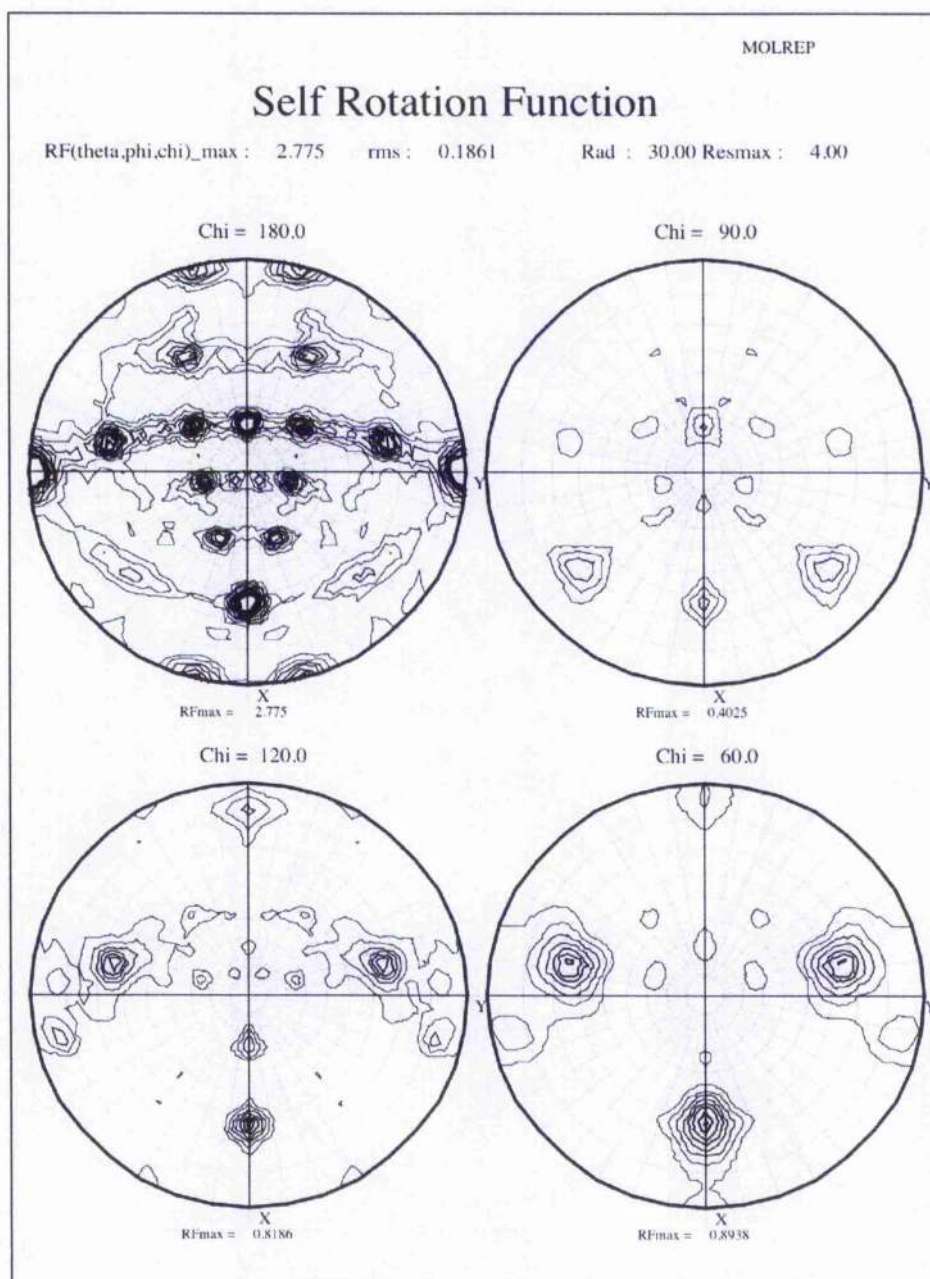


Figure 5.9 The self-rotation function of SeMet PrxIII C168S

The self-rotation function was calculated by the program MOLREP with data in the 10-4 Å resolution range and an integration radius of 30 Å with chi angle at 180, 120, 90 and 60 degrees.

5.1.7 Locating the Se

Datasets of the inflection and remote wavelengths were processed using the same protocol as the peak wavelength dataset. Three wavelengths (peak, inflection and remote) data were merged into one datafile by CAD from the CCP4 package. The multiwavelength anomalous diffraction (MAD) methods were tried in order to locate the selenium atoms from the two methionine residues in each subunit. AutoSHARP (Fortelle and Bricogne, 1997; Vourrhein, 2005), Shake and Bake (Weeks, 1999), Solve-Resolve (Terwilliger and Berendzen, 1999) and Shelx (Schneider, 1997) all failed to locate the selenium atoms. For example, ShelxD was used to search for 24 Se atoms (12 molecules in the asymmetric unit, 2 Se atoms per molecule) using data in the 20-5Å resolution range, with minimum allowed distance between sites set to 3.5Å and tried for 20 cycles. After running, the program gave the message "No suitable Patterson vectors found". Solve was used to search data in the 10-4.5Å resolution range for 24 Se atoms in 2640 residues. The program was able to find 5 heavy atoms. However, Rcsolve couldn't improve the electron density maps to make them interpretable. Similar failures were encountered with AutoSHARP and Shake and Bake. The reasons for failing to locate Se atoms could be due to either the quality of the data and/or lack of phasing power (one Se atom per 110 residues).

5.1.8 PHASER

Due to the failure to locate the selenium atoms from MAD data, the molecular replacement approach was applied to the peak dataset. This again proved unsuccessful using an automated version of MOLREP, AMoRe and PHASER (see section 5.1.4 for details). A less automated approach for searching for oligomer structure in PHASER, which was discussed on the CCP4 bulletin board (www.ccp4.ac.uk), was introduced. The approach suggests that for an oligomeric structure, it is better to search for a monomer and use the solution file of the monomer to find other monomers. An initial solution set was obtained by PHASER (Storoni *et al.*, 2004) using a dimer of TPxB B (PDB ID 1qmv) as a model to search for only one dimer. Data from 20-4.0Å resolution were used. Applying the solution a new run of PHASER was employed to search for another two dimers and

a solution locating a semi-circular, trimeric assembly of dimers was obtained (Fig 5.10a). On searching for another hexamer, a second independent half ring was found (Fig 5.10b). The best Z-score for the Fast Rotation Function was 12.51 (the second best with 10.94 Z-score) and for the Fast Translation Function was 11.72 (9.53 for the second best one). No clashes were found from the program after Packing and the log-likelihood gain was 783.23 (a relatively high score for PHASER) after refinement. Applying the crystallographic 2-fold symmetry along the *b* axis to these solutions gave two interlocked dodecameric ring structures.

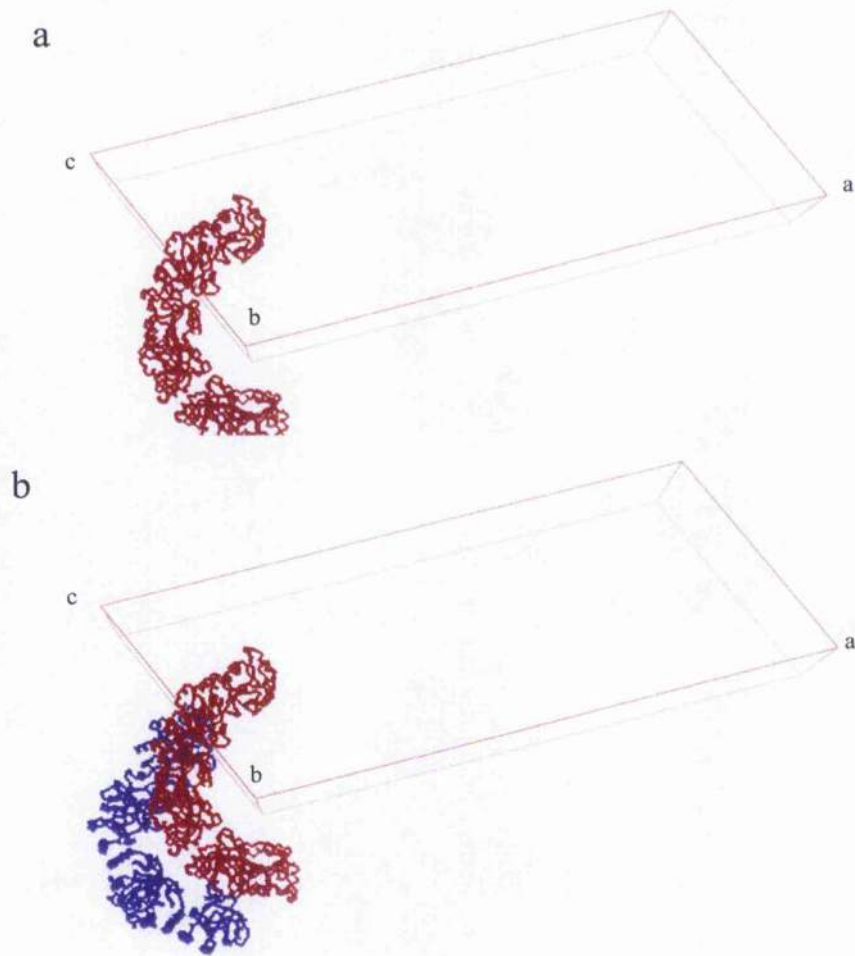


Figure 5.10 Phaser solution

a) The first semi-ring trimer dimer found by PHASER. b) The second half ring. Instead of forming a full ring, the second half ring is independent of the first ring. The view is from close to the b-axis. The figure was produced using the program PyMOL(Delano, 2002)

5.1.9 Model building and refinement

This structure was refined in ten cycles of rigid body refinement, with a dodecameric ring treated as 12 domains, using the program REFMAC5 (Murshudov *et al.*, 1997). After correcting the model to the PrxIII sequence, 5 rounds of restrained refinement with tight NCS restraints reduced R_{work} from 0.400 to 0.299, R_{free} from 0.405 to 0.356 and increased FOM from 0.598 to 0.711. An averaged map was calculated to give a much better quality map for model building. Individual residue refinements were interspersed with manual rebuilding using the programs COOT (Emsley and Cowtan, 2004) and Quanta (Accelrys). The quality of the electron density allowed modelling of amino acid residues 2-163 (of 195) for each monomer. Nine water molecules were found per asymmetric unit. Several more rounds of restrained refinement with tight NCS restraints reduced R_{work} to 0.223, R_{free} to 0.265 with good stereochemistry (Table 5.4).

$R_{work}/R_{free}(\%)$	22.3/26.5
R.m.s deviations	
Bond lengths (Å)	0.019
Bond angles (°)	1.76
Ramachandran plot (%)	
Core region	89.0
Allowed	9.3
Generously allowed	1.7
Forbidden	0

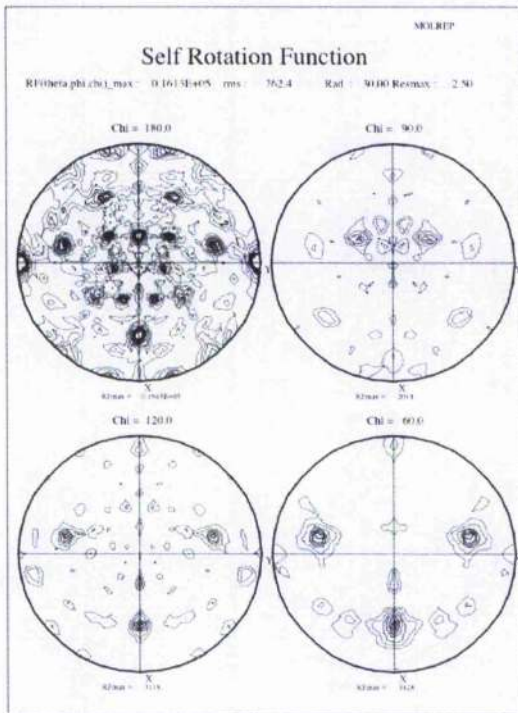
*Parentheses refer to final resolution shell.

Table 5.4 Refinement statistics of SeMet PrxIII C168S

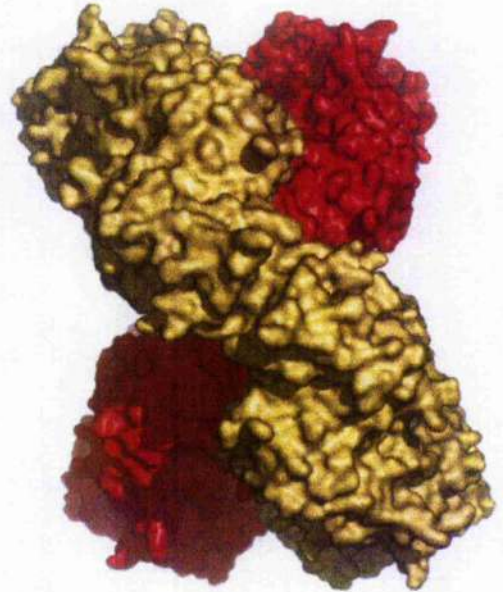
5.1.10 Self-rotation Function

The model produces an explanation for the self-rotation function data in Fig 5.9. The two lines of six 2-fold peaks ($\phi = 64, \varphi = +150$; $\phi = 38, \varphi = +130$; $\phi = 25, \varphi = +75$; $\phi = 38, \varphi = -23$; $\phi = 64, \varphi = 0$) represent the 2-fold axes in the plane of the ring. Because the ring was composed of six homodimers, there are 12 2-fold axes on the plane, which gives a 30 degree angle between adjacent axes. The two 2-fold peaks at $\phi = 66, \varphi = 104$ and $\phi = 66, \varphi = -104$, with coincident 3-fold ($\chi = 120$) and 6-fold ($\chi = 60$) axes, are the two 6-fold axes perpendicular to the planes of the rings. These two 6-fold axes are perpendicular to the 2 lines of six 2-fold axes as well. The large, apparently 6-fold, peak at $\phi = 64, \varphi = 0$ is actually the tail of a peak arising from a improper rotation of 55 degree (Fig 5.11c) which is the angle between two planes of the rings (Fig 5.11b). In addition, another 2-fold peak at $\phi = 26, \varphi = 180$ is an axis in the plane of the page and runs vertically through the centre of the model shown in Fig 5.11b. The two peaks at $\phi = 90, \varphi = 90$ and $\phi = 90, \varphi = -90$ are the crystallographic 2-fold symmetry since the spacegroup is C2.

a)



b)



c)

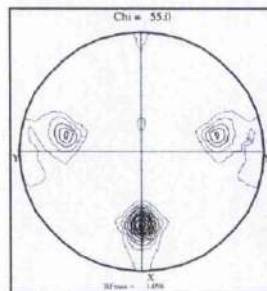


Figure 5.11 Self-rotation function explanation

a) The self-rotation function calculated by MOLREP. b) The side view of the 2-ring catenane structure. c) Same parameters as (a) but with chi angle at 55 degrees.

5.1.11 The anomalous signal contained contribution from the Se atoms

Although the MAD procedures failed to locate selenium atoms, applying the phases obtained from PHASER to the MAD data, anomalous peaks were found and located exactly at the positions of the Se atoms of the selenomethionine residues. Although some of the 12 anomalous peaks are weak, most of them are relatively strong (over 5 sigma).

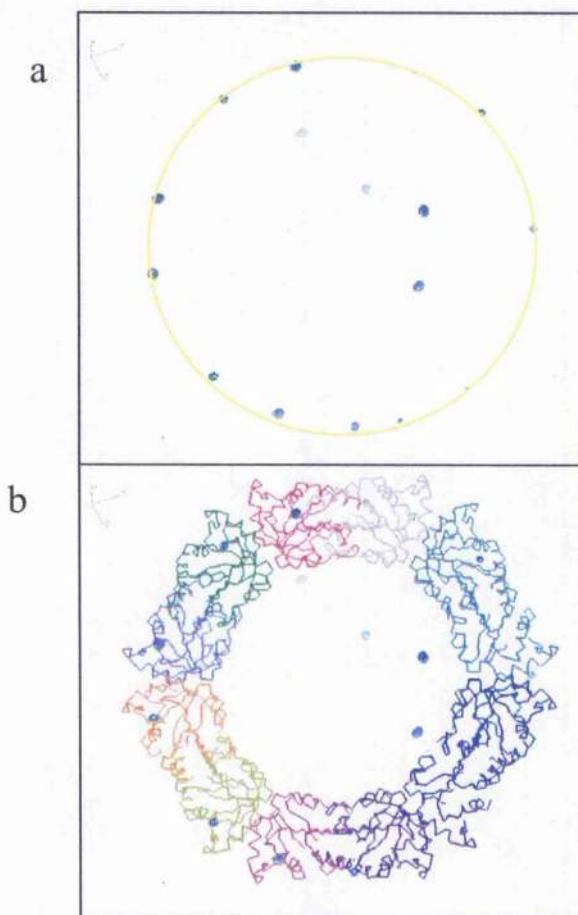


Fig 5.12 Anomalous peaks

a) The electron density map at 4 sigma by applying the MR phase to MAD data showing the anomalous signal. The yellow circle indicates the 12 peaks in one ring. **b)** By comparing the model, all the anomalous signals are accurately located at Met95.

5.2 Discussion

Wild-type PrxIII only yielded needle-like crystals that diffracted poorly with crystallization conditions containing 2M ammonium sulphate and 5% isopropanol. Better crystals were obtained from a C168S mutant around those conditions. The best crystals of PrxIII C168S were obtained from 1.7M ammonium sulphate and 5% isopropanol and diffracted to 3.47Å resolution. However, no solution could be obtained by Molecular Replacement (MR) using different Prxs as search model in various MR programs. Therefore SeMet was introduced to solve the phase problem. Apart from overexpression, the SeMet protein behaved similarly to the wild-type enzyme. Similar crystals were obtained in the conditions as previously described. Higher concentrations of protein gave bigger and better crystals; therefore, very high (38 mg/ml) concentrations of protein were used to obtain large, well-ordered crystals with a diffraction to 3.3Å resolution.

Eventually PHASER revealed a solution that was completely unexpected. The 3.3Å data enabled the main chain of the protein to be easily traced. In addition side chains within the areas of strong secondary structure were determined without any difficulties. However, the electron density in some mobile parts is very poor making it impossible to locate the position of the side chains. While the average map, comprising 12 subunits, gave a much better map overall, it did not improve much in some areas and the density map was so poor that no model could be built beyond residue 163. It is very unfortunate that the conserved C-terminal cysteine 168 could not be located and therefore, valuable information about the active site is not available.

With tight NCS restraints and manual refinement, the R_{work} dropped to 0.223 and R_{free} to 0.265, which is very good at this resolution, with good stereochemistry (Table 5.4). The structure coordinates and structure factors have been deposited to the Protein Data Bank with ID 1ZYE. The structure will be discussed in the next chapter.

Although bias could have been introduced from the search model by molecular replacement, there are several pieces of evidence that support the model. Firstly,

the R factor went down after refinement with good stereochemistry and no clashes were found with the model. Secondly, the anomalous signal contributed from Se atoms located exactly at the positions of the sulfur atoms of the methionine residues. Thirdly, analysis of the intensity distribution showed conclusively that it was not a twinned crystal. Finally, the independent program Self-rotation Function result matches the model perfectly with all the major peaks explained.

Chapter 6

Structure Analysis

6.1 Introduction

The typical 2-Cys Prxs are the largest class of Prxs and are identified by the conservation of their two redox-active cysteines, the N-terminal peroxidatic cysteine (generally near residue 50) and the resolving C-terminal cysteine (near residue 170). All the typical 2-Cys Prxs show very similar monomer structures with a thioredoxin fold, consisting of a seven stranded β -sheet with parallel and anti-parallel alignments. The sheet is surrounded by four or five α -helices of varying length. Typical 2-Cys Prxs form stable homodimers with the two subunits arranged in a "head-to-tail" fashion. The dimer interface, which has an NCS 2-fold, is created mainly by the formation of an anti-parallel β -sheet ($\beta 7$ from each monomer), which produces a 14-stranded, twisted β -sheet running through the centre of the dimer.

Crystal structures of 17 Prxs have been elucidated so far in a variety of redox and oligomeric states. Although the monomer or the dimer is the biological functional unit, most Prxs will further assemble into decameric rings (Wood *et al.*, 2003). There are two exceptions from *Mycobacterium tuberculosis*, one is a 1-Cys Prx with an octameric organisation (Li *et al.*, 2005) and another is a typical 2-Cys Prx which has been shown to exist as a dodecamer (Guimaraes *et al.*, 2005). The oligomeric properties of 2-Cys Prxs have been studied using a variety of methods. Factors such as ionic strength, pH, magnesium or calcium concentration have been shown to affect the oligomeric states of Prxs. However, reduction of the active-site disulphide bond of typical 2-Cys Prxs is shown as the primary factor contributing to stabilization of the ring structures (Wood *et al.*, 2002) and our results (see chapter 4). The exact relationship between peroxidase activity and oligomeric state is still unclear, but they appear to be closely linked.

The dimerization interfaces of Prxs were described by Sarma *et al* (2005) as A-type and B-type interfaces. The first structure of a Prx, human Prx VI (Choi *et al.*, 1998), which is a dimer in the crystal structure, has a β -sheet-based interface. They called this the B-type interface (for β -sheet). In all the crystal structures of typical

2-Cys Prxs, apart from HBP23 (see table 1.1), the protein further assembles into a ring structure formed by a pentamer or hexamer of dimers. Recent studies on the structure of hybrid PrxV (Kim *et al.*, 2003) and *E. coli* Tpx (Choi *et al.*, 2003) show they form a dimer with a different loop-based interface. Sarma *et al.* (2003) call this the A-type interface (for alternate). The dimer-dimer interfaces in the decameric and dodecamer structures are also A-type interfaces, so the decamers and dodecamers are built up using both of these interfaces. In AhpC, it has been shown that it will dissociate into B-type dimers during the catalytic cycle (Wood *et al.*, 2002). Thus, B-type dimers only exist in the typical 2-Cys Prxs while the A-type interface is much more widespread. For these reasons, Sarma and co-workers hypothesized that the A-type dimerization interface preceded the B-type interface in evolution.

An overlay of the dimer interfaces of typical 2-Cys Prxs is shown in Fig 6.1. From this figure we can tell, apart from the M1AhpC (blue line), other typical 2-Cys Prxs share very similar structures (see section 6.2.1 for detail).

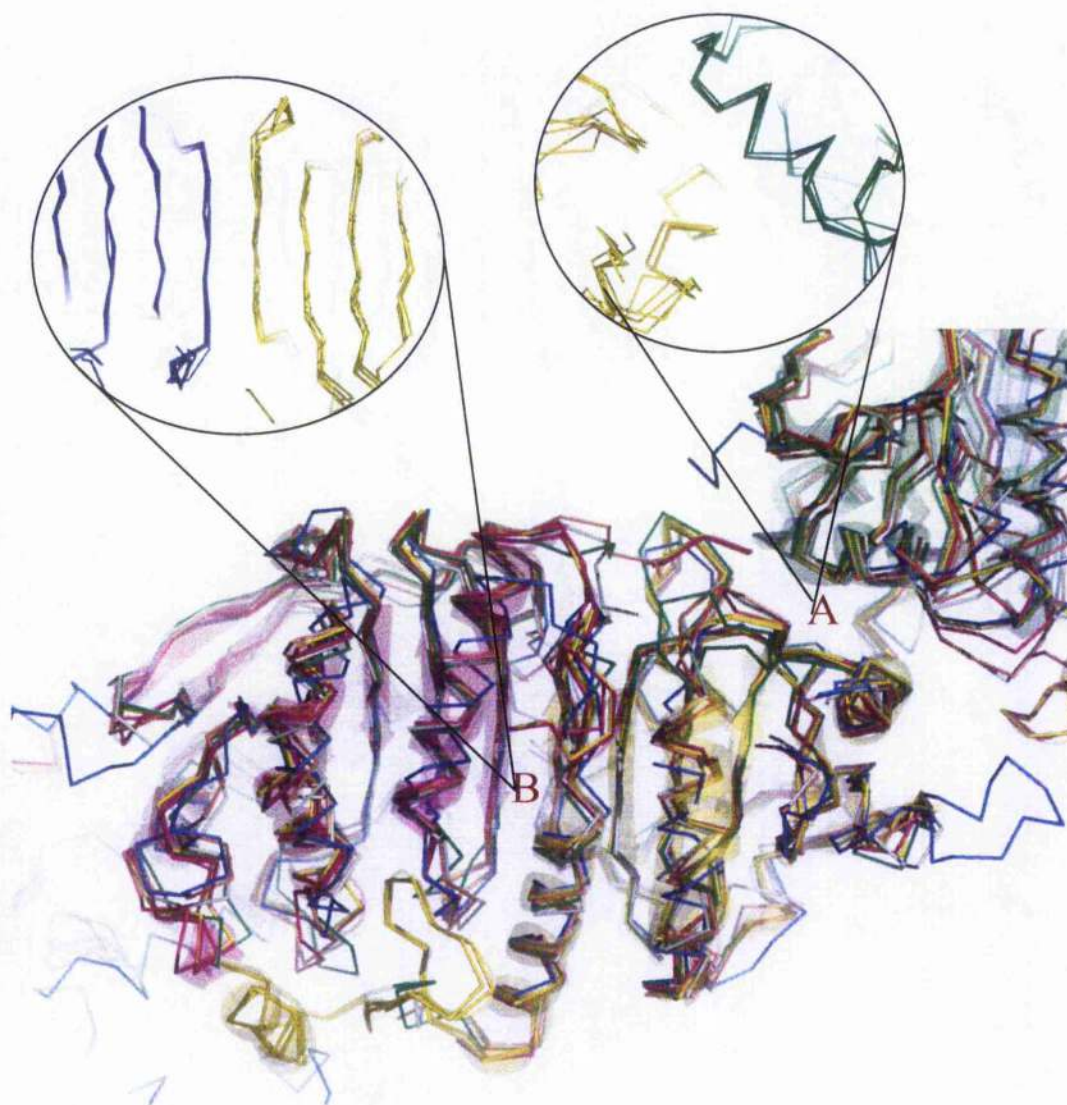


Figure 6.1 The overlay of typical 2-Cys Prxs

All structures are overlaid to chain A of TPxB (pdb 1qmv). Different subunits are shown by transparent cartoon in different colours. The interface between monomer A (yellow) and B (purple) is the B-type interface while the interface between A and C (green) is the A-type. The blue C α indicates MtAhpC. The B-type and A-type interfaces are highlighted. The figure was produced using the program PyMOL(Delano, 2002).

6.2 Results

6.2.1 Monomer structure

Monomeric bovine PrxIII C168S is a compact globular structure, with the typical thioredoxin fold of the Prx family constructed around a seven-stranded twisted mixed β -sheet, in the order $\beta 5$ - $\beta 4$ - $\beta 3$ - $\beta 6$ - $\beta 7$, surrounded by five α -helices of varying length (Fig 6.2). One face of this central β -sheet has two helices ($\alpha 2$ and $\alpha 5$) packed against it, with the other face being covered by helix $\alpha 4$ and a $\beta\beta\alpha$ structure from the N-terminal part of the protein, comprising a β -hairpin ($\beta 1$ - $\beta 2$) and following helix ($\alpha 1$). Another helix $\alpha 3$, which joins strands $\beta 4$ and $\beta 5$, is on the periphery of the monomer where it participates in oligomerization.

The PrxIII monomer structure is very close to other typical 2-Cys Prxs except MtAhpC, which forms a dodecamer rather than a decamer in the crystal structure (Fig 6.1). Firstly, MtAhpC has two additional helical structures between residues 19 and 34. Secondly, $\alpha 2$ of PrxIII has a position shift compared to the helix equivalent to $\alpha 2$ in MtAhpC. There is no significant difference in the rest of the structure. This is very surprising because only PrxIII and MtAhpC form dodecamers. However, although MtAhpC is classed as a typical 2-Cys Prx, its catalytic mechanism is different from others. It has two C-terminal Cys which compete with each other for the N-terminal Cys. This might explain the differences in sequence and structures.

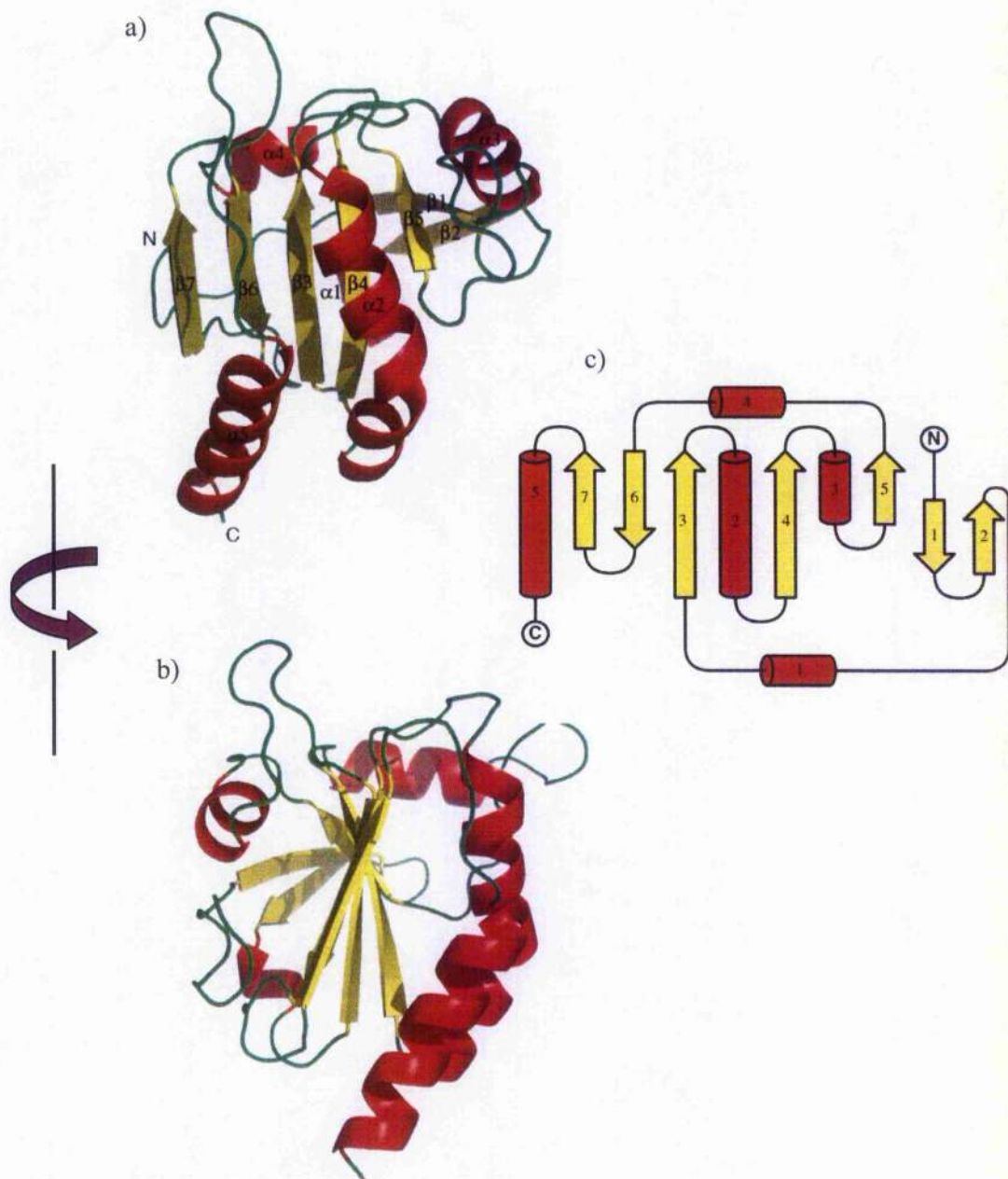


Figure 6.2 Cartoon diagram of the PrxIII monomer

a) Secondary structural elements are labelled, and N and C termini are indicated. **b)** as for a) after 90 degree rotation along the vertical axis. **c)** topology diagram of PrxIII monomer. The figure was produced using the program PyMOL(Delano, 2002) and Topdraw (CCP4, 1994).

6.2.2 Dimer structure

Stable dimers are formed across a non-crystallographic 2-fold axis that extends the central β -sheet and buries a total of 1772 \AA^2 of solvent accessible surface (886 \AA^2 per monomer). The dimer interface, which is similar to that formed in other typical 2-Cys Prx structures, is created mainly by the formation of an anti-parallel β -sheet by six mainchain hydrogen bonds involving His 136, Leu 137, Ser 138, Val 139, Asn 140 (Fig 6.3). A 14-stranded, twisted β -sheet running through the centre of the dimer was produced (Fig 6.4).

From the structure-based sequence alignment (Fig 6.5), it is clear that Prxs share very close secondary structure. PrxIII has a much higher sequence homology to decameric Prxs (63% to TPxB) than to the dodecamer Prx, MtAhpC (33%), although they have the same quaternary structure.

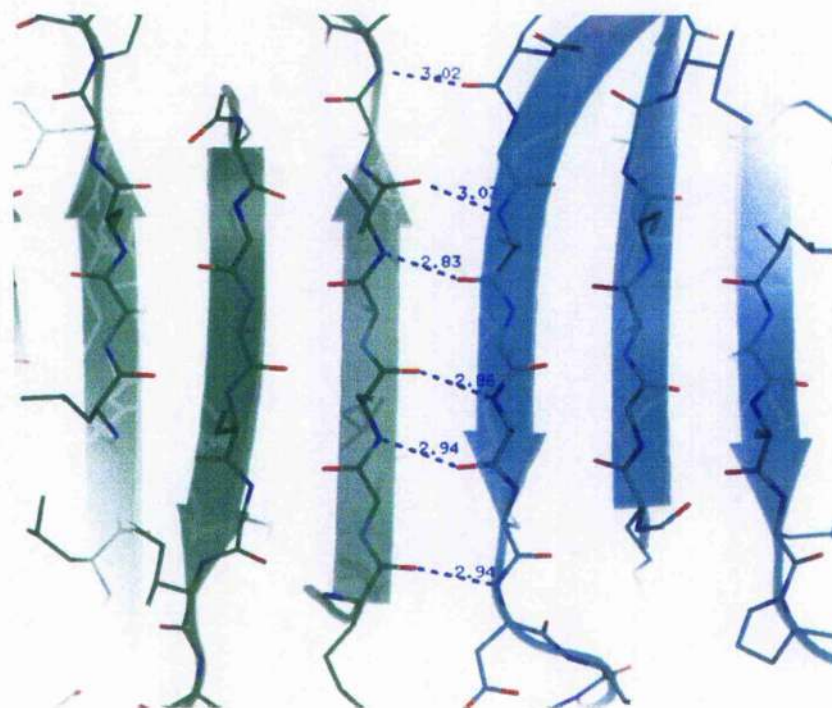


Figure 6.3 Hydrogen bonds between a pair of anti-parallel β -sheets on the PrxIII dimer interface.

Green and cyan present different subunits. Hydrogen bonds were drawn by dotted lines with the distances marked (\AA). The figure was produced using the program PyMOL(Delano, 2002).

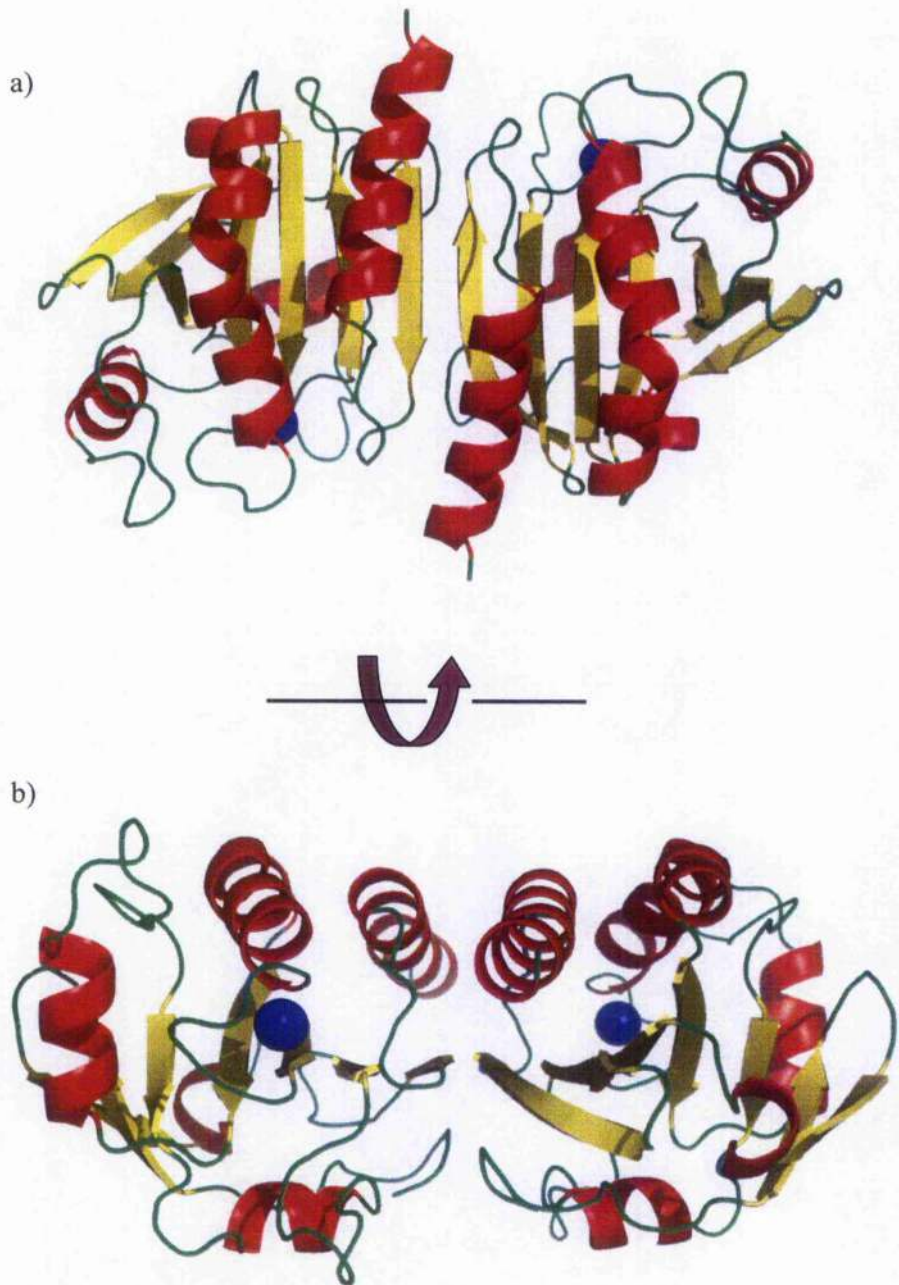


Figure 6.4 Cartoon diagram of the PrxIII dimer

a) The dimer interface is created mainly by the formation of an anti-parallel β -sheet. Cys 47 is highlighted as a blue ball. Cys 168 is close to the C-terminal of the model (5 residues) but no model can be built due to poor electron density in this region. **b)** as for a) after 90 degree rotation along the horizontal axis. The figure was produced using the program PyMOL (Delano, 2002).

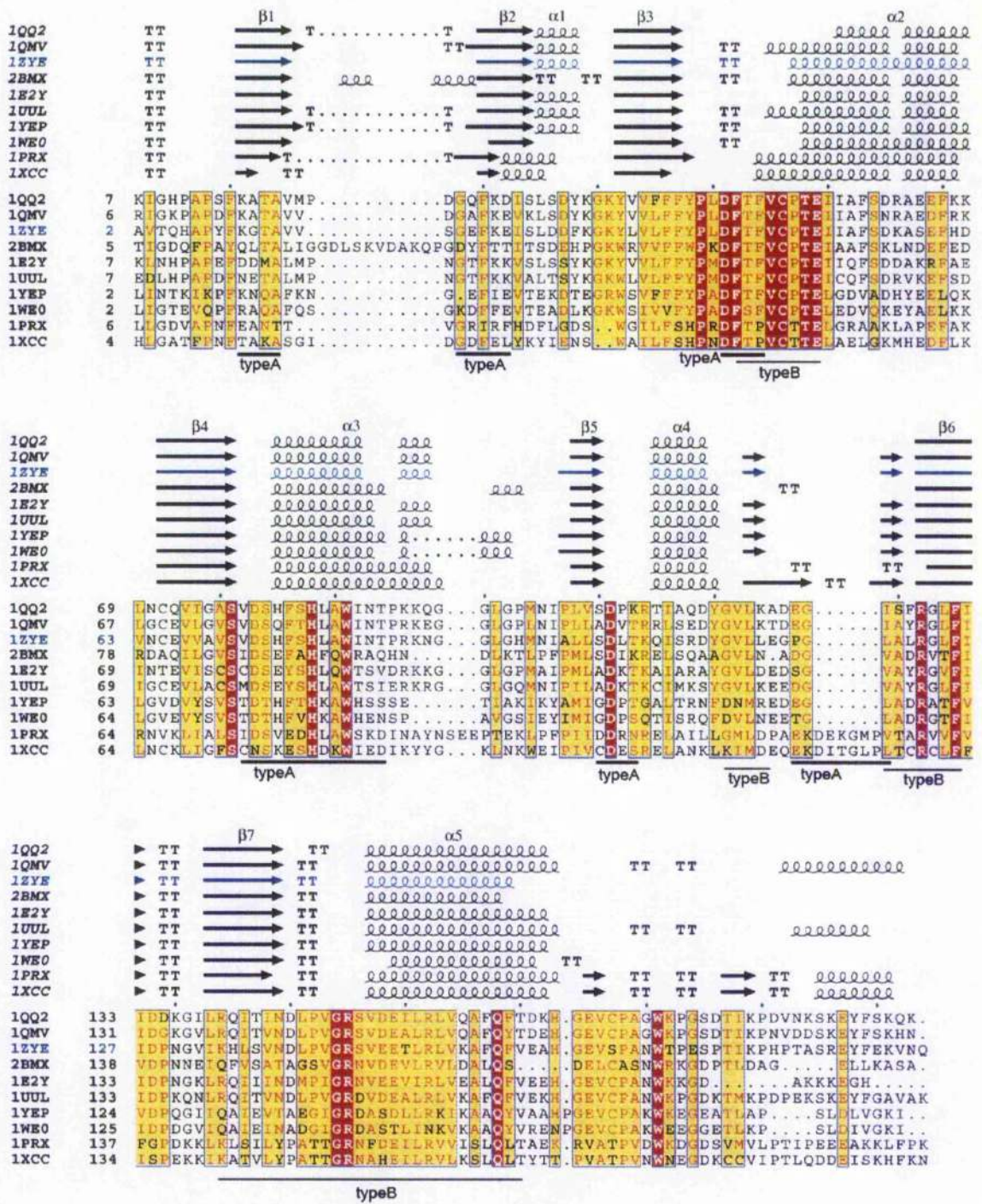


Figure 6.5 Structure based sequence alignment of selected Prxs

Residues involved in secondary structure are indicated by coils (helices) and arrows (strands) above the sequences. Regions involved in the type A and B oligomeric interfaces are also indicated by A or B below the sequences. 1PRX and 1XCC are 1-Cys Prxs and the rest are 2-Cys Prxs. In 2-Cys Prxs, 1QQ2 is dimer, 1E2Y, 1UUL, 1YEP, 1WE0 are decamers. 1ZYE and 2BMX are dodecamers. 1ZYE (PrxIII) is shown in blue. See Table 1.1 for PDB ID details of individual Prxs.

6.2.3 Dodecamer structure

The 6-fold NCS-related dimers are assembled into a dodecameric ring structure with outer and inner diameters of 150 and 70 Å respectively (*cf* 130 and 60 Å for the decameric Prxs) (Fig 6.6a). The dimer-dimer interfaces within the ring are formed mainly by hydrophobic residues (Leu 41, Phe 43, Phe 45, Val 73, Phe 77, Leu 103, Leu 120) burying 635Å² of solvent accessible surface per monomer (Fig 6.7 and 6.8). A similar dodecameric ring structure has recently been reported for the crystal structure of MtAhpC_{C176S} (Guimaraes *et al.*, 2005) (Fig 6.6b). This, and our result, shows that 2-Cys Prxs oligomers are not restricted to forming decameric toroids.

The sequence alignment on the type A dimer interface of PrxIII (1ZYE), HBP23 (1QQ2), TPxB (1QMV) and MtAhpC (2BMX) are highly homologous (8 out of 18 are identical, 9 are conservative substitutions indicating no significant difference between them (Fig 6.5 and Table 6.1).

1ZYE (12mer) This work	1QQ2 (dimer) HBP23	1QMV (10mer) TPxB	2BMX (12mer) MtAhpC
41 L	Conserved	Conserved	K
42 D	Conserved	Conserved	Conserved
43 F	Conserved	Conserved	Conserved
44 T	Conserved	Conserved	Conserved
45 F	Conserved	Conserved	I
73 V	Conserved	Conserved	Conserved
74 D	Conserved	Conserved	Conserved
75 S	Conserved	Conserved	Conserved
77 F	Conserved	Conserved	Conserved
78 S	S	T	A
81 A	Conserved	Conserved	Q
103 L	P	V	I
104 T	K	T	K
105 K	R	R	R
109 R	Q	E	Q
118 P	E	E	D
119 G	Conserved	Conserved	Conserved
120 L	I	I	V

Table 6.1 Sequences alignment of the PrxIII residues involved in the A-type dimer interface against other Prxs.

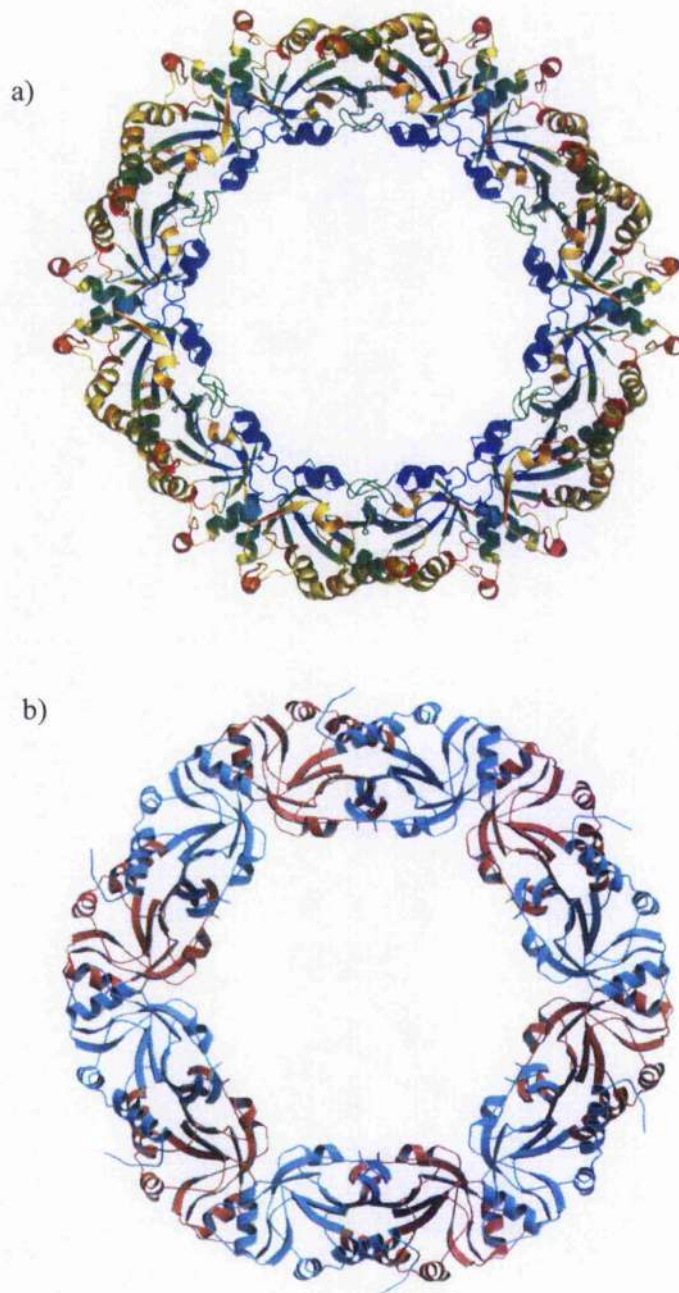


Figure 6.6 The Prx dodecamer

a) PrxIII dodecamer shown as a cartoon diagram and colouring is added using atomic B-factors. High B-factor is red and low B-factor is blue. The figure was produced using the program PyMOL (Delano, 2002). **b)** Crystal structure of MtAhpC_{C176S}. Taken from (Guimaraes *et al.*, 2005).

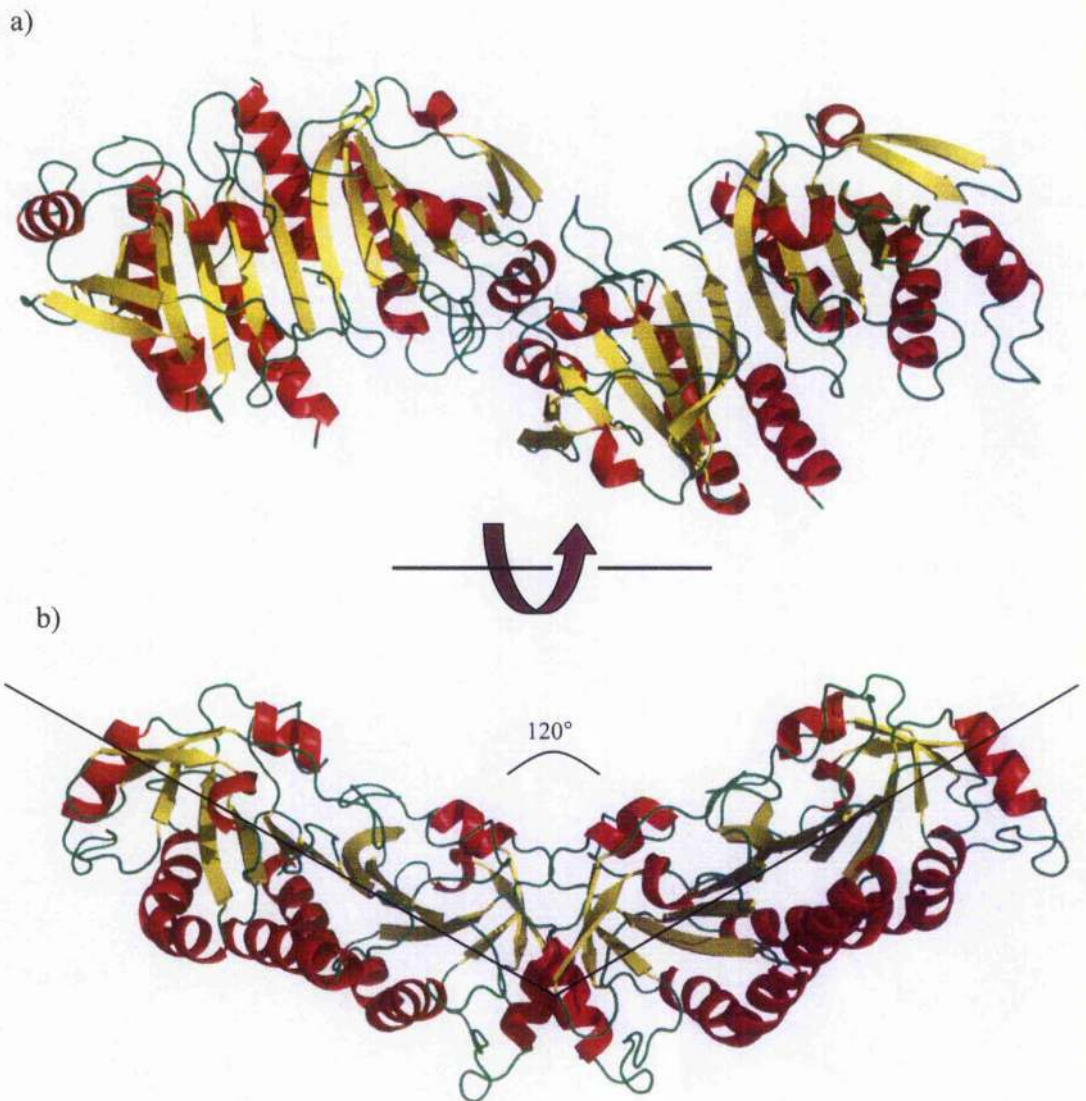


Figure 6.7 Cartoon diagram of the PrxIII dimer-dimer interaction

a) A-type interface characterized by mostly hydrophobic interactions across a non-crystallographic 2-fold axis. The interface is contributed mainly by α_3 and the loop region. **b)** as for a) after 90 degree rotation along the horizontal axis showing the two dimers lie at 120 degrees to each other (compared to 108 degrees for the decamer) which will give a dodecamer in the whole ring structure. The figure was produced using the program PyMOL (Delano, 2002).

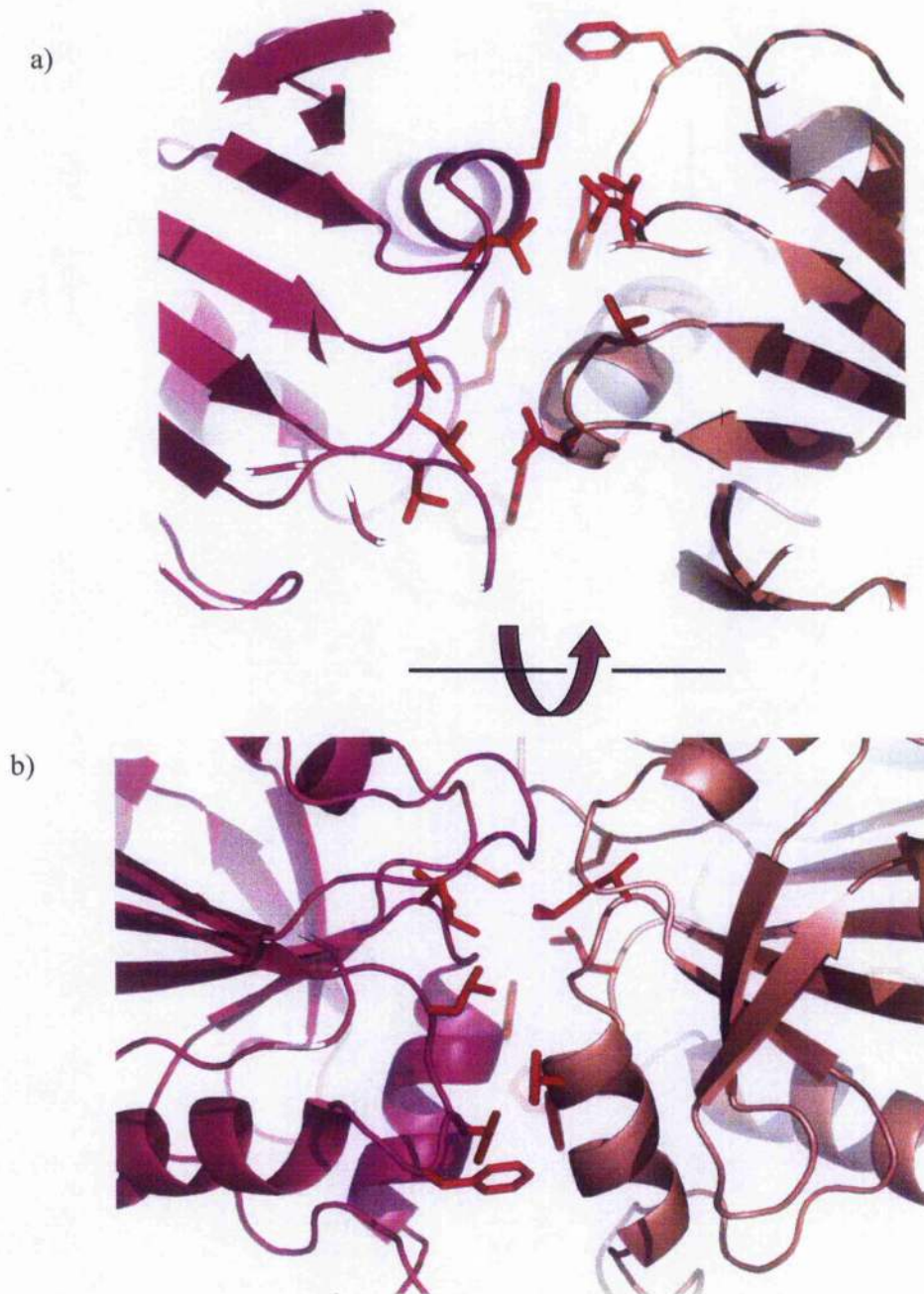


Figure 6.8 Detail of PrxIII type A dimer interface

Different subunits of the structure are shown in different colours as a cartoon diagram. **a)** the hydrophobic residues involved in the type A dimer interface are shown in red stick. **b)** as for a) after 90 degree rotation along the vertical axis. The figure was produced using the program PyMOL (Delano, 2002).

6.2.4 Catenane structure

The most surprising feature of the crystal structure of PrxIII C168S is its presence as a 2-ring catenane comprising two interlocking dodecameric toroids (Fig 6.9a). The planes of the rings are not at right angles, but are inclined at an angle of 55 degrees (Fig 6.9b), which allows a larger contact surface between the rings. This arrangement explains a large peak in the self-rotation function at $\chi = 55$ degrees with a coincident 2-fold NCS axis (Fig 5.12). There are twelve areas of contact burying 5067 \AA^2 of solvent accessible surface between the rings (Fig 6.10). These contacts arise from four NCS-related copies of three distinct interfaces. The prominent feature of the first contact area is Lys 88, which projects into a polar cavity at the dimer-dimer interface and forms a hydrogen bond with Thr 104 (Fig 6.10b). The second contact area is stabilized by a pair of NCS two-fold related hydrogen bonds between Lys 12 and Tyr 10 (Figure 6.10d). The contacts in the third area are also polar (Figure 6.10c). A salt bridge is clearly formed between Arg 109 and Glu 67, but other hydrogen bond contacts cannot be defined due to the resolution and accuracy of the structure.

The sequence alignment of the ring-ring interaction domain shows no significant difference between PrxIII and TPxB, while quite large differences exist between PrxIII and MtAhpC (Table 6.2). This may suggest that TPxB has the potential to form a catenane but due to its smaller ring size (10mer, not 12mer), it may not be able to accommodate another polypeptide chain within its central cavity. One interesting point is, in the crystal structure of TPxB, the crystal packing shows that two decamer rings lie at 60 degrees to each other (Fig 6.11). There are several contacts between the two rings which also including the equivalent residue to Lys 88 of PrxIII (Lys 92 in TPxB). This may suggest that there are similar contacts between dimers but the interaction or the orientation are slightly different which will determine the final quaternary structure.

For the MtAhpC, although the size of the ring is similar to PrxIII (12mer), the absence of necessary amino acids, such as Lys 88, to promote inter-toroid contacts may inhibit catenane formation.

1ZYE (catenane) This work	2BMX (12mer) MtAhpC	1QMV (10mer) TPxB
Lys 88	none	Conserved
Thr 104	Lys	Conserved
Tyr 10	Ala	Ser
Lys 12	Gln	Conserved
Glu 67	Gln	Conserved
Arg 109	Gln	Glu

Table 6.2 Sequence alignment of the residues involved ring-ring interactions

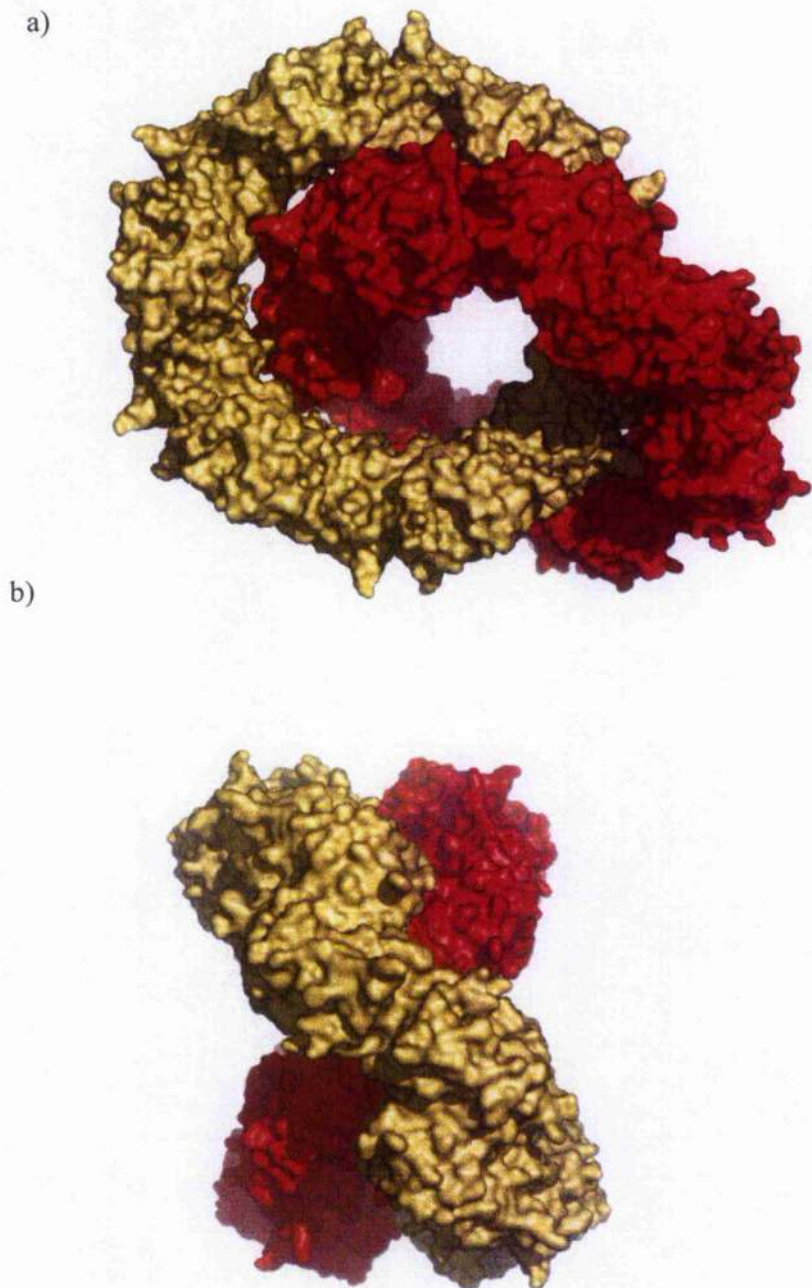


Figure 6.9 Surface diagram of the catenane structure of PrxIII C168S

a) The overall structure of the two interlocking rings. Shown in red and gold respectively; **b)** side view of the 2-ring catenane structure illustrating that the planes of the 2 rings lie at an angle of 55 degrees to each other. The figure was produced using the program PyMOL (Delano, 2002).

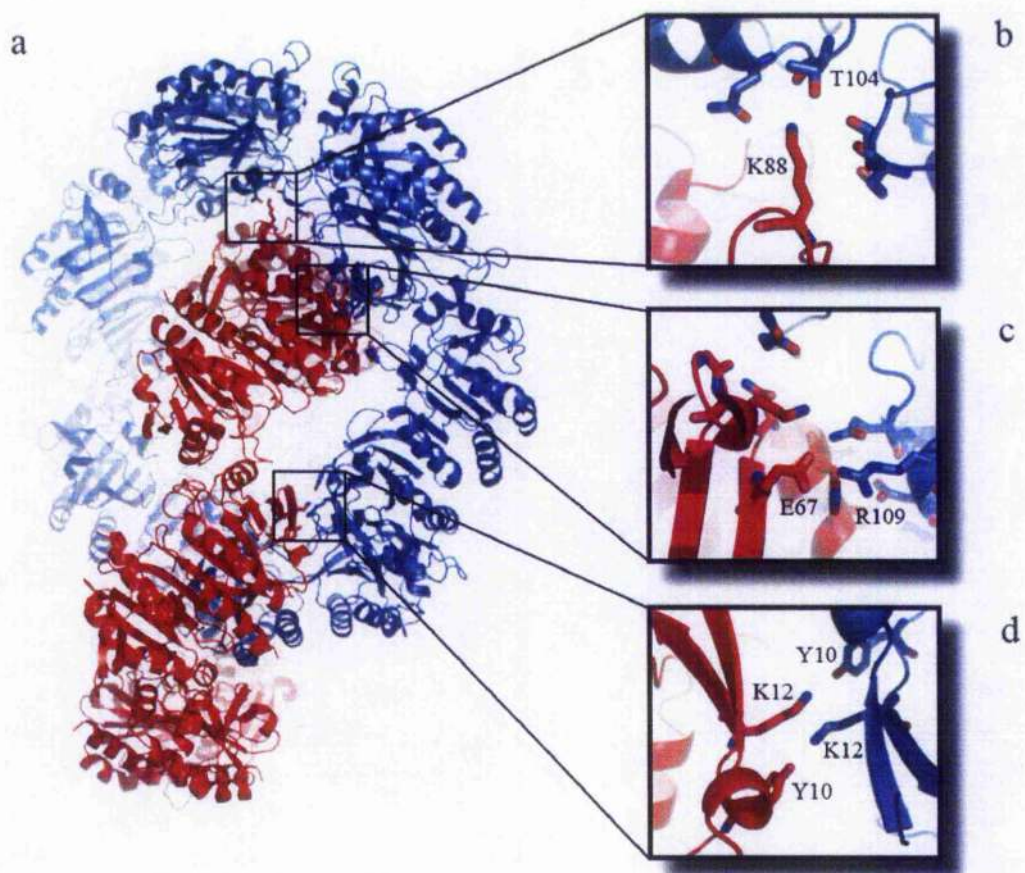


Figure 6.10 Sites of interaction between the two interlocked rings.

a) An overview of the 3 main sites of polar contact between the 2 interlocked dodecameric rings depicted in red and blue, respectively. These are each replicated 4 times in the overall structure; **b-d**) detailed representation of the polar contacts between the two rings; **b**) hydrogen bond between K88 and Thr104 located in a polar cavity; **c**) salt bridge between E67 and R109; **d**) 2-fold related hydrogen bonds between K12 and Y10. The figure was produced using the program PyMOL (Delano, 2002).

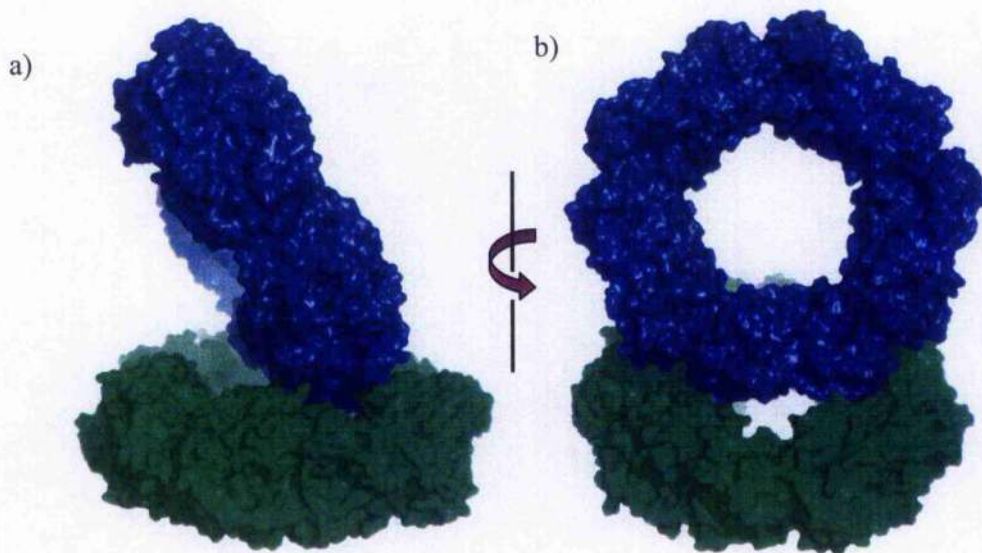


Figure 6.11 Surface diagram of the crystal packing of TPxB

a) The packing of two-ring structure of TPxB in the crystal. The two rings are showing in blue and green respectively. **b)** as for a) after 90 degree rotation along the vertical axis. The figure was produced using the program PyMOL (Delano, 2002).

6.3 Discussion

Catenane, as a word to describe macrocyclic molecules which are held together only mechanically without the aid of a chemical bond, was mentioned by Willstätter in a seminar at Zürich a century ago (Sauvage and Dietrich-Buchecker, 1999). The existence of the first chemical catenane was confirmed by a mass spectrometry measured by Schill in 1967 (Schill, 1967). In the same year, catenated DNA molecules were observed in the mitochondria of HeLa cells and human leukaemic leucocytes (Clayton and Vinograd, 1967; Hudson and Vinograd, 1967). Since then, catenated DNA has been found to be common in nature and has been discovered in a number of diverse biological systems.

As proteins have limited flexibility in their polypeptide chains, it was thought to be very difficult to form a knot or a catenated quaternary structure. However, although very rare, they do exist. Besides the so called “pseudo-knots” where cysteine residues lie close enough to become crosslinked to give extra stability to the fold (Tamaoki *et al.*, 1998), there are “topological” knot proteins such as acetohydroxy acid isomeroreductase (PDB ID: 1yve) with the backbone chain tangled together (Biou *et al.*, 1997; Taylor and Lin, 2003).

There are three previous examples of protein catenanes cited in the literature and two of them are rather specialised cases. One is a totally artificially-produced peptide catenane based on a small segment of a dimeric mutant of the p53tet protein generated *in vitro* using chemical techniques. Another one is a viral capsid assembly of 420 subunits where the subunits are topologically linked by covalent (isopeptide) bonds creating a form of protein ‘chain mail’ which is highly resistant to degradation. The third example is the crystal structure of RecR from *Deinococcus radiodurans*, which is involved in homologous recombinational DNA repair in prokaryotes (Lee *et al.*, 2004) (PDB ID: 1VDD). Four RecR monomers form a ring-shaped tetramer of 222 symmetry with a central hole of 30-35 Å diameter. In the crystal, two tetramers are concatenated (see Fig 6.12). PrxIII C168S represents another example of a classical, naturally-occurring, interlocked 2-ring protein structure, a protein catenane.

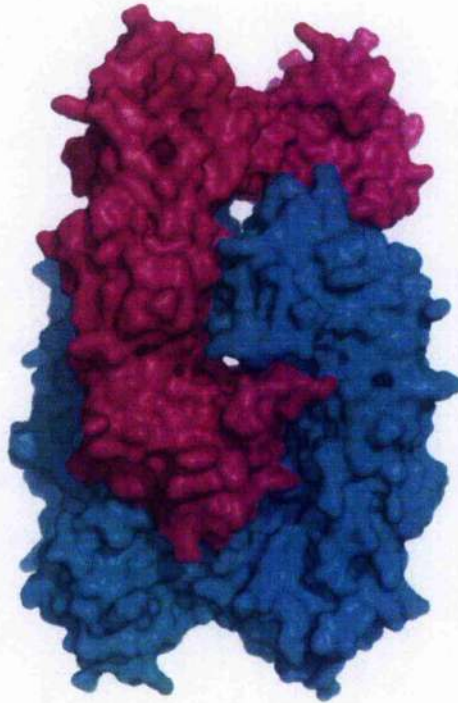


Figure 6.12 Crystal structure of *Deinococcus radiodurans* RecR octamer

Two tetramers (pink and cyan) are concatenated to form an octameric structure in the crystal. The figure was produced using the program PyMOL (Delano, 2002).

Preliminary data from analytical ultracentrifugation (AUC) (data not shown) and EM (Fig 6.13) studies indicate that the PrxIII C168S preparations employed for crystallisation contain a mixed population of single and double-ring oligomers. The oligomerization of the protein is concentration dependent. This was also reported in the other catenane structure (Lce *et al.*, 2004). A RecR tetramer (one ring) structure is found at 1 mg/ml and an octamer (two rings) structure is formed at 5mg/ml protein concentration.

We have no data indicating how the 2-ring catenane structure is formed but the crystal structure does provide some important insights into possible mechanisms of assembly (Fig 6.14). Dimeric units can interact in two different modes that are not mutually exclusive. One mode produces the dimer-dimer contacts, primarily hydrophobic, associated with ring generation in this and other Prx structures. The other mode gives polar contacts that could potentially initiate catenane formation at any stage during single toroid assembly by allowing two rings to form simultaneously around each other. A general model illustrating catenane formation arising from polar contacts between two basic dimeric units is described. At present it is unclear whether the fraction of the mixed population represented by the concatenated rings is assembled *in vivo* during overexpression in *E. coli*, or arises as a result of increasing protein concentration. A likely scenario is that interlocked double rings, single rings and a small population of dimers are in dynamic equilibrium in solution, so that during the crystallisation process *in vitro*, where there is a very high concentration of protein, formation of crystals from the catenated rings would be the most favoured event.

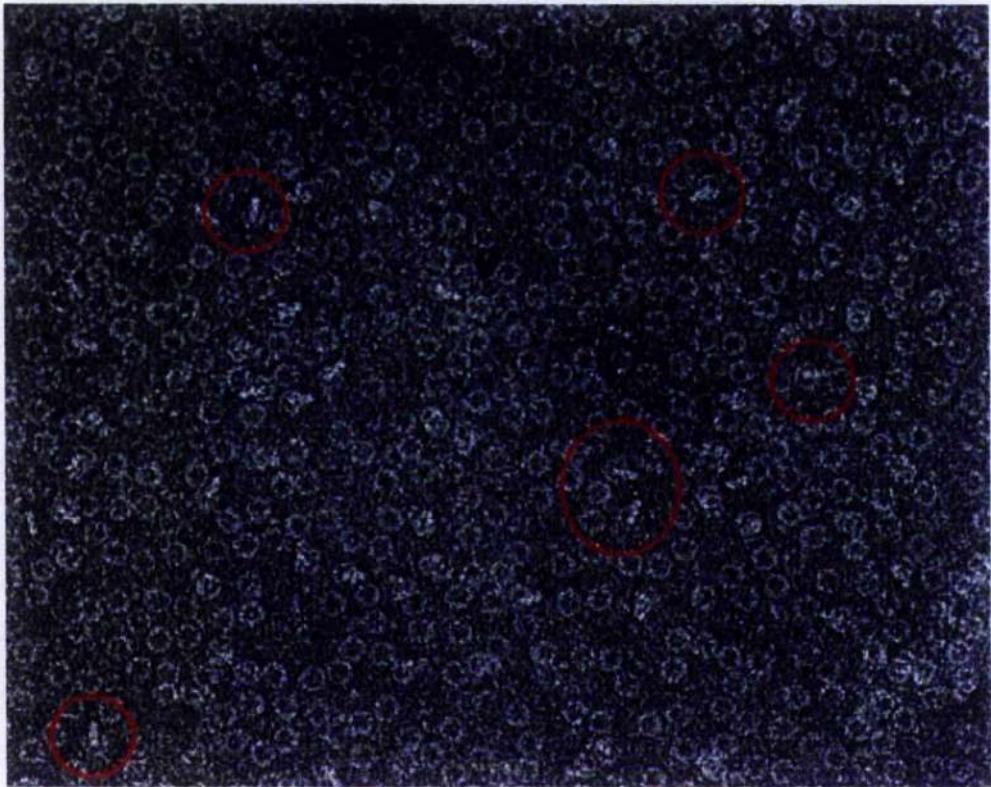


Figure 6.13 Electron Micrograph of PrxIII C168S

Red circles highlight some of the protein catenanes. Picture was kindly taken and provided by Dr Bhella from IBLS, University of Glasgow.

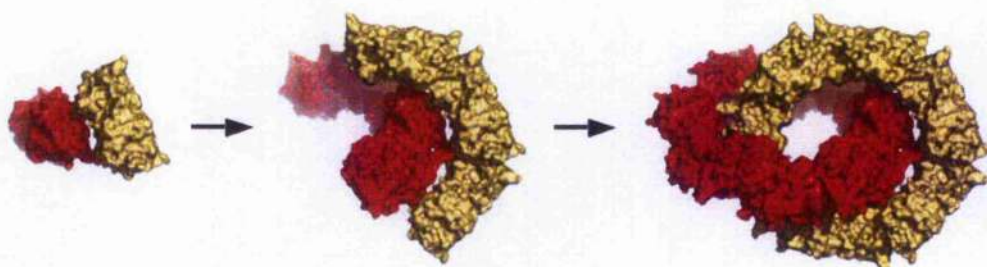


Figure 6.14 General model for mechanism of assembly of the 2-ring catenane structure.

Polar contacts between adjacent dimers (shown in red and gold), potentially occurring at any stage during single toroid formation, provide the basis for initiating the generation of a second topologically-linked ring leading to the overall 2-ring catenane structure. The figure was produced using the program PyMOL (Delano, 2002).

Chapter 7

Conclusions

7.1 Possible multiple functions of Prxs

The peroxiredoxins (Prxs) are a ubiquitous family of antioxidant enzymes that reduce hydrogen peroxide to water and were originally identified for their key role in antioxidant defence stemming from their peroxidase activity. However, in recent years, Prxs have also been implicated in regulating intracellular levels of H_2O_2 and are now considered to display multiple functions e.g. in limiting damage to ROS, in regulating H_2O_2 -mediated signalling pathways (Wood *et al.*, 2003) and also more recently in serving as molecular chaperones under some conditions (Jang *et al.*, 2004). Their vital contribution to antioxidant defence has been emphasised by their high abundance and ubiquitous distribution in both bacterial and mammalian cells. In the latter, they can account for 0.1-0.8% of total cellular protein (Chae *et al.*, 1999) and up to 5% of mitochondrial matrix protein (Chae *et al.*, 1994).

Prxs function as thioredoxin-dependent hydroperoxide reductases and typical 2-Cys enzymes, such as PrxIII, are organised as homodimers in which the adjacent subunits interact in a 'head-to-tail' fashion. During the catalytic cycle, the N-terminal cysteine is oxidised to a cysteine sulphenic acid by its peroxide substrate, which subsequently forms an inter-subunit disulphide bond with the conserved C-terminal cysteine of its partner. Atypical 2-Cys Prxs exist as monomers and generate an intramolecular disulphide bond during the reaction cycle (Seo *et al.*, 2000).

The peroxidatic cysteine (N-terminal cysteine) can be over-oxidised to yield inactive sulphinic ($-SO_2H$) or sulphonic ($-SO_3H$) acid forms. Studies of the susceptibility of eukaryotic Prxs to overoxidation and increasing evidence for their multiple roles has led to the development of the floodgate theory (as described in Chapter 1) that proposes a scheme for their involvement in cell signalling events. Wood *et al.* (Wood *et al.*, 2003) were the first to point out that bacterial 2-Cys Prxs are much less sensitive to oxidative inactivation than are eukaryotic 2-Cys Prxs. They concluded that this enhanced sensitivity of 2-Cys Prxs is not a limitation of the 2-Cys Prx catalytic mechanism, but is a feature that has been selected for during

the evolution of eukaryotes. Thus, in eukaryotes, when H_2O_2 concentrations are low, Prxs will primarily act in an anti-oxidant capacity. However, when H_2O_2 concentrations are elevated sufficiently, Prxs become temporarily inactivated and H_2O_2 serves as a messenger inducing the expression of specific groups of genes required for the development of an appropriate stress response or ultimately activating the apoptotic pathway.

7.2 Overoxidation of PrxIII

As shown in this thesis, PrxIII is also susceptible to overoxidation and loses peroxidase activity at increased H_2O_2 levels in the range $50\mu M$ to $1mM$. From SDS-PAGE analysis of H_2O_2 -mediated PrxIII oxidation, the appearance of abnormal oxidation states of PrxIII is also readily detectable at similar elevated levels of peroxide. Indeed, the PrxIII pathway reaches maximal activity at H_2O_2 concentrations of $5\mu M$ or less suggesting that this enzyme operates most efficiently at substrate levels in the micromolar or submicromolar range.

7.3 PrxIII pathway

Bovine PrxIII was cloned previously in our laboratory (Gourlay *et al.*, 2003); however PrxIII requires its cognate partners, mammalian mitochondrial thioredoxin (Trx2) and mammalian mitochondrial thioredoxin reductase (TRR2), to reconstitute the complete antioxidant defence system. To establish a direct *in vitro* assay for PrxIII, Trx2 and TRR2 were cloned, overexpressed and purified in this study. As TRR2 is a SeCys protein, a suitable SECIS for the translation of its penultimate SeCys codon was introduced by incorporating it into the reverse primer for PCR. A combination of different approaches was used for the successful overexpression of active TRR2. Overexpression in the modified rich LB media at $15^\circ C$ in the presence of low IPTG concentrations gave good overexpression of soluble enzyme. Moreover, the addition of the SECIS at the C-terminal of the insert, in the presence of $1\mu M Na_2SeO_3$ and co-expression of the SelABC plasmid ensured an optimal supply of the relevant tRNA, tRNA synthase and elongation factor for translation of the UGA SeCys codon. To develop the optimal conditions for determination of pathway activity, different concentrations of pathway components were varied independently in the reconstitution mix to achieve a situation where PrxIII levels

were rate limiting to the overall reaction. A relatively high concentration of TRR2 was required, presumably reflecting the low specific activity of the recombinant enzyme compared to its wild-type counterpart.

Assays showed that NADPH-linked oxidation needed the presence of all three enzymes to reduce H_2O_2 . PrxIII was also shown to reduce other organic peroxides, although with lower activities. Cys47 and Cys168, but not Cys66, proved to be crucial for peroxiredoxin activity. Interestingly, at high H_2O_2 concentrations in the non-physiological range, TRR2 also had the capacity to reduce H_2O_2 directly in an NADPH-dependent manner. This property is also found in mammalian TRR1 although it is not clear if this has any physiological relevance (Zhong and Holmgren, 2002).

7.4 Srx and Molecular Chaperone Function

Until recently the overoxidation of Prxs was thought to be irreversible. However, Woo *et al.* (2003) showed that the sulphinic acid form of PrxI, produced during the exposure of cells to H_2O_2 , is rapidly reconverted to the catalytically active thiol form. A protein called sulphiredoxin (Srx), which was first identified in yeast and is conserved in higher eukaryotes, was found to be able to reduce cysteine-sulphinic acid in the yeast peroxiredoxin Tsa1 (Biteau *et al.*, 2003). This ability of eukaryotic cells to repair overoxidized Prxs suggests that the function of this class of enzymes may be modulated by their oxidation state.

In this context, cytosolic PrxI and PrxII were found to be responsible for yeast survival after heat shock although the ability of cytosolic PrxI to protect cells lacking PrxI/II under these conditions is not exclusively due to its peroxidase activity (Jang *et al.*, 2004). These authors also report that heat shock and/or oxidative stress induces a structural change in PrxI which results in a functional switch from a peroxidase to a molecular chaperone *in vitro*. They have developed a new model taking into account these additional observations. At low ROS concentrations, Prxs are present mainly as the standard low molecular weight species i.e. dimers or decamers in the case of PrxI with normal peroxidase activity. However, when yeast was placed under extreme conditions like heat shock or

oxidative stress, PrxI shifts to previously unrecognized high molecular weight state, the structure of which is not clear at present. In this model, overoxidation of Cys47 acts as a highly efficient "H₂O₂-sensor" and induces this structural change with the aid of the Trx system. The novel structural switch is associated with functional change and this Prx now exhibits chaperone-like activity, enhancing cell survival under stress conditions. After oxidative stress, the cyst-sulphinic acid can be reduced to cyst-thiol by Srx and the high molecular weight complex dissociates into decamers and/or dimers, thus restoring peroxidase activity.

Although not included in this study, it will be necessary in future to investigate possible chaperone-related functions of PrxIII and its ability to assemble into a high M_r super-chaperone complex.

7.5 PrxIII oligomerization

Gel filtration chromatography was used to determine under which conditions the PrxIII dodecamer would dissociate to dimers. The results show that redox state, protein concentration and the N-terminal His-tag all affect the oligomerization of PrxIII. Structural studies of other Prxs show that there is a conformational change at the active site from reduced form to oxidized form, and that part of this active site is involved in the dimer-dimer interaction. Since the dimer-dimer interaction is contributed mainly from hydrophobic interactions, it is not hard to understand that at low protein concentrations it will form dimers but a mixture of dimers and dodecamers when the concentration is high. Interestingly the presence or absence of the N-terminal His-tag appears to affect the dimer-dimer interaction also. In the PrxIII pathway assay, (preliminary data, not shown) both the presence or absence of the His-tag has no obvious affect on the ability of PrxIII to sustain overall NADPH-linked reduction of H₂O₂. Recently, we have also constructed S78V, I and D mutants of PrxIII which all display altered oligomer stability so it will be of interest in future to test their ability to function as thioredoxin-dependent peroxidases and further examine the relationship between the dimer-dodecamer switch and the regulation or alteration of function. It should be noted that GFC is not a suitable technique for resolving the different higher M_r oligomeric state of PrxIII since they all have a similar hydrodynamic radius.

7.6 Crystal structure of PrxIII

Crystal structures have now been reported for 3 atypical 2-Cys, 8 typical 2-Cys and 4 1-Cys Prxs. In 5 of the typical 2-Cys structures, the basic dimeric unit is further assembled into decameric rings. In the remaining 2-Cys and 1-Cys Prxs, the structures are monomers or dimers, with three exceptions. Recently an octameric organisation has been reported for a 1-Cys Prx from *Mycobacterium tuberculosis* (Li *et al.*, 2005) and another 2-Cys Prx from the same organism has been shown to exist as a dodecamer (Guimaraes *et al.*, 2005). The third one is bovine PrxIII, the protein studied in this thesis, which also forms a dodecamer. As the basic functional unit of all Prxs is either a monomer or dimer, the precise relationship between peroxidase activity and the oligomeric state of these enzymes is unclear at present. Electron Microscopy (EM) studies (Gourlay *et al.*, 2003; Wood *et al.*, 2003) have shown that PrxIII exists as an oligomeric ring (previously thought to be decameric) enclosing a central cavity, although its overall dimensions are, in fact, slightly larger than other typical decameric Prx structures.

In this study, the PrxIII crystal structure was solved which further reveals that the toroid is composed of 12 (not 10) monomers with a 6(2,2) symmetry. Surprisingly, two PrxIII rings are mechanically interlocked in the crystal to form a protein catenane. Interestingly, the catenane form represents only a small proportion (3-5%) of the total PrxIII population, as observed by EM studies at dilute concentration (10-50µg/ml). Preliminary AUC data (not shown) suggest that 2-ring catenane formation is concentration dependent. Dimeric units can interact in two different modes that are not mutually exclusive. One mode produces the dimer-dimer contacts, primarily hydrophobic, associated with ring generation in this and other Prx structures. The other mode involve polar contacts that could potentially initiate catenane formation at any stage during single toroid assembly by allowing two rings to form simultaneously around each other. A general model illustrating catenane formation arising from polar contacts between two basic dimeric units is described. At present it is unclear whether the fraction of the mixed population represented by the concatenated rings is assembled *in vivo* during overexpression in *E. coli*, or arises as a result of increasing protein concentration. A likely scenario is

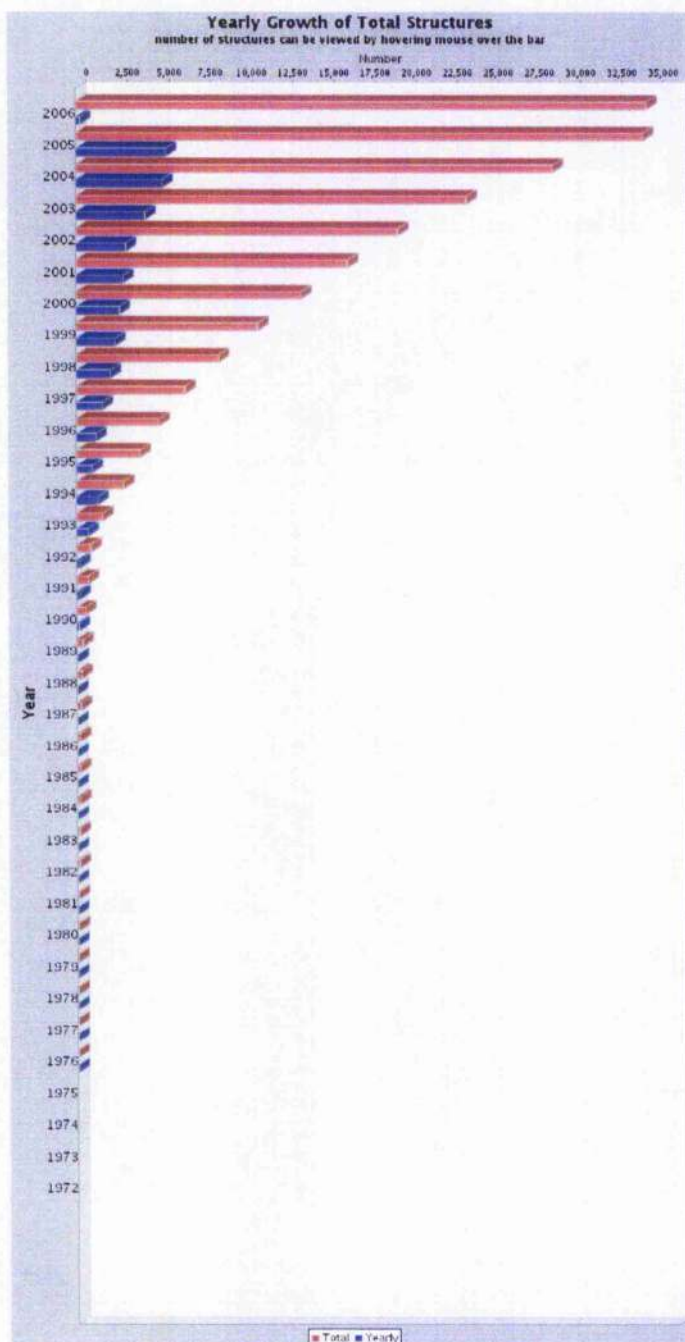
that interlocked double rings, single rings and a small population of dimers are in dynamic equilibrium in solution, so that during the crystallisation process *in vitro*, where there is a very high concentration of protein, formation of crystals from the catenated rings would be the most favoured event.

Whether the catenane form of PrxIII has any physiological function is not clear. The observation that Prxs can protect cells from heat shock in a peroxidase-independent process might provide new insights into possible novel functions. It should be noted that the Prx structure undergoes large conformational changes in the monomer during oxidation and reduction. The two catalytic cysteines are separated by approximately 13Å in the reduced state but form a disulphide bond in the oxidized enzyme. Thus, the reduced enzyme and the conserved cysteine mutants (eg the C168S mutant of PrxIII) that are incapable of disulphide bond formation are structurally equivalent to the overoxidised form. During catalysis, the structure will transform rapidly between its oxidised and reduced states, a process that also involves transient generation of covalent links between adjacent monomers in the basic functional dimeric unit. However, there is increasing evidence to show that the conserved cysteines may play a role as hydrogen peroxide "sensors" in addition to their catalytic role. At elevated hydrogen peroxide levels, Prx will be overoxidised triggering assembly into high molecular weight complexes with altered functions. It is possible that the ability of Prxs to associate into oligomeric rings of various sizes, super chaperone complexes or even catenane structures might be essential for activating these novel functional properties. In this connection, a screen for unknown candidate proteins which can interact with Prxs in their various oligomeric states might provide important clues as to the diversity of physiological roles attributable to this interesting family of antioxidant enzymes.

There are three previous examples of protein catenanes cited in the literature and two of them are rather specialised cases. One is a totally artificially-produced peptide catenane based on a small segment of a dimeric mutant of the p53tet protein generated *in vitro* using chemical techniques. The other one is a viral capsid assembly of 420 subunits where the subunits are topologically linked by covalent (isopeptide) bonds creating a form of protein 'chain mail' which is highly resistant

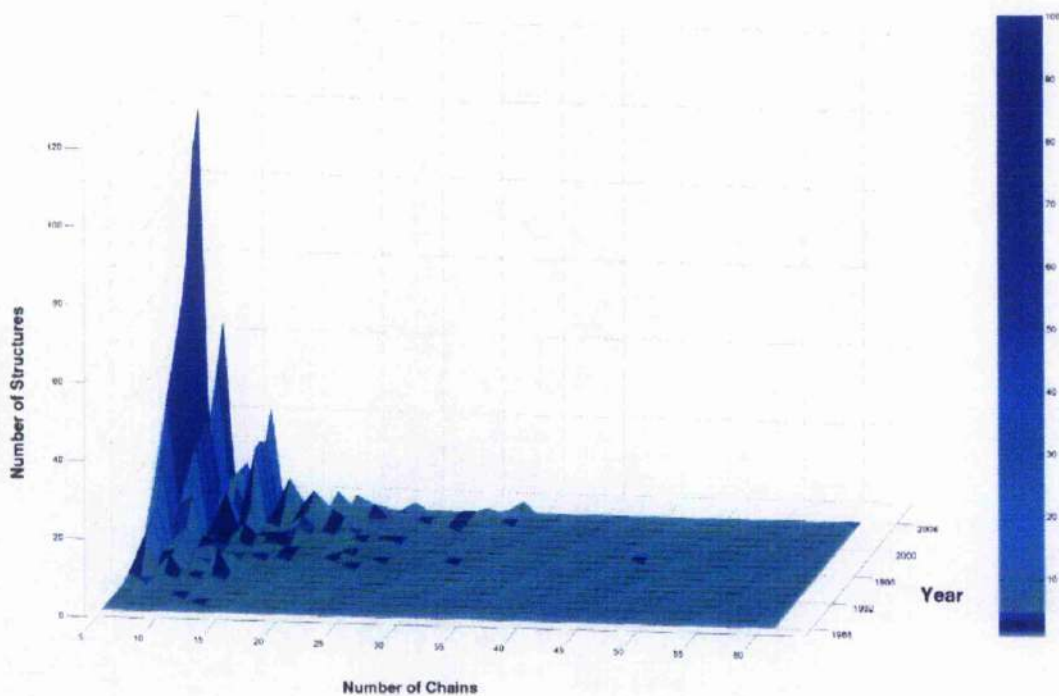
to degradation. The third case is the crystal structure of RecR from *Deinococcus radiodurans*, which is involved in homologous recombinational DNA repair in prokaryotes (PDB id: 1VDD) and is also present as a protein catenane (Lcc *et al.*, 2004). The structures of RecR and PrxIII C168S show that proteins are also able to form catenanes although these are extremely rare at present.

Appendix



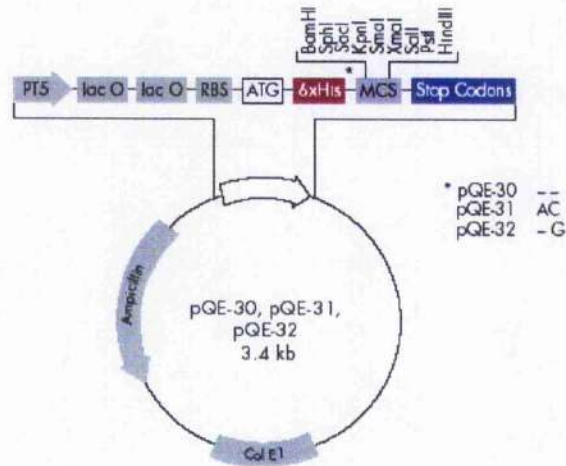
Appendix I The Growth of PDB content

Growth in the number of structures deposited per year (blue) and total holdings of the PDB (red) are shown from the time that the PDB was founded. The numbers used for year 2006 are projected based on actual entries available at the time of writing this thesis. Adapted from <http://www.rcsb.org/pdb>.

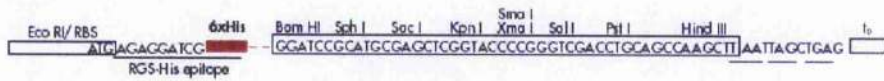


Appendix II Complexity of structures in the PDB

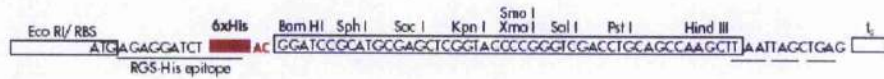
This three-dimensional contour plot displays the PDB holdings with 5 or more chains in the asymmetric unit as a function of time. The plot shows that there has been an increase in number of structures with a higher number of chains per asymmetric unit between 1989 and 2004. The colour bar on the right defines the number of structures in each group. Taken from (Dutta and Berman, 2005)



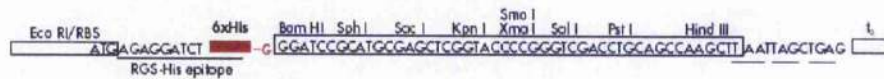
pQE-30



pQE-31



pQE-32



Appendix III Plasmid maps of pQE 30, 31 and 32 vectors

There is an N-terminal 6x His-tag sequence followed by the multiple cloning sites. The different sequences between the His-tag and multiple cloning sites are highlighted in red.

References

- Alphey, M. S., Bond, C. S., Tetaud, E., Fairlamb, A. H. and Hunter, W. N. (2000). "The structure of reduced trypanothione peroxidase reveals a decamer and insight into reactivity of 2Cys-peroxiredoxins." *J Mol Biol* **300**(4): 903-16.
- Anestai, K. and Arner, E. S. (2003). "Rapid induction of cell death by selenium-compromised thioredoxin reductase 1 but not by the fully active enzyme containing selenocysteine." *J Biol Chem* **278**(18): 15966-72.
- Araki, M., Nanri, H., Ejima, K., Murasato, Y., Fujiwara, T., Nakashima, Y. and Ikeda, M. (1999). "Antioxidant function of the mitochondrial protein SP-22 in the cardiovascular system." *J Biol Chem* **274**(4): 2271-8.
- Arner, E. S., Sarioglu, H., Lottspeich, F., Holmgren, A. and Bock, A. (1999). "High-level expression in *Escherichia coli* of selenocysteine-containing rat thioredoxin reductase utilizing gene fusions with engineered bacterial-type SECIS elements and co-expression with the selA, selB and selC genes." *J Mol Biol* **292**(5): 1003-16.
- Arcott, L. D., Gromer, S., Schirmer, R. H., Becker, K. and Williams, C. H., Jr. (1997). "The mechanism of thioredoxin reductase from human placenta is similar to the mechanisms of lipoamide dehydrogenase and glutathione reductase and is distinct from the mechanism of thioredoxin reductase from *Escherichia coli*." *Proc Natl Acad Sci U S A* **94**(8): 3621-6.
- Avraham, K. B., Schickler, M., Sapoznikov, D., Yarom, R. and Groner, Y. (1988). "Down's syndrome: abnormal neuromuscular junction in tongue of transgenic mice with elevated levels of human Cu/Zn-superoxide dismutase." *Cell* **54**(6): 823-9.
- Biou, V., Dumas, R., Cohen-Addad, C., Douce, R., Job, D. and Pebay-Peyroula, E. (1997). "The crystal structure of plant acetohydroxy acid isomeroreductase complexed with NADPH, two magnesium ions and a herbicidal transition state analog determined at 1.65 Å resolution." *EMBO J* **16**(12): 3405-15.

- Birringer, M., Pilawa, S. and Flohe, L. (2002). "Trends in selenium biochemistry." *Nat Prod Rep* **19**(6): 693-718.
- Biteau, B., Labarre, J. and Toledano, M. B. (2003). "ATP-dependent reduction of cysteine-sulphinic acid by *S. cerevisiae* sulphiredoxin." *Nature* **425**(6961): 980-4.
- Biterova, E. I., Turanov, A. A., Gladyshev, V. N. and Barycki, J. J. (2005). "Crystal structures of oxidized and reduced mitochondrial thioredoxin reductase provide molecular details of the reaction mechanism." *Proc Natl Acad Sci U S A* **102**(42): 15018-23.
- Bodenstein, J. and Follmann, H. (1991). "Characterization of two thioredoxins in pig heart including a new mitochondrial protein." *Z Naturforsch [C]* **46**(3-4): 270-9.
- Boveris, A. and Chance, B. (1973). "The mitochondrial generation of hydrogen peroxide. General properties and effect of hyperbaric oxygen." *Biochem J* **134**(3): 707-16.
- Brigelius-Flohe, R. (1999). "Tissue-specific functions of individual glutathione peroxidases." *Free Radic Biol Med* **27**(9-10): 951-65.
- Bryk, R., Griffin, P. and Nathan, C. (2000). "Peroxynitrite reductase activity of bacterial peroxiredoxins." *Nature* **407**(6801): 211-5.
- Bryk, R., Lima, C. D., Erdjument-Bromage, H., Tempst, P. and Nathan, C. (2002). "Metabolic enzymes of mycobacteria linked to antioxidant defense by a thioredoxin-like protein." *Science* **295**(5557): 1073-7.
- Buettner, C., Harnoy, J. W. and Larsen, P. R. (1998). "The 3'-untranslated region of human type 2 iodothyronine deiodinase mRNA contains a functional selenocysteine insertion sequence element." *J Biol Chem* **273**(50): 33374-8.
- Burke-Gaffney, A., Callister, M. E. and Nakamura, H. (2005). "Thioredoxin: friend or foe in human disease?" *Trends Pharmacol Sci* **26**(8): 398-404.
- Cadenas, E., Boveris, A., Ragan, C. I. and Stoppani, A. O. (1977). "Production of superoxide radicals and hydrogen peroxide by NADH-ubiquinone reductase and ubiquinol-cytochrome c reductase from beef-heart mitochondria." *Arch Biochem*

Biophys **180**(2): 248-57.

- CCP4 (1994). "The CCP4 Suite - Programs for Protein Crystallography." *Acta Crystallographica Section D-Biological Crystallography* **50**: 760-763.
- Chae, H. Z., Kang, S. W. and Rhee, S. G. (1999). "Isoforms of mammalian peroxiredoxin that reduce peroxides in presence of thioredoxin." *Methods Enzymol* **300**: 219-26.
- Chae, H. Z., Robison, K., Poole, L. B., Church, G., Storz, G. and Rhee, S. G. (1994). "Cloning and sequencing of thiol-specific antioxidant from mammalian brain: alkyl hydroperoxide reductase and thiol-specific antioxidant define a large family of antioxidant enzymes." *Proc Natl Acad Sci USA* **91**(15): 7017-21.
- Chance, B., Sies, H. and Boveris, A. (1979). "Hydroperoxide metabolism in mammalian organs." *Physiol Rev* **59**(3): 527-605.
- Chang, T. S., Cho, C. S., Park, S., Yu, S., Kang, S. W. and Rhee, S. G. (2004). "Peroxiredoxin III, a mitochondrion-specific peroxidase, regulates apoptotic signaling by mitochondria." *J Biol Chem* **279**(40): 41975-84.
- Chang, T. S., Jeong, W., Choi, S. Y., Yu, S., Kang, S. W. and Rhee, S. G. (2002). "Regulation of peroxiredoxin I activity by Cdc2-mediated phosphorylation." *J Biol Chem* **277**(28): 25370-6.
- Chauhan, R. and Mande, S. C. (2001). "Characterization of the Mycobacterium tuberculosis H37Rv alkyl hydroperoxidase AhpC points to the importance of ionic interactions in oligomerization and activity." *Biochem J* **354**(Pt 1): 209-15.
- Chen, Y., Cai, J., Murphy, T. J. and Jones, D. P. (2002). "Overexpressed human mitochondrial thioredoxin confers resistance to oxidant-induced apoptosis in human osteosarcoma cells." *J Biol Chem* **277**(36): 33242-8.
- Chenna, R., Sugawara, H., Koike, T., Lopez, R., Gibson, T. J., Higgins, D. G. and Thompson, J. D. (2003). "Multiple sequence alignment with the Clustal series of programs." *Nucleic Acids Res* **31**(13): 3497-500.
- Choi, H. J., Kang, S. W., Yang, C. H., Rhee, S. G. and Ryu, S. E. (1998). "Crystallization

and preliminary X-ray studies of hORF6, a novel human antioxidant enzyme." *Acta Crystallogr D Biol Crystallogr* **54** (Pt 3): 436-7.

Choi, J., Choi, S., Cha, M. K., Kim, I. H. and Shin, W. (2003). "Crystal structure of *Escherichia coli* thiol peroxidase in the oxidized state: insights into intramolecular disulfide formation and substrate binding in atypical 2-Cys peroxiredoxins." *J Biol Chem* **278**(49): 49478-86.

Choi, M. H., Lee, J. K., Kim, G. W., Kim, B. U., Han, Y. H., Yu, D. Y., Park, H. S., Kim, K. Y., Lee, J. S., Choi, C., Bae, Y. S., Lee, B. I., Rhee, S. G. and Kang, S. W. (2005). "Regulation of PDGF signalling and vascular remodelling by peroxiredoxin II." *Nature* **435**(7040): 347-53.

Clayton, D. A. and Vinograd, J. (1967). "Circular dimer and catenate forms of mitochondrial DNA in human leukaemic leucocytes." *J Pers* **35**(4): 652-7.

Conrad, M., Jakupoglu, C., Moreno, S. G., Lippl, S., Banjac, A., Schneider, M., Beck, H., Hatzopoulos, A. K., Just, U., Sinowatz, F., Schmahl, W., Chien, K. R., Wurst, W., Bornkamm, G. W. and Brielmeier, M. (2004). "Essential role for mitochondrial thioredoxin reductase in hematopoiesis, heart development, and heart function." *Mol Cell Biol* **24**(21): 9414-23.

Damdimopoulos, A. E., Miranda-Vizuete, A., Pelto-Huikko, M., Gustafsson, J. A. and Spyrou, G. (2002). "Human mitochondrial thioredoxin. Involvement in mitochondrial membrane potential and cell death." *J Biol Chem* **277**(36): 33249-57.

de Haan, J. B., Bladier, C., Griffiths, P., Kelner, M., O'Shea, R. D., Cheung, N. S., Bronson, R. T., Silvestro, M. J., Wild, S., Zheng, S. S., Beart, P. M., Hertzog, P. J. and Kola, I. (1998). "Mice with a homozygous null mutation for the most abundant glutathione peroxidase, Gpx1, show increased susceptibility to the oxidative stress-inducing agents paraquat and hydrogen peroxide." *J Biol Chem* **273**(35): 22528-36.

Declercq, J. P., Evrard, C., Clippe, A., Stricht, D. V., Bernard, A. and Knoops, B. (2001). "Crystal structure of human peroxiredoxin 5, a novel type of mammalian peroxiredoxin at 1.5 Å resolution." *J Mol Biol* **311**(4): 751-9.

- Deiss, L. P. and Kimchi, A. (1991). "A genetic tool used to identify thioredoxin as a mediator of a growth inhibitory signal." *Science* **252**(5002): 117-20.
- Delano, W. L. (2002). The PyMOL Molecular Graphics System, Delano Scientific, San Carlos, CA, USA.
- Dutta, S. and Berman, H. M. (2005). "Large macromolecular complexes in the Protein Data Bank: a status report." *Structure* **13**(3): 381-8.
- Echalier, A., Trivelli, X., Corbier, C., Rouhier, N., Walker, O., Tsan, P., Jacquot, J. P., Aubry, A., Krimm, I. and Lancelin, J. M. (2005). "Crystal structure and solution NMR dynamics of a D (type II) peroxiredoxin glutaredoxin and thioredoxin dependent: a new insight into the peroxiredoxin oligomerism." *Biochemistry* **44**(6): 1755-67.
- Emsley, P. and Cowtan, K. (2004). "Coot: model-building tools for molecular graphics." *Acta Crystallogr D Biol Crystallogr* **60**(Pt 12 Pt 1): 2126-32.
- Esworthy, R. S., Ho, Y. S. and Chu, F. F. (1997). "The Gpx1 gene encodes mitochondrial glutathione peroxidase in the mouse liver." *Arch Biochem Biophys* **340**(1): 59-63.
- Fortelle, E. d. L. and Bricogne, G. (1997). "Maximum-Likelihood Heavy-Atom Parameter Refinement for the Multiple Isomorphous Replacement and Multiwavelength Anomalous Diffraction Methods." *Methods in Enzymology* **276**: 472-494.
- Fridovich, I. (1995). "Superoxide radical and superoxide dismutases." *Annu Rev Biochem* **64**: 97-112.
- Fujii, J. and Ikeda, Y. (2002). "Advances in our understanding of peroxiredoxin, a multifunctional, mammalian redox protein." *Redox Rep* **7**(3): 123-30.
- Gasdaska, P. Y., Gasdaska, J. R., Cochran, S. and Powis, G. (1995). "Cloning and sequencing of a human thioredoxin reductase." *FEBS Lett* **373**(1): 5-9.
- Gazaryan, I. G., Krasnikov, B. F., Ashby, G. A., Thorneley, R. N., Kristal, B. S. and Brown, A. M. (2002). "Zinc is a potent inhibitor of thiol oxidoreductase activity and stimulates reactive oxygen species production by lipoamide dehydrogenase." *J*

Biol Chem **277**(12): 10064-72.

- Ge, K., Xue, A., Bai, J. and Wang, S. (1983). "Keshan disease-an endemic cardiomyopathy in China." *Virchows Arch A Pathol Anat Histopathol* **401**(1): 1-15.
- Georgiou, G. and Masip, L. (2003). "Biochemistry. An overoxidation journey with a return ticket." *Science* **300**(5619): 592-4.
- Gouet, P., Courcelle, E., Stuart, D. I. and Metoz, F. (1999). "ESPrpt: analysis of multiple sequence alignments in PostScript." *Bioinformatics* **15**(4): 305-8.
- Gourlay, L. J., Bhella, D., Kelly, S. M., Price, N. C. and Lindsay, J. G. (2003). "Structure-function analysis of recombinant substrate protein 22 kDa (SP-22). A mitochondrial 2-CYS peroxiredoxin organized as a decameric toroid." *J Biol Chem* **278**(35): 32631-7.
- Gromer, S., Johansson, L., Bauer, H., Arscott, L. D., Rauch, S., Ballou, D. P., Williams, C. H., Jr., Schirmer, R. H. and Arner, E. S. (2003). "Active sites of thioredoxin reductases: why selenoproteins?" *Proc Natl Acad Sci U S A* **100**(22): 12618-23.
- Grundner-Culemann, E., Martin, G. W., 3rd, Harney, J. W. and Berry, M. J. (1999). "Two distinct SECIS structures capable of directing selenocysteine incorporation in eukaryotes." *RNA* **5**(5): 625-35.
- Guimaraes, B. G., Souchou, H., Honore, N., Saint-Joanis, B., Brosch, R., Shepard, W., Cole, S. T. and Alzari, P. M. (2005). "Structure and mechanism of the alkyl hydroperoxidase AhpC, a key element of the *Mycobacterium tuberculosis* defense system against oxidative stress." *J Biol Chem* **280**(27): 25735-42.
- Hattori, F., Murayama, N., Noshita, T. and Oikawa, S. (2003). "Mitochondrial peroxiredoxin-3 protects hippocampal neurons from excitotoxic injury in vivo." *J Neurochem* **86**(4): 860-8.
- Hirotsu, S., Abe, Y., Okada, K., Nagahara, N., Hori, H., Nishino, T. and Hakoshima, T. (1999). "Crystal structure of a multifunctional 2-Cys peroxiredoxin heme-binding protein 23 kDa/proliferation-associated gene product." *Proc Natl Acad Sci U S A* **96**(22): 12333-8.

- Ho, Y. S., Magnenat, J. L., Bronson, R. T., Cao, J., Gargano, M., Sugawara, M. and Funk, C. D. (1997). "Mice deficient in cellular glutathione peroxidase develop normally and show no increased sensitivity to hyperoxia." *J Biol Chem* **272**(26): 16644-51.
- Hofmann, B., Hecht, H. J. and Flohe, L. (2002). "Peroxiredoxins." *Biol Chem* **383**(3-4): 347-64.
- Holmgren, A. (1995). "Thioredoxin structure and mechanism: conformational changes on oxidation of the active-site sulfhydryls to a disulfide." *Structure* **3**(3): 239-43.
- Huber, R. E. and Criddle, R. S. (1967). "Comparison of the chemical properties of selenocysteine and selenocystine with their sulfur analogs." *Arch Biochem Biophys* **122**(1): 164-73.
- Hudson, B. and Vinograd, J. (1967). "Catenated circular DNA molecules in HeLa cell mitochondria." *Nature* **216**(5116): 647-52.
- Jang, H. H., Lee, K. O., Chi, Y. H., Jung, B. G., Park, S. K., Park, J. H., Lee, J. R., Lee, S. S., Moon, J. C., Yun, J. W., Choi, Y. O., Kim, W. Y., Kang, J. S., Cheong, G. W., Yun, D. J., Rhee, S. G., Cho, M. J. and Lee, S. Y. (2004). "Two enzymes in one; two yeast peroxiredoxins display oxidative stress-dependent switching from a peroxidase to a molecular chaperone function." *Cell* **117**(5): 625-35.
- Jeong, W., Park, S. J., Chang, T. S., Lee, D. Y. and Rhee, S. G. (2006). "Molecular mechanism of the reduction of cysteine sulfenic acid of peroxiredoxin to cysteine by mammalian sulfiredoxin." *J Biol Chem*.
- Kang, S. W., Chae, H. Z., Seo, M. S., Kim, K., Baines, I. C. and Rhee, S. G. (1998). "Mammalian peroxiredoxin isoforms can reduce hydrogen peroxide generated in response to growth factors and tumor necrosis factor-alpha." *J Biol Chem* **273**(11): 6297-302.
- Kim, S. J., Woo, J. R., Hwang, Y. S., Jeong, D. G., Shin, D. H., Kim, K. and Ryu, S. E. (2003). "The tetrameric structure of Haemophilus influenza hybrid Prx5 reveals interactions between electron donor and acceptor proteins." *J Biol Chem* **278**(12): 10790-8.

- Kitano, K., Kita, A., Hakoshima, T., Niimura, Y. and Miki, K. (2005). "Crystal structure of decameric peroxiredoxin (AhpC) from *Amphibacillus xylanus*." *Proteins* **59**(3): 644-7.
- Kitano, K., Niimura, Y., Nishiyama, Y. and Miki, K. (1999). "Stimulation of peroxidase activity by decamerization related to ionic strength: AhpC protein from *Amphibacillus xylanus*." *J Biochem (Tokyo)* **126**(2): 313-9.
- Kokoszka, J. E., Coskun, P., Esposito, L. A. and Wallace, D. C. (2001). "Increased mitochondrial oxidative stress in the Sod2 (+/-) mouse results in the age-related decline of mitochondrial function culminating in increased apoptosis." *Proc Natl Acad Sci U S A* **98**(5): 2278-83.
- Koshkin, A., Nunn, C. M., Djordjevic, S. and Ortiz de Montellano, P. R. (2003). "The mechanism of *Mycobacterium tuberculosis* alkylhydroperoxidase AhpD as defined by mutagenesis, crystallography, and kinetics." *J Biol Chem* **278**(32): 29502-8.
- Kristensen, P., Rasmussen, D. E. and Kristensen, B. I. (1999). "Properties of thiol-specific anti-oxidant protein or calpromotin in solution." *Biochem Biophys Res Commun* **262**(1): 127-31.
- Kryukov, G. V., Castellano, S., Novoselov, S. V., Lobanov, A. V., Zehtab, O., Guigo, R. and Gladyshev, V. N. (2003). "Characterization of mammalian selenoproteomes." *Science* **300**(5624): 1439-43.
- Laskowski, R. A., Macarthur, M. W., Moss, D. S. and Thornton, J. M. (1993). "Procheck - a Program to Check the Stereochemical Quality of Protein Structures." *Journal of Applied Crystallography* **26**: 283-291.
- Lee, B. I., Kim, K. H., Park, S. J., Eom, S. H., Song, H. K. and Suh, S. W. (2004). "Ring-shaped architecture of RecR: implications for its role in homologous recombinational DNA repair." *EMBO J* **23**(10): 2029-38.
- Lee, S. R., Kim, J. R., Kwon, K. S., Yoon, H. W., Levine, R. L., Ginsburg, A. and Rhee, S. G. (1999). "Molecular cloning and characterization of a mitochondrial selenocysteine-containing thioredoxin reductase from rat liver." *J Biol Chem*

- Legault, J., Carrier, C., Petrov, P., Renard, P., Remacle, J. and Mirault, M. E. (2000). "Mitochondrial GPx1 decreases induced but not basal oxidative damage to mtDNA in T47D cells." *Biochem Biophys Res Commun* **272**(2): 416-22.
- Li, S., Peterson, N. A., Kim, M. Y., Kim, C. Y., Hung, L. W., Yu, M., Lekin, T., Segelke, B. W., Lott, J. S. and Baker, E. N. (2005). "Crystal Structure of AlpE from *Mycobacterium tuberculosis*, a 1-Cys peroxiredoxin." *J Mol Biol* **346**(4): 1035-46.
- Low, S. C. and Berry, M. J. (1996). "Knowing when not to stop: selenocysteine incorporation in eukaryotes." *Trends Biochem Sci* **21**(6): 203-8.
- Makino, N., Mochizuki, Y., Bannai, S. and Sugita, Y. (1994). "Kinetic studies on the removal of extracellular hydrogen peroxide by cultured fibroblasts." *J Biol Chem* **269**(2): 1020-5.
- Marklund, S. I., Holme, E. and Hellner, L. (1982). "Superoxide dismutase in extracellular fluids." *Clin Chim Acta* **126**(1): 41-51.
- Matthews, B. W. (1968). "Solvent content of protein crystals." *J Mol Biol* **33**(2): 491-7.
- McCord, J. M. and Fridovich, I. (1969). "Superoxide dismutase. An enzymic function for erythrocyte hemocuprein." *J Biol Chem* **244**(22): 6049-55.
- Miranda-Vizuete, A., Damdimopoulos, A. E. and Spyrou, G. (2000). "The mitochondrial thioredoxin system." *Antioxid Redox Signal* **2**(4): 801-10.
- Mizohata, E., Sakai, H., Fusatomi, E., Terada, T., Murayama, K., Shirouzu, M. and Yokoyama, S. (2005). "Crystal structure of an archaeal peroxiredoxin from the aerobic hyperthermophilic crenarchaeon *Aeropyrum pernix* K1." *J Mol Biol* **354**(2): 317-29.
- Murshudov, G. N., Vagin, A. A. and Dodson, E. J. (1997). "Refinement of macromolecular structures by the maximum-likelihood method." *Acta Crystallogr D Biol Crystallogr* **53**(Pt 3): 240-55.

- Navaza, J. (1994). "Amore - an Automated Package for Molecular Replacement." *Acta Crystallographica Section A* **50**: 157-163.
- Panfilì, E., Sandri, G. and Ernster, L. (1991). "Distribution of glutathione peroxidases and glutathione reductase in rat brain mitochondria." *FEBS Lett* **290**(1-2): 35-7.
- Pedrajas, J. R., Kosmidou, E., Miranda-Vizuete, A., Gustafsson, J. A., Wright, A. P. and Spyrou, G. (1999). "Identification and functional characterization of a novel mitochondrial thioredoxin system in *Saccharomyces cerevisiae*." *J Biol Chem* **274**(10): 6366-73.
- Pedrajas, J. R., Miranda-Vizuete, A., Javanmard, N., Gustafsson, J. A. and Spyrou, G. (2000). "Mitochondria of *Saccharomyces cerevisiae* contain one-conserved cysteine type peroxiredoxin with thioredoxin peroxidase activity." *J Biol Chem* **275**(21): 16296-301.
- Peng, X., Lingxia, Z., Schrauzer, G. N. and Xiong, G. (2000). "Selenium, boron, and germanium deficiency in the etiology of Kashin-Beck disease." *Biol Trace Elem Res* **77**(3): 193-7.
- Pineyro, M. D., Pizarro, J. C., Lema, F., Pritsch, O., Cayota, A., Bentley, G. A. and Robello, C. (2005). "Crystal structure of the trypanothione peroxidase from the human parasite *Trypanosoma cruzi*." *J Struct Biol* **150**(1): 11-22.
- Putnam, C. D., Arvai, A. S., Bourne, Y. and Tainer, J. A. (2000). "Active and inhibited human catalase structures: ligand and NADPH binding and catalytic mechanism." *J Mol Biol* **296**(1): 295-309.
- Rabilloud, T., Heller, M., Gasnier, F., Luche, S., Rey, C., Aebersold, R., Benahmed, M., Louisot, P. and Lunardi, J. (2002). "Proteomics analysis of cellular response to oxidative stress. Evidence for in vivo overoxidation of peroxiredoxins at their active site." *J Biol Chem* **277**(22): 19396-401.
- Radi, R., Turrens, J. F., Chang, L. Y., Bush, K. M., Crapo, J. D. and Freeman, B. A. (1991). "Detection of catalase in rat heart mitochondria." *J Biol Chem* **266**(32): 22028-34.
- Rosen, D. R., Siddiqui, T., Patterson, D., Figlewicz, D. A., Sapp, P., Hentati, A.,

- Donaldson, D., Goto, J., O'Regan, J. P., Deng, H. X. and et al. (1993). "Mutations in Cu/Zn superoxide dismutase gene are associated with familial amyotrophic lateral sclerosis." *Nature* **362**(6415): 59-62.
- Rosenblum, J. S., Gilula, N. B. and Lerner, R. A. (1996). "On signal sequence polymorphisms and diseases of distribution." *Proc Natl Acad Sci U S A* **93**(9): 4471-3.
- Rotruck, J. T., Pope, A. L., Ganther, H. E., Swanson, A. B., Hafeman, D. G. and Hoekstra, W. G. (1973). "Selenium: biochemical role as a component of glutathione peroxidase." *Science* **179**(73): 588-90.
- Russel, M. and Model, P. (1988). "Sequence of thioredoxin reductase from *Escherichia coli*. Relationship to other flavoprotein disulfide oxidoreductases." *J Biol Chem* **263**(18): 9015-9.
- Saitoh, M., Nishitoh, H., Fujii, M., Takeda, K., Tobiume, K., Sawada, Y., Kawabata, M., Miyazono, K. and Ichijo, H. (1998). "Mammalian thioredoxin is a direct inhibitor of apoptosis signal-regulating kinase (ASK) 1." *EMBO J* **17**(9): 2596-606.
- Sandalova, T., Zhong, L., Lindqvist, Y., Holmgren, A. and Schneider, G. (2001). "Three-dimensional structure of a mammalian thioredoxin reductase: implications for mechanism and evolution of a selenocysteine-dependent enzyme." *Proc Natl Acad Sci U S A* **98**(17): 9533-8.
- Sarma, G. N., Nickel, C., Rahlfs, S., Fischer, M., Becker, K. and Karplus, P. A. (2005). "Crystal structure of a novel *Plasmodium falciparum* 1-Cys peroxiredoxin." *J Mol Biol* **346**(4): 1021-34.
- Sauvage, J.-P. and Dietrich-Buchecker, C. (1999). *Molecular catenanes, rotaxanes and knots : a journey through the world of molecular topology*. Weinheim ; New York, Wiley-VCH.
- Scandalios, J. G. (2002). "The rise of ROS." *Trends Biochem Sci* **27**(9): 483-6.
- Schill, W. V. a. G. (1967). "Das massenspektrum einer catena-verbindung." *Tetrahedron* **23**(7): 3079.

- Schneider, G. M. S. a. T. R. (1997). "SHELXL: High-resolution refinement." *Methods in Enzymology* **277**: 319-343.
- Schroder, F., Littlechild, J. A., Lebedev, A. A., Errington, N., Vagin, A. A. and Isupov, M. N. (2000). "Crystal structure of decameric 2-Cys peroxiredoxin from human erythrocytes at 1.7 Å resolution." *Structure Fold Des* **8**(6): 605-15.
- Seo, M. S., Kang, S. W., Kim, K., Baines, I. C., Lee, T. H. and Rhee, S. G. (2000). "Identification of a new type of mammalian peroxiredoxin that forms an intramolecular disulfide as a reaction intermediate." *J Biol Chem* **275**(27): 20346-54.
- Smeets, A., Evrard, C., Landtmeters, M., Marchand, C., Knoop, B. and Declercq, J. P. (2005). "Crystal structures of oxidized and reduced forms of human mitochondrial thioredoxin 2." *Protein Sci* **14**(10): 2610-21.
- Spyrou, G., Enmark, E., Miranda-Vizuete, A. and Gustafsson, J. (1997). "Cloning and expression of a novel mammalian thioredoxin." *J Biol Chem* **272**(5): 2936-41.
- Stadtman, T. C. (1996). "Selenocysteine." *Annu Rev Biochem* **65**: 83-100.
- Storoni, L. C., McCoy, A. J. and Read, R. J. (2004). "Likelihood-enhanced fast rotation functions." *Acta Crystallogr D Biol Crystallogr* **60**(Pt 3): 432-8.
- Sun, Q. A. and Gladyshev, V. N. (2002). "Redox regulation of cell signaling by thioredoxin reductases." *Methods Enzymol* **347**: 451-61.
- Tamaoki, H., Miura, R., Kusunoki, M., Kyogoku, Y., Kobayashi, Y. and Moroder, L. (1998). "Folding motifs induced and stabilized by distinct cystine frameworks." *Protein Eng* **11**(8): 649-59.
- Tamura, T. and Stadtman, T. C. (1996). "A new selenoprotein from human lung adenocarcinoma cells: purification, properties, and thioredoxin reductase activity." *Proc Natl Acad Sci U S A* **93**(3): 1006-11.
- Taylor, S. D., Davenport, L. D., Speranza, M. J., Mullenbach, G. T. and Lynch, R. E.

- (1993). "Glutathione peroxidase protects cultured mammalian cells from the toxicity of adriamycin and paraquat." *Arch Biochem Biophys* **305**(2): 600-5.
- Taylor, W. R. and Lin, K. (2003). "Protein knots: A tangled problem." *Nature* **421**(6918): 25.
- Terwilliger, T. C. and Berendzen, J. (1999). "Automated MAD and MIR structure solution." *Acta Crystallogr D Biol Crystallogr* **55** (Pt 4): 849-61.
- Turrens, J. E. (1997). "Superoxide production by the mitochondrial respiratory chain." *Biosci Rep* **17**(1): 3-8.
- Ursini, F., Maiorino, M. and Gregolin, C. (1985). "The selenoenzyme phospholipid hydroperoxide glutathione peroxidase." *Biochim Biophys Acta* **839**(1): 62-70.
- Vonrhein, C., Blanc, E., Roversi, P & Bricogne, G. (2005). "Automated structure solution with autoSHARP." *Crystallographic Methods*.
- Wallace, D. C. (1999). "Mitochondrial discases in man and mouse." *Science* **283**(5407): 1482-8.
- Watabe, S., Hasegawa, H., Takimoto, K., Yamamoto, Y. and Takahashi, S. Y. (1995). "Possible function of SP-22, a substrate of mitochondrial ATP-dependent protease, as a radical scavenger." *Biochem Biophys Res Commun* **213**(3): 1010-6.
- Watabe, S., Hiroi, T., Yamamoto, Y., Fujioka, Y., Hasegawa, H., Yago, N. and Takahashi, S. Y. (1997). "SP-22 is a thioredoxin-dependent peroxide reductase in mitochondria." *Eur J Biochem* **249**(1): 52-60.
- Watabe, S., Kohno, H., Kouyama, H., Hiroi, T., Yago, N. and Nakazawa, T. (1994). "Purification and characterization of a substrate protein for mitochondrial ATP-dependent protease in bovine adrenal cortex." *J Biochem (Tokyo)* **115**(4): 648-54.
- Weeks, C. M. M., R (1999). "The design and implementation of SnB v2.0." *J. Appl. Cryst.* **32**: 120-124.
- Weichsel, A., Gasdaska, J. R., Powis, G. and Montfort, W. R. (1996). "Crystal structures of

reduced, oxidized, and mutated human thioredoxins: evidence for a regulatory homodimer." *Structure* 4(6): 735-51.

Wonacott, A. J. (1977). *Geometry of the rotation method*. Amsterdam, North-Holland Publishing Company.

Wong, C. M., Chun, A. C., Kok, K. H., Zhou, Y., Fung, P. C., Kung, H. F., Jeang, K. T. and Jin, D. Y. (2000). "Characterization of human and mouse peroxiredoxin IV: evidence for inhibition by Prx-IV of epidermal growth factor- and p53-induced reactive oxygen species." *Antioxid Redox Signal* 2(3): 507-18.

Wood, Z. A., Poole, L. B., Hantgan, R. R. and Karplus, P. A. (2002). "Dimers to doughnuts: redox-sensitive oligomerization of 2-cysteine peroxiredoxins." *Biochemistry* 41(17): 5493-504.

Wood, Z. A., Poole, L. B. and Karplus, P. A. (2003). "Peroxiredoxin evolution and the regulation of hydrogen peroxide signaling." *Science* 300(5619): 650-3.

Wood, Z. A., Schroder, E., Robin Harris, J. and Poole, L. B. (2003). "Structure, mechanism and regulation of peroxiredoxins." *Trends Biochem Sci* 28(1): 32-40.

Yang, K. S., Kang, S. W., Woo, H. A., Hwang, S. C., Chae, H. Z., Kim, K. and Rhee, S. G. (2002). "Inactivation of human peroxiredoxin I during catalysis as the result of the oxidation of the catalytic site cysteine to cysteine-sulfinic acid." *J Biol Chem* 277(41): 38029-36.

Zhong, L., Arner, E. S., Ljung, J., Ashund, F. and Holmgren, A. (1998). "Rat and calf thioredoxin reductase are homologous to glutathione reductase with a carboxyl-terminal elongation containing a conserved catalytically active penultimate selenocysteine residue." *J Biol Chem* 273(15): 8581-91.

Zhong, L., Arner, E. S. and Holmgren, A. (2000). "Structure and mechanism of mammalian thioredoxin reductase: the active site is a redox-active selenolthiol/selenenylsulfide formed from the conserved cysteine-selenocysteine sequence." *Proc Natl Acad Sci USA* 97(11): 5854-9.

Zhong, L. and Holmgren, A. (2000). "Essential role of selenium in the catalytic activities

of mammalian thioredoxin reductase revealed by characterization of recombinant enzymes with selenocysteine mutations." *J Biol Chem* 275(24): 18121-8.

Zhong, L. and Holmgren, A. (2002). "Mammalian thioredoxin reductases as hydroperoxide reductases." *Methods Enzymol* 347: 236-43.